STEADY STATE & TRANSIENT ULTRASONIC FIELD MODELING IN MULTILAYERED LIQUID USING DISTRIBUTED POINT SOURCE METHOD (DPSM)

A

Thesis Report

Submitted in the partial fulfillment of the requirement

for the award of the degree of

Master of Engineering
in
CAD/CAM & Robotics

Submitted By

Shavinder Singh

801081028

Under the Guidance of

Mr. Sandeep Sharma
Assistant Professor,
Department of Mechanical Engineering,
Thapar University, Patiala

Department of Mechanical Engineering,

Thapar University,

Patiala. – 147004

July 2012

ACKNOWLEDGEMENT

I take this opportunity to express my sincere gratitude to **Mr. Sandeep Sharma, Assistant Professor**, **MED, Thapar University, Patiala** for giving me the opportunity of doing my thesis work under his guidance. I am also thankful to him for his constant supervision and valuable suggestions.

It is my proud privilege to express regards and sincere gratitude to **Dr. Shruti Sharma**, **Assistant Professor, CED, Thapar University, Patiala** for her patient listening of my ideas and also suggesting new ways for implementing my ideas by her expert guidance throughout my work.

I am also thankful to **Dr. Ajay Batish, Professor & Head Mechanical Engineering Department, Thapar University, Patiala** for the motivation and inspiration that triggered me for my thesis work.

I also take this opportunity to thank all my close friends, my family, entire faculty and staff of **Mechanical Engineering Department, Thapar University, Patiala** for their help, inspiration and moral support, which went a long way in successfully completion of this report.

Shavinder Singh

(801081028)

Certificate

This is to certify that the work in this thesis report entitled **" Steady & Transient State Ultrasonic Field Modeling in Multi-layered Liquid using Distributed Point Source Method (DPSM) "** submitted in partial fulfillment of requirement for the award of **Master of Engineering Degree in CAD/CAM & Robotics** in Mechanical Engineering Department of Thapar University, Patiala, is an authentic record of work carried out by me under the guidance of **Mr Sandeep Sharma, Assistant Professor, Mechanical Engineering Department, Thapar University, Patiala.**

The matter embodied in this report has not been submitted in part or full to any university or institute for the award of any degree.

Shavinder Singh

Shavinder Singh

801081028

M.E. (CCR)

Dated:

This is to certify that above declaration made by the student concerned is correct to the best of my knowledge and belief.

Mr. Sandeep Sharma

Assistant Professor

Department of Mechanical Engineering

Thapar University

Patiala – 147004

Dr. Ajay Batish

Professor and Head
Deptt. of Mechanical Engg.
Thapar University, Patiala

Dr. S.K Mohapatra

Professor and Head
Dean of Academic Affairs
Thapar University, Patiala

ABSTRACT

In the field of non-destructive evaluation (NDE), the newly developed distributed point source method (DPSM) is gradually gaining popularity. DPSM is a semi-analytical technique used to calculate the ultrasonic fields (pressure, velocity and displacement fields) generated by ultrasonic transducers of finite dimension immersed in homogeneous or non-homogeneous media. In this work the technique is extended to model the transducer immersed in triple layered non-homogeneous fluid and the propagation of steady & transient wave and its pressure generated with transducer is placed at both normal and non-normal angles. DPSM is a frequency based technique. Wave propagation tone burst signal is used. For modeling of transient transmitted & reflected signals are observed at different locations & arrival times are studied. Input transient tone burst signal in time domain is transferred to frequency domain. These frequency components in DPSM module is executed & pressure values are computed at desired target points. Inverse FFT is used to convert the frequency domain results into time domain.

Finally, key characteristics of ultrasonic wave propagation like location of Near Field Zone, Angle of Divergence (formulated in homogeneous fluid) & Snell's Law (formulated in triple layered non-homogeneous fluid) have been validated for the obtained results. The empirical & computed DPSM results are found to be matching with reasonable accuracy.

Keywords: DPSM, FFT, Triple Layered Non-Homogeneous Fluid, Wave Propagation, Transient, Transducer, Double Interface

CONTENTS

LIST OF FIGURES

List of Tables

CHAPTER ONE

INTRODUCTION

1.1 Structural Health Monitoring (SHM)

Structural Health Monitoring (SHM) involves the application of wave propagation to civil and mechanical structures and aims to assist engineers in realizing the full benefits of structural health monitoring. Health of several structures is monitored by recording propagation of stress waves through them. The wave characteristics change due to the deterioration in the structure and they are sensitive to the location, extent and character of damage. However, for a successful monitoring a priori knowledge of the wave characteristic due to different cases is imperative.

The process of implementing a damage detection and characterization strategy for engineering structures (mechanical, aerospace & civil) is referred to as Structural Health Monitoring (SHM). Here damage is defined as changes to the material and/or geometric properties of a structural system, including changes to the boundary conditions and system connectivity, which adversely affect the system's performance. The SHM process involves the observation of a system over time using periodically sampled dynamic response measurements from an array of sensors, the extraction of damage-sensitive features from these measurements, and the statistical analysis of these features to determine the current state of system health [1], [19].

Structural health monitoring (SHM) aims to give, at every moment during the life of a structure, a diagnosis of the "state" of the constituent materials, of the different parts and of the full assembly of these parts constituting the structure as a whole. The state of the structure must remain in the domain specified in the design, although this can be altered by normal aging due to usage, by the action of the environment and by accidental events.

Motivation for SHM

- Nearly all in-service structure requires some form of maintenance for monitoring their integrity and health condition to prolong their lifespan or to prevent catastrophic failure.
- Current schedule-driven inspection and maintenance techniques can be time consuming, labour-intensive and expensive.

- Recent advances in smart structures technologies, sensors and actuators, new diagnostic technologies allows for the detection of the damage to both existing and new structure in real time with minimal human involvement.

Applications of SHM

Though there are tremendous amount of fields where structural health monitoring can be utilized but the most exploited fields are:

- Mechanical engineering
- Civil engineering
- Pipeline engineering
- Aerospace field

1.2 Various Techniques for SHM

Structural Health Monitoring (SHM) is estimating the state of structural health, for detecting the changes in the structure that affect its performance. Two major factors that are considered in structural health monitoring are time-scale of change which deals how quickly the change occurs and Severity of change which deals the degree of change.

Global technique and Local technique are the two different types of techniques available to assess the health of structure are enlisted and they are further divided into sub category, which is shown with the help of a **Figure 1.1**.

Global techniques are employed by carrying out dynamic analysis of the structure in order to identify the damage, its approximate location and its severity, reducing the need for manual inspection. Global techniques are very attractive to civil engineers because they can be implemented without direct access to structural member and no previous knowledge of the damage of the structure is needed. Local techniques are most widely used for assessing the health of the mechanical structures

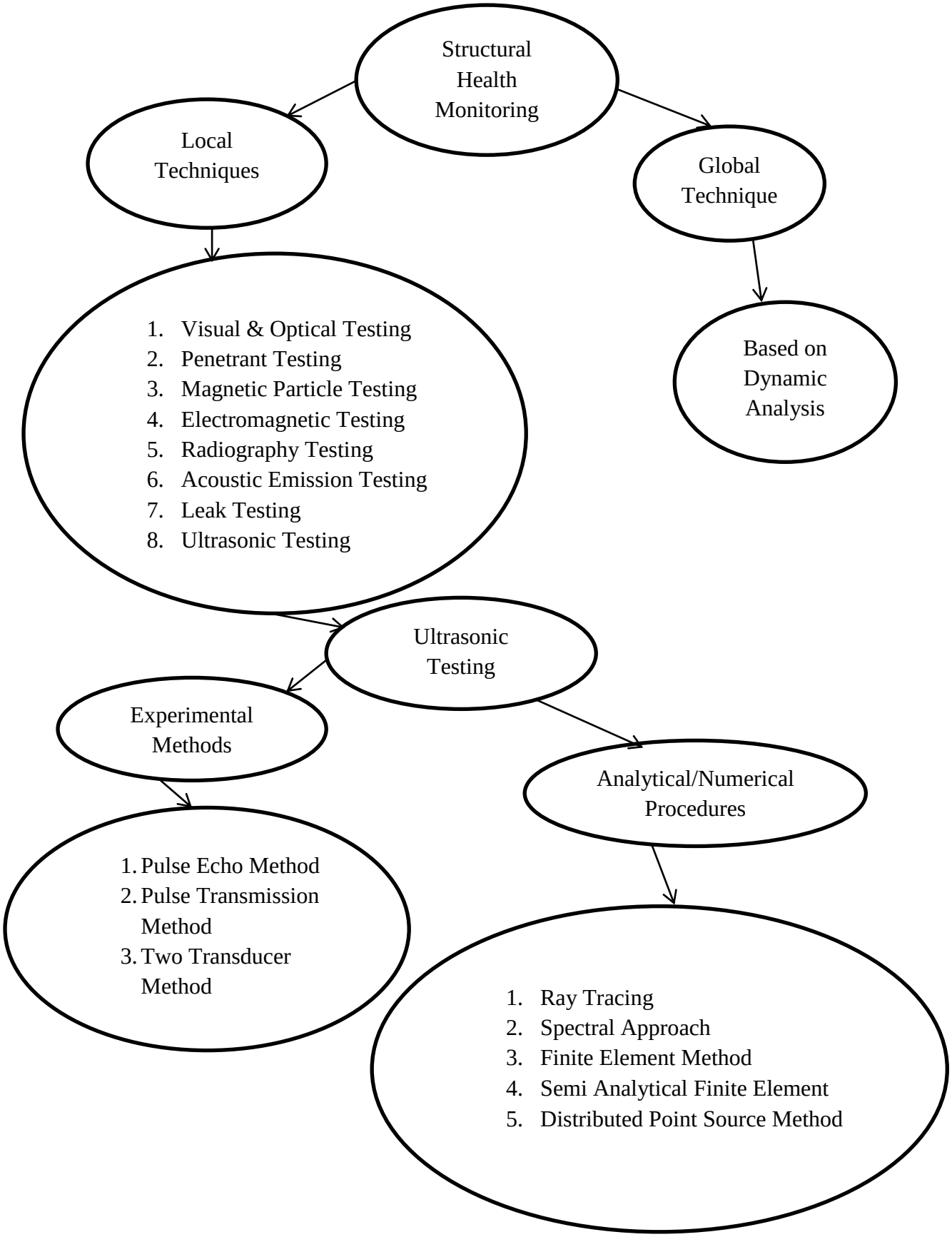

Figure 1.1: Techniques of SHM

The various Global Techniques, shown in **Figure 1.1**, have Non-destructive Methods like ultrasonic testing has emerged as most effective testing technique for SHM because of the economic benefits and reduction in testing time. In next section several NDT techniques have been discussed which are used in different field of application

NDT signifies the method of testing where testing of specimen is done without changing its geometry and physical properties. NDT is classified into various methods of non-destructive testing, which work on different principles and can be implemented where it can improve the performance of NDT [2].

Following are the commonly used NDT techniques

- **Visual and Optical Testing**-Visual inspection involves using an inspector's eyes to look for defects. The inspector may also use special tools such as magnifying glasses or mirrors gain access and more closely inspect the subject area.
- **Penetrant Testing**- Test specimens are coated with visible or fluorescent dye solution. Excess dye is then wiped out from the surface, and a developer is applied. The developer acts as blotter, drawing trapped penetrant out of imperfections open to the surface. With visible dyes, vivid colour contrasts between the penetrant and developer make “bleed out" easy to see.
- **Magnetic Particle Testing (MT*)*** - In this method a magnetic field in a ferromagnetic material is induced and then dusting the surface with iron particles (either dry or suspended in liquid) is done. Surface and near-surface imperfections distort the magnetic field and concentrate iron particles near imperfections, previewing a visual indication of the flaw.
- **Electromagnetic Testing (ET) or Eddy Current Testing** - Eddy currents are generated in a conductive material by an induced alternating magnetic field and they flow in circles at just below the surface of the material. Interruptions in the flow of eddy currents, caused by imperfections, dimensional changes, or changes in the materials conductive and permeability properties, can be detected with the proper equipment.
- **Radiography (RT)** - Radiography involves the use of penetrating gamma or X-radiation to examine parts and products for imperfections. An X-ray generator or radioactive isotope is used as a source of radiation. The resulting shadowgraph shows the dimensional features of the part. Possible imperfections are indicated as

density changes on the film in the same manner as medical X-ray shows broken bones.

- **Acoustic Emission Testing (AE)** - When a solid material is stressed, imperfections within the material emit short bursts of acoustic energy called "emissions." as in ultrasonic testing; acoustic emissions can be detected by special receivers. Emission sources can be evaluated through the study of their intensity, rate, and location
- **Leak Testing (LT)** - Several techniques are used to detect and locate leaks in pressure containment parts, pressure vessels, and structures. Leaks can be detected by using electronic listening devices, pressure gauge measurements, liquid and gas penetrant techniques, and/or a simple soap-bubble test.
- **Ultrasonic Testing (UT)** - In Ultrasonic Testing (UT), very short ultrasonic pulse-waves with center frequencies ranging from 0.1-15 MHz and occasionally up to 50 MHz are launched into materials to detect internal flaws or to characterize materials. The technique is also commonly used to determine the thickness of the test object. Ultrasonic testing is often performed on steel and other metals and alloys, though it can also be used on concrete, wood and composites, albeit with less resolution. It is a form of non-destructive testing used in many industries including aerospace, automotive and other transportation sectors.

  In ultrasonic testing, an ultrasound transducer connected to a diagnostic machine is passed over the object being inspected. The transducer is typically separated from the test object by a couplant (such as oil) or by water, as in immersion testing.

  There are two methods of receiving the ultrasound waveform, reflection and attenuation. In reflection (or pulse-echo) mode, the transducer performs both the sending and the receiving of the pulsed waves as the "sound" is reflected back to the device. Reflected ultrasound comes from an interface, such as the back wall of the object or from an imperfection within the object. The diagnostic machine displays these results in the form of a signal with amplitude presenting the intensity of the reflection and the distance, representing the arrival time of the reflection. In attenuation (or through-transmission) mode, a transmitter sends ultrasound through one surface, and a separate receiver detects the amount that has reached it on another surface after traveling through the medium. Imperfections or other degradation in the space between the transmitter and receiver reduce the amount of sound transmitted, thus revealing their presence. Using the couplant increases the efficiency of the

process by reducing the losses in the ultrasonic wave energy due to separation between the surfaces.

1.3 Basic Terminology related to Wave Propagation

- **Sound Waves**: - Sound waves are simply organized mechanical vibrations traveling through a medium, which may be a solid, a liquid, or a gas. These waves will travel through a given medium at a specific speed or velocity, in a predictable direction, and when they encounter a boundary with a different medium they will be reflected or transmitted according to simple rules. This is the principle of physics that underlies ultrasonic flaw detection
- **Frequency**: - All sound waves oscillate at a specific frequency, or number of vibrations or cycles per second, which we experience as pitch in the familiar range of audible sound. Human hearing extends to a maximum frequency of about 20,000 cycles per second (20 KHz), while the majority of ultrasonic flaw detection applications utilize frequencies between 500 KHz to 10 MHz At frequencies in the Megahertz range, sound energy does not travel efficiently through air or other gasses, but it travels freely through most liquids and common engineering materials.
- **Wave Speed**: - The speed of a sound wave varies depending on the medium through which it is traveling, affected by the medium's density and elastic properties. Different types of sound waves will travel at different velocities.
- **Wave length of a wave**: - Wavelength is related to frequency and velocity by the simple equation Wavelength (λ) =velocity (V)/frequency (f). In ultrasonic flaw detection, the generally accepted lower limit of detection for a small flaw is one-half wavelength, and anything smaller than that will be invisible. In ultrasonic thickness gauging, the theoretical minimum measurable thickness is one wavelength
- **Acoustic Impedance**: - Sound travels through materials under the influence of sound pressure. Because molecules or atoms of a solid are bound elastically to one another, the excess pressure results in a wave propagating through the solid. The Acoustic Impedance (Z) of a material is defined as the product of its density (ρ) and acoustic velocity (V).

$$Z = \rho V$$

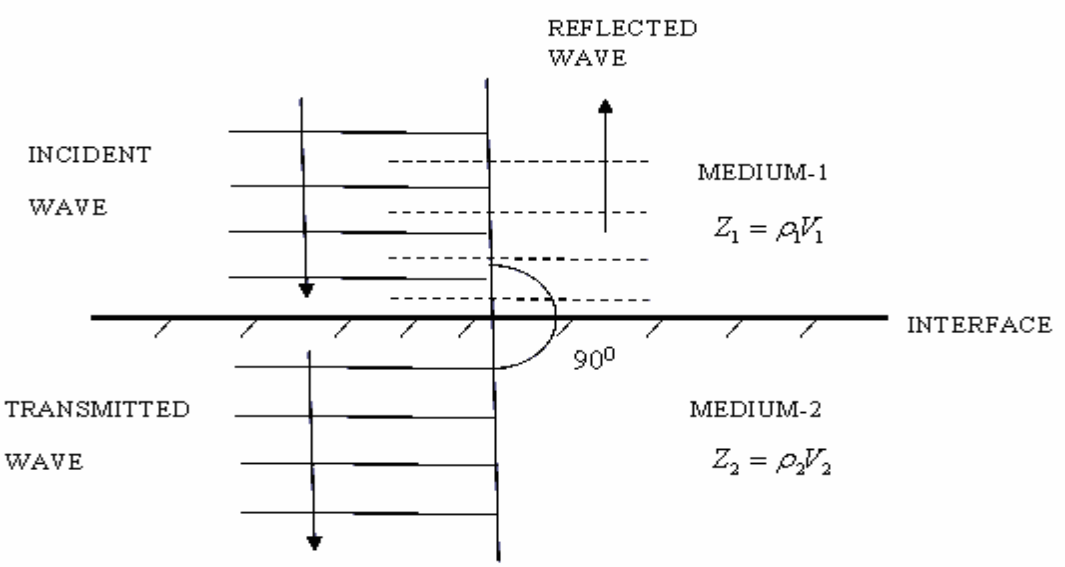

Figure 1.2: Reflection and Transmission of sound wave at normal incidence [2]

1.3.1 Refraction & Snell's Law

When an ultrasonic wave passes through an interface between two materials at an oblique angle, and the materials have different indices of refraction, both reflected and refracted waves are produced. This also occurs with light. Refraction takes place at an interface due to the different velocities of the acoustic waves within the two materials. The velocity of sound in each material is determined by the material properties (elastic modulus and density) for that material. Snell's Law describes the relationship between the angles and the velocities of the waves. Snell's law equates the ratio of material velocities V_1 and V_2 to the ratio of the sine's of incident (Q_1) and refracted (Q_2) angles, as shown in the following **Figure 1.3** and equation.

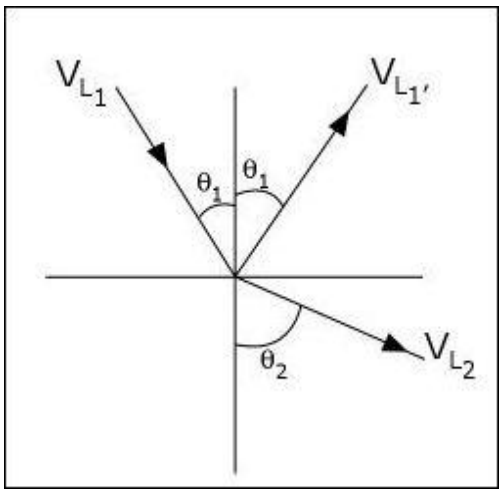

$$\frac{Sin\ \theta_1}{V_{L_1}} = \frac{Sin\ \theta_2}{V_{L_2}} \qquad \text{Eq-1.1}$$

where, V_{L_1} & V_{L_2} are the longitudinal wave velocities in material 1 and material 2 respectively

Figure 1.3: Snell's Law & its Equation [2]

1.3.2 Beam Spread & Beam Divergence

The transducer creates the sound field, which resembles a cylindrical mass in front of the transducer. However, the energy in the beam does not remain in a cylinder, but instead spreads out as it propagates through the material. The phenomenon is usually referred to as beam spread but is sometimes also referred to as beam divergence or ultrasonic diffraction. It should be noted that there is actually a difference between beam spread and beam divergence. Beam spread is a measure of the whole angle from side to side of the main lobe of the sound beam in the far field. Beam divergence is a measure of the angle from one side of the sound beam to the central axis of the beam in the far field, as shown in **Figure1.4**. Therefore, beam spread is twice the beam divergence.

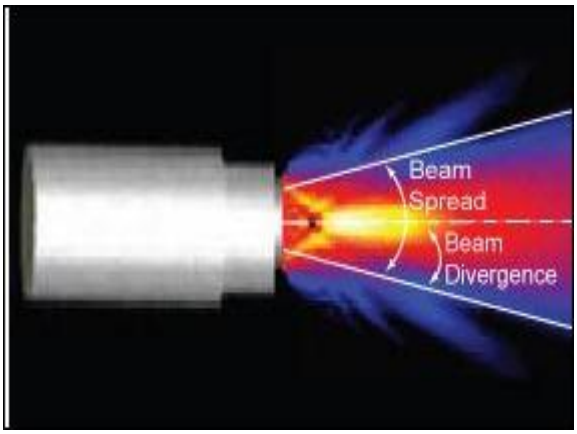

Figure 1.4 : Beam Divergence and Beam Spread [2]

$$\sin\theta = 1.2\frac{V}{DF} \qquad \text{Eq-1.2}$$

where, θ is beam divergence angle from centre line to point where signal is at its half strength.

V = Sound Velocity in material

D = Diameter of the transducer.

F = Frequency of the transducer

1.3.3 Reflection and Transmission Coefficients: Ultrasonic waves are reflected at boundaries where there is a difference in acoustic impedances (Z) of the materials on each side of the boundary as shown in the **Figure 1.2**. This difference in Z is commonly referred to as the impedance mismatch. The greater the impedance mismatch, the greater the percentage of energy that will be reflected at the interface or boundary between one medium and another. The fraction of the incident wave intensity that is refracted can be derived because particle velocity and local particle pressures must be continuous across the boundary. When the acoustic impedances of the materials on both sides of the boundary are known, the fraction of the incident wave intensity that is reflected can be calculated with the equation below. The value produced is known as the reflection coefficient.

$$\text{Reflection coefficient, R} = \frac{(Z_2 - Z_1)}{(Z_2 + Z_1)}$$

Transmission coefficient, T = $\frac{2Z_2}{(Z_2-Z_1)}$

1.3.4 Near Field Zone

The near field Zone is a region of the pressure field around transducer surface. This term describe the way of the characteristics of a pressure field change with distance from the transducer surface to the target points. This phenomenon plays a vital role in ultrasonic testing in any media. The basic equation for this Near Field is given by

$$N_f = \frac{D^2}{4\lambda} \qquad \text{for } \lambda << D \qquad \text{Eq-1.3}$$

1.4 Modes of Wave Propagation

The ultrasonic waves propagate in a number of ways in a medium. On the basis of the mode of particle displacement, these waves can be classified as:

a) Longitudinal or Compressional waves (L-waves)
b) Transverse or Shear waves (S-waves)
c) Surface or Rayleigh waves
d) Lamb or Plate waves or Guided waves

a) Longitudinal or Compressional waves (L-waves)

In longitudinal waves, the oscillations occur in the longitudinal direction or the direction of wave propagation. Since compressional and dilatational forces are active in these waves, they are also called pressure or compressional waves. Compression waves can be generated in liquids, as well as solids because the energy travels through the atomic structure by a series of comparison and expansion (rarefaction) movements **Figure 1.3**.

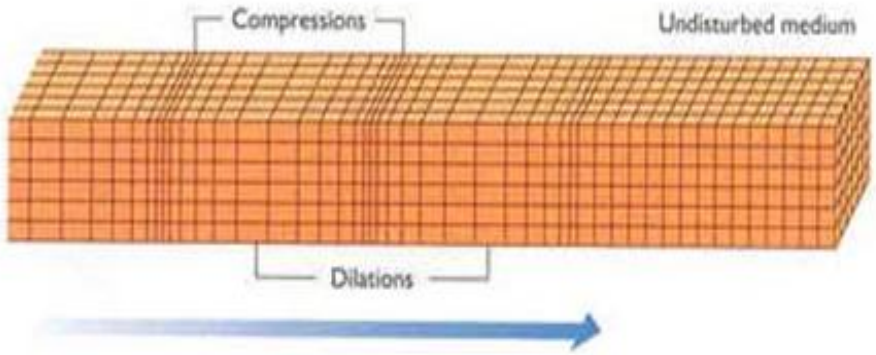

Figure 1.5: Propagation of Longitudinal waves [3]

b) Transverse or Shear waves

In the transverse or shear wave, the particles oscillate at a right angle or transverse to the direction of propagation **Figure 1.4**.

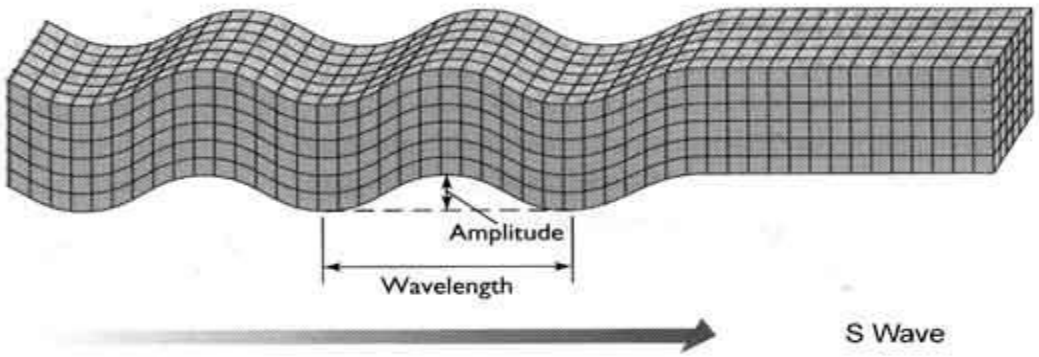

Figure 1.6: Propagation of Transverse or Shear waves [4]

Shear waves require an acoustically solid material for effective propagation, and therefore, are not effectively propagated in materials such as liquids or gasses. Shear waves are relatively weak when compared to longitudinal waves as shown in **Figure 1.6**.

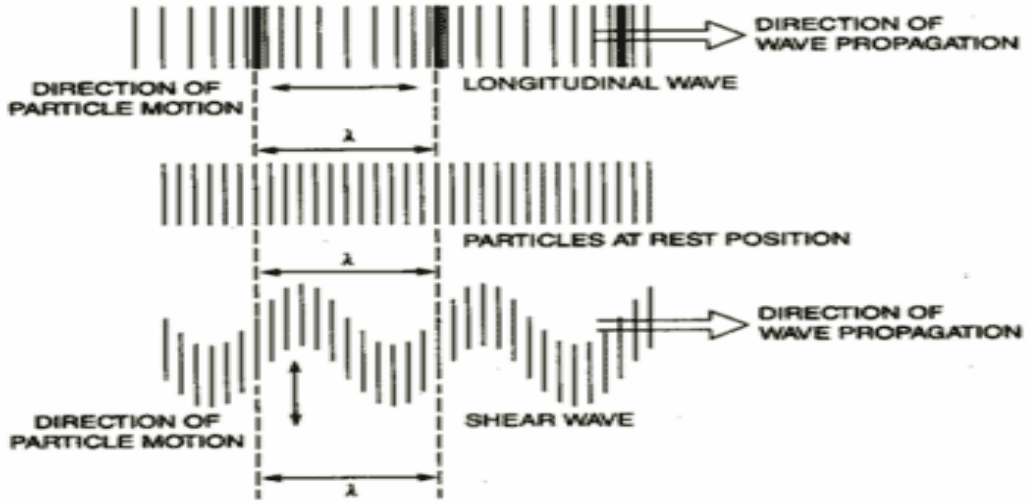

Figure 1.7: Particle Movement Showing the Propagation of Longitudinal and Shear Waves [2]

(c) Surface (or Rayleigh) waves

Surface (or Rayleigh) waves travel the surface of a relatively thick solid material penetrating to a depth of one wavelength. The particle movement has an elliptical orbit as shown in the image and animation below. Rayleigh waves, as shown in **Figure 1.8**, are useful because they are very sensitive to surface defects and they follow the surface around curves. Because of this, Rayleigh waves can be used to inspect areas that other waves might have difficulty reaching.

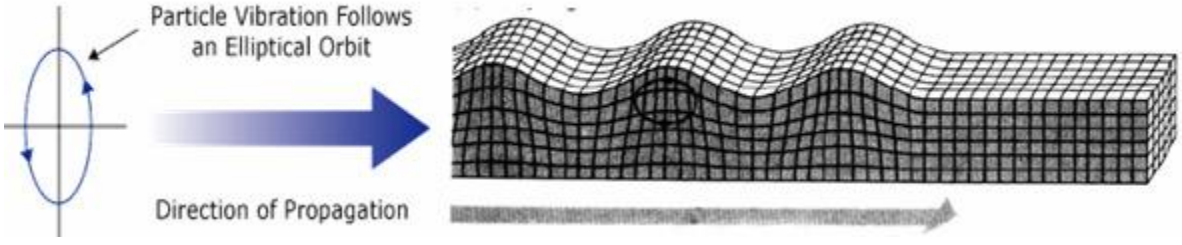

Figure 1.8: Propagation of Surface or Rayleigh Waves [5]

d) Lamb or Plate waves or Guided waves

Plate waves can be propagated only in very thin metals. Lamb waves are the most commonly used plate waves in NDT. Lamb waves are complex vibrational waves that travel through the entire thickness of a material. Propagation of lamb waves depends on the density and the elastic material properties of a component. They are also influenced a great deal by the test frequency and material thickness

The different modes of wave propagation discussed above, out of these modes longitudinal wave and shear waves are two most commonly used for ultrasonic testing in SHM.

1.5 Ultrasonic Testing in SHM

Ultrasonic testing (UT) uses high frequency sound energy to conduct examinations and make measurements. A typical UT inspection system consists of several functional units, such as the pulser/receiver, transducer, and display devices as shown in **Figure 1.9**. A pulser/receiver is an electronic device that can produce high voltage electrical pulses. Driven by the pulser, the transducer generates high frequency ultrasonic energy. The sound energy is introduced and propagates through the materials in the form of waves. When there is a discontinuity (such as a crack) in the wave path, part of the energy will be reflected back from the flaw surface. The reflected wave signal is transformed into an electrical signal by the transducer and is displayed on a screen.

Ultrasonic Testing is a very useful and versatile NDT method. Some of the advantages of Ultrasonic Testing that are often cited include:

- It is sensitive to both surface and subsurface discontinuities.
- The depth of penetration for flaw detection or measurement is superior to other NDT methods.
- Only single-sided access is needed when the pulse-echo technique is used.
- It is highly accurate in determining reflector position and estimating size and shape.
- Minimal part preparation is required.
- Electronic equipment provides instantaneous results.
- Detailed images can be produced with automated systems.
- It has other uses, such as thickness measurement, in addition to flaw detection.

As with all NDT methods, Ultrasonic Testing also has its limitations, which include:

- Surface must be accessible to transmit ultrasound.

- Skill and training is more extensive than with some other methods.
- It normally requires a coupling medium to promote the transfer of sound energy into the test specimen.
- Materials that are rough, irregular in shape, very small, exceptionally thin or not homogeneous are difficult to inspect.
- Cast iron and other coarse grained materials are difficult to inspect due to low sound transmission and high signal noise.
- Linear defects oriented parallel to the sound beam may go undetected.
- Reference standards are required for both equipment calibration and the characterization of flaws

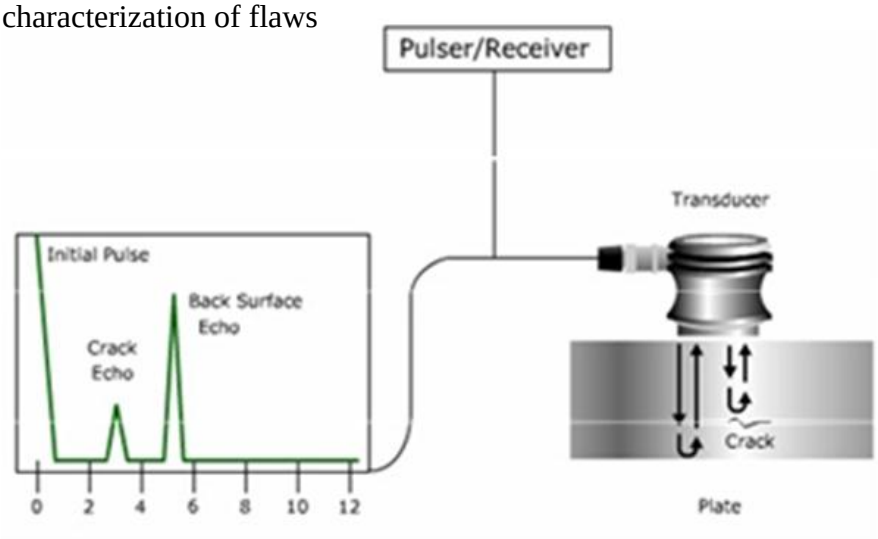

Figure 1.9: General ultrasonic Inspection Principle of pulse echo method [2]

1.5.2 Experimental Methods for Ultrasonic Testing

a) Pulse-echo method
b) Through transmission method
c) Two transducer method

(a) Pulse-echo Method In the pulse-echo method, a piezoelectric transducer with its longitudinal axis located perpendicular to and mounted on or near the surface of the test material is used to transmit and receive ultrasonic energy. The ultrasonic waves are reflected by the opposite face of the material or by discontinuities, layers, voids, or inclusions in the material, and received by the same transducer where the reflected energy is converted into an electrical signal as shown in **Figure 1.10**. The electrical signal is computer processed for display on a video monitor or TV screen.

The display can show the relative thickness of the material, depth into the material where flaws are located, and (with proper scanning hardware and software), where the flaws are located in the X-Y plane

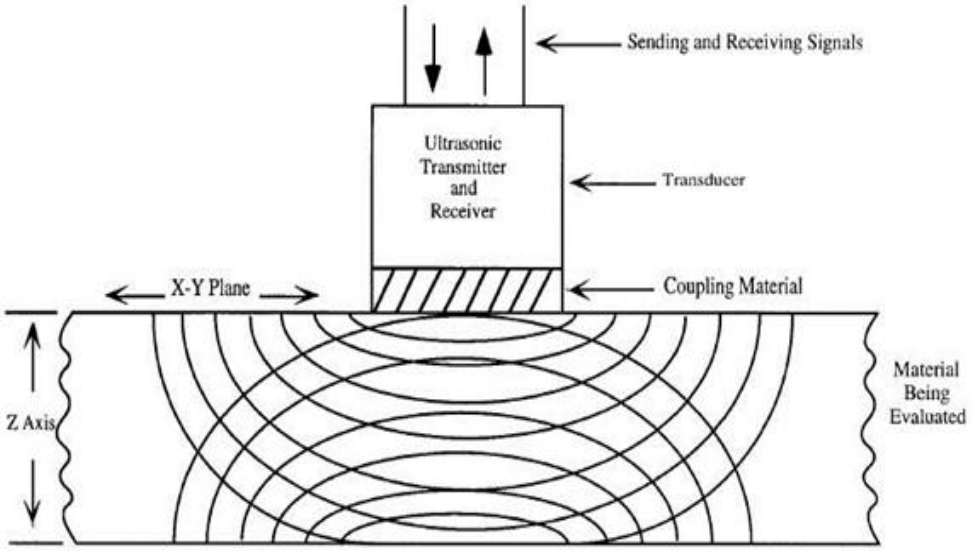

Figure 1.10: Principle of pulse echo method of inspection [6]

(b) **Through transmission Method** In the through-transmission method, an ultrasonic transmitter is used on one side of the material while a detector is placed on the opposite side. One unit acts as transmitter and the other unit as receiver as shown in Figure 1.11. The beam from the transmitter T travels through the material to its opposite surface where the receiving transducer R is placed. Scanning of the material using this method will result in the location of defects, flaws, and inclusions in the X-Y plane.

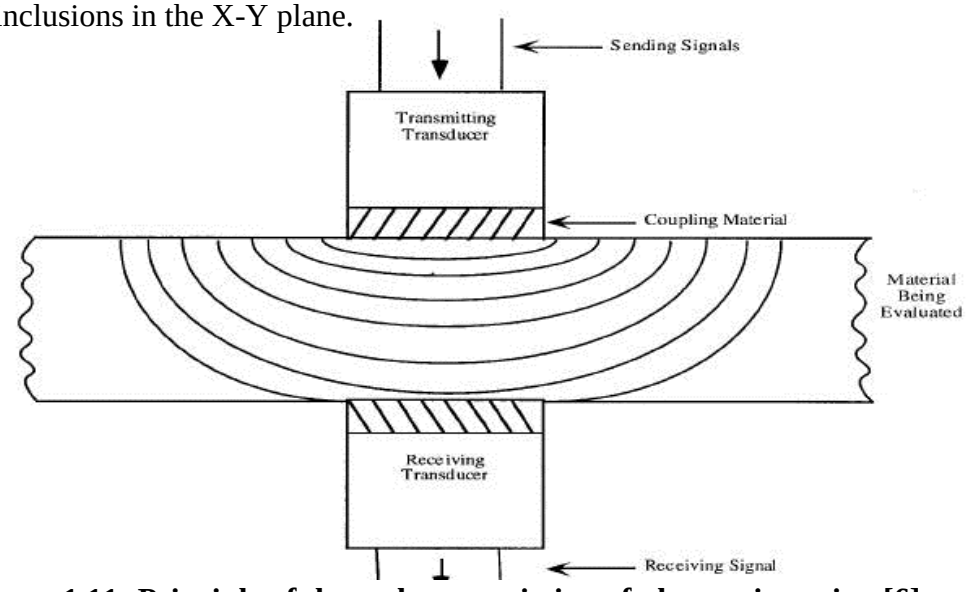

Figure 1.11: Principle of through transmission of ultrasonic testing [6]

(c) Two Transducer Method The pulse echo method can be used with either single or double crystal unit in single transducer unit the probe acts as both transmitter and receiver. In two transducer arrangement, one transmits and other receives the ultrasonic waves .These are placed on same side of specimen ,pulse wave is send in to the specimen by the transducer T, And the echoes reflected from the back surface or any defect are received by the transducer R and displayed on the flaw detector screen. For specific applications like wall thickness measurement special type of transducers in which the transmitting and the receiving crystals are housed in a single unit are also used .These transducers are popularly known as 'twin' or T-R probes.

1.6 Concluding Remarks

This chapter deals with the various Non-Destructive testing methods available for SHM of infrastructure. The ultrasonic testing procedures and various Ultrasonic Testing methods have been discussed.

The following chapter discusses the various numerical/analytical modeling procedures available for the same.

CHAPTER TWO

NUMERICAL/ANALYTICAL TECHNIQUES FOR MODELING WAVE PROPAGATION

2.1 General

Modeling has been an integral part of NDT since its earliest applications [7]. It has been used for several of the common NDT methods including radiography, ultrasonics, eddy current, remote field and a variety of others.

However, the concept of modeling may vary from method to method or even from user to user. To allow for a general approach that encompasses as many NDT modeling concepts as possible, a definition of NDT modeling is proposed for this. Generically we may state that:

"Model, models, or modeling may refer to a pattern, plan, representation, or description designed to show the structure or workings of an object, system, or concept."

For NDT applications modeling is a tool that assists in the understanding of NDT method and its application to a test piece. Such a definition allows for both the visualisation and more common mathematical methods of modeling.

Definition of modeling is quite synonymous with "simulation" [8] and is primarily concerned with the mathematical case:

"The benefit of mathematical modeling codes for modern NDT is well-known, as they are increasingly applied to simulate ultrasonic experiments in real-life inspection. They yield valuable information on the propagation of ultrasound and its interaction with defects and allow for visualization of sound fields and sensitivity zones of ultrasonic transducers."

Depending on the extent or type of the modeling, the main expectations from modeling may include:

- Volume coverage by the test setup
- Improved understanding of basic principle
- Improvement of the inspection technique

- Refinement of sensor design to optimise sensor placement and detection capabilities
- POD (Probability of Detection) evaluation on more specific structures by mixing real and virtual data.

Not all applications require elaborate modeling calculations. Likewise, not all modeling calculations provide the desired solutions to the applications under scrutiny. Thus it is required to pick and choose from the modeling options available and decide when a modelled solution is desirable for an application. It requires the comprehensive knowledge of the available modeling options available.

2.2 Classification of NDT Modeling Methodologies

Based on the definition of modeling, various methodologies may be classified into three general categories;

1. Simple Geometric modeling
2. Mathematic computations
3. Visualisation

Simple Geometric options include lines or curves representing the sensing fields. These entities may be manually or computer drawn. These entities may be extended to indicate skips and are used to indicate either the coverage of the technique or the point of interaction of the beam with an indication. These simple entity drawings sufficed for decades. By producing scale drawings and assuming the beam followed simple straight lines it was even possible to predict the locations where mode conversion would occur.

The second option, mathematic computations, generally consider field source strength and effects of the test method and take into account the attenuation effects of the tested material. Depending on the detail to which the parameters are considered and the methodology used, the complexity of the mathematics varies. The basic mathematic principles underlying sound propagation include the principles of continuum mechanics, which include the laws that deal with conservation of mass, changes in momentum, changes in energy brought about by work and heat transfer, symmetry conditions, and properties of the substances through which sound can propagate. Mathematic modeling has used a variety of methodologies including FEM, BEM (Boundary Element Method) ,FDM (Finite Difference Method) etc.

The third option, visualisation methods, uses the actual sensor or field effects and adapts methods of displaying the field. For some NDT methods this is done as part of the normal

test (e.g. fluoroscopy) but we do not generally consider fluoroscopy a modeling visualisation method. The main beneficiary of NDT visualisation has been the ultrasonic method. Ultrasound has been displayed using schlieren, photoelastic and acoustography techniques.

The following list of the software available is based primarily on various available numerical modeling softwares for the non-destructive testing are given in the **Table 2.1, 2.2, 2.3, 2.4**.

Table 2.1: Softwares for Ultrasonic Numerical Modeling [7]

Product / Software Name	**Type (Models which part)**	**Modeling Technique /Approach Employed**
I3D	Transducer, Geometry	Ray Tracing
Wave2000	Transducer	2D Finite Difference
Wave2500 & Wave3000	Transduces	Full time domain solution to the 3D-axisymmetric viscoelastic wave equation
EWE	Geometry	FEM
Integrated Sound Software	Acoustic field simulation	Boundary element method with simplest elements in 2-D, 3-D, and axi-symmetric acoustic (or Helmholtz) problems
PizeoFLEX	Transducer	FEM, 2D and 3D Piezoelectric Modeling

PiezoCAD	Transducer	Chain matrix technique to calculate the system characteristics from electric terminals to the front acoustic port (KLM)
Utrasim	Transducer (Ultrasound Field Simulation)	Numerical integration of sub-elements of a transducer
3D-CAD	Geometry	Ray Trace

Table 2.2: Softwares for Guided Wave Numerical Modeling [7]

Product / Software Name	**Type (Models which part)**	**Modeling Technique /Approach Employed**
DISPERSE	Modelled guided waves-solution to dispersion curves	Transfer matrix. Solve dispersion relations via root finding routines
ABAQUS	Guided Waves	Finite Element Method

Table 2.3: Software for Acoustic Emission Numerical Modeling [7]

Product / Software Name	Type (Models which part)	Modeling Technique /Approach Employed
AGU-Vallen wavelet	Modelled dispersion curves	Calculate and display the wavelet transform on individual waveforms

Table 2.4: Softwares for X-Ray numerical modeling [7]

Product / Software Name	Type (Models which part)	Modeling Technique /Approach Employed
XRSIM	Geometry	Film Density analysis using different radiation sources and film grades
X-ray NDT Simulation	Geometry	Ray-Tracing and on the X-ray attenuation law

The various modeling packages, which are available commercially, are shown on **Table 2.1, 2.2, 2.3, 2.4** can be used on the demanding application. The back hand principle on which these various modeling packages work are like ray tracing, FEM, SAFE etc. These Numerical principles are discussed in next section.

2.3 Numerical Techniques

Various methods for numerical modeling of wave propagation problems either use time based approach or frequency based techniques. Some of them are hybrid or extended from them using certain manipulations. Key characteristics of wave propagation problems are that the frequency content of the exciting force is very high. At very high frequencies the system becomes mass dominated where inertial effects need to be very accurately modeled. Some popular techniques of modeling wave propagation include:

1. Ray Tracing Method
2. Spectral Approach
3. Finite Element Approach
4. Distributed Point Source Method (DPSM)
5. Semi-Analytical Finite Element (SAFE)

2.3.1 Ray Tracing Method

In this method, the path of waves emerging out of a point or a group of points is traced as rays through all interfaces. Ray tracing is useful when only a few trains of wave emerge and they traverse through simple interfaces **Figure 2.1**.

A simple elegant, one-dimensional model based on ray tracing the path travelled by wave movement insight into stress wave management issues. Ray Tracing is a unique method working independent of time or spectral approach.

Ray Tracing method applied to FGMs

Ray tracing method has wide applications in characterization of materials. So, it is used as a very promising means for characterization of functionally graded materials (FGMs).The method was adopted, to characterize the discretely graded FGM, is a simple reflection-transmission method. When the stress waves come across an interface, some part of it is reflected and the remaining is transmitted in the next layer. The behaviour of these waves, moving across the FGM is traced and hence it is called as the ray-tracing method.

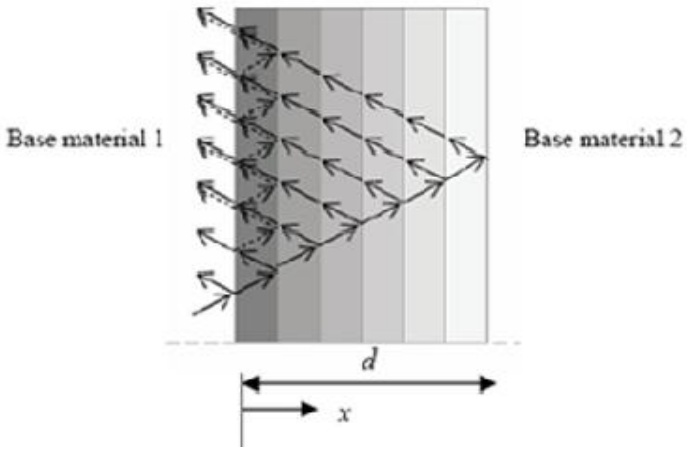

Figure 2.1: 1-D stress wave propagation through discretely layered FGM [9]

The amount of stress wave reflection and transmission can be given by simple laws of physics.

$f_i = (2/(1+\propto))f_t$

$f_r = ((1-\propto)/(1+\propto))\ f_t$

Where f_i is the amount of stress in the incident wave, f_t is the amount of stress in the transmitted wave; f_r is the amount of stress in the reflected wave, and α is the ratio of the acoustic impedance of base material 1 to the acoustic impedance of base material 2 as discussed in Chapter One. For unit area it becomes the characteristic impedance which is the material property.

If d is the thickness of the graded layer and m is the number of graded layers, then the thickness of each layer is$\frac{d}{m}$, and the total time, t, it takes for the incident wave to travel through a layer and then get reflected back is:

$$t= \frac{2d}{c \times m}$$

Where, c is the longitudinal wave speed of the layer.

Limitations in this method

- This method is limited only up to 1-dimension wave propagation and cannot be extended to 2 or 3 dimensions
- It cannot be used for arbitrary forcing functions.

2.3.2 Spectral Approach

One of the shortcomings of Ray Tracing Method is its difficulty in extending it to two-dimensional wave propagation & key issue in modeling of wave propagation is that the frequency content of the exciting force is very high. It requires a very fine mesh of finite elements is necessary to adequately model the problem. This problem can be alleviated by using frequency-based methods, such as the spectral method instead of the time-based techniques. It has many advantages over time-based approaches like it takes very less time for running simulation models. In addition, the inertial effects are exactly represented in it and hence often-exact solutions are obtained for the transformed partial differential equation. In this method, the governing partial differential wave equation is reduced to a set of ordinary differential equations. Their solution is easier than the original differential equation. However, often-approximate solutions are sought. The transformation occurs as a result of Fast Fourier transformation (FFT). These solutions to the governing equations are used as shape functions for spectral element formulation. In addition, often the resulting element is super convergent and very few elements are required to model the system.

Spectral analysis method is a means of solving wave propagation problems in structures. While it is possible to solve structural dynamics problems by starting with partial differential equations of motion and integrating, the task is horrendously large even for the biggest computer available. It has been known long back that an arbitrary time signal can be thought of as the superposition of many sinusoidal components. This is the basis of Fourier (or spectral) analysis. In wave analysis, the time domain for the disturbance is from minus infinity to plus infinity and thus the components have a continuous distribution (known as Continuous Fourier transform). However, the numerical evaluation of the transform requires discretizing the distribution in some manner, and the one chosen here is by the way of discrete Fourier transform (DFT). This has two advantages. First, many of the ideas and methods of time series analysis can be borrowed and used for present purposes. Second, it allows the use of the very efficient Fast Fourier Transform (FFT) computer algorithm.

The significance of the spectral approach to waves coupled with the use of the differential equations is that once the signal is characterized at one space position then it is known at all positions, therefore propagating it becomes a fairly simple matter. This section illustrates the basic algorithm for doing this.

Basic Algorithm

In its simplest terms, the solutions to a waves problems is represented as,

$$u(x) = \sum_n \{ C_1 e^{ik_1 x} + C_2 e^{ik_2 x} + \ldots\ldots + C_{mn} e^{ik_m x} \} e^{i\omega t} = \sum F_n G(K_{mn} x) e^{i\omega t}$$

where G is the analytically known transfer function of the problems. It is a function of position x and has different numerical values at each frequency. F_n is the amplitude spectrum; this is known from the input conditions or from some measurement. This F_nG is recognized as the Fourier transform of the solution. K is the Wave Number, ω is spectral relation, C is constant for integration, and m is different values for different modes. Of course it is different at each position but once it is evaluated at a particular position then its inverse immediately gives the time history of the solution at that point. **Figure 2.3** is a flow diagram for its evaluation. Briefly, the time input F(t) is converted to its spectrum F_n through a use of the forward FFT. The transform solution is the obtained by evaluating the product, at each frequency.

$$u_n = F_n G(K_{mn})$$

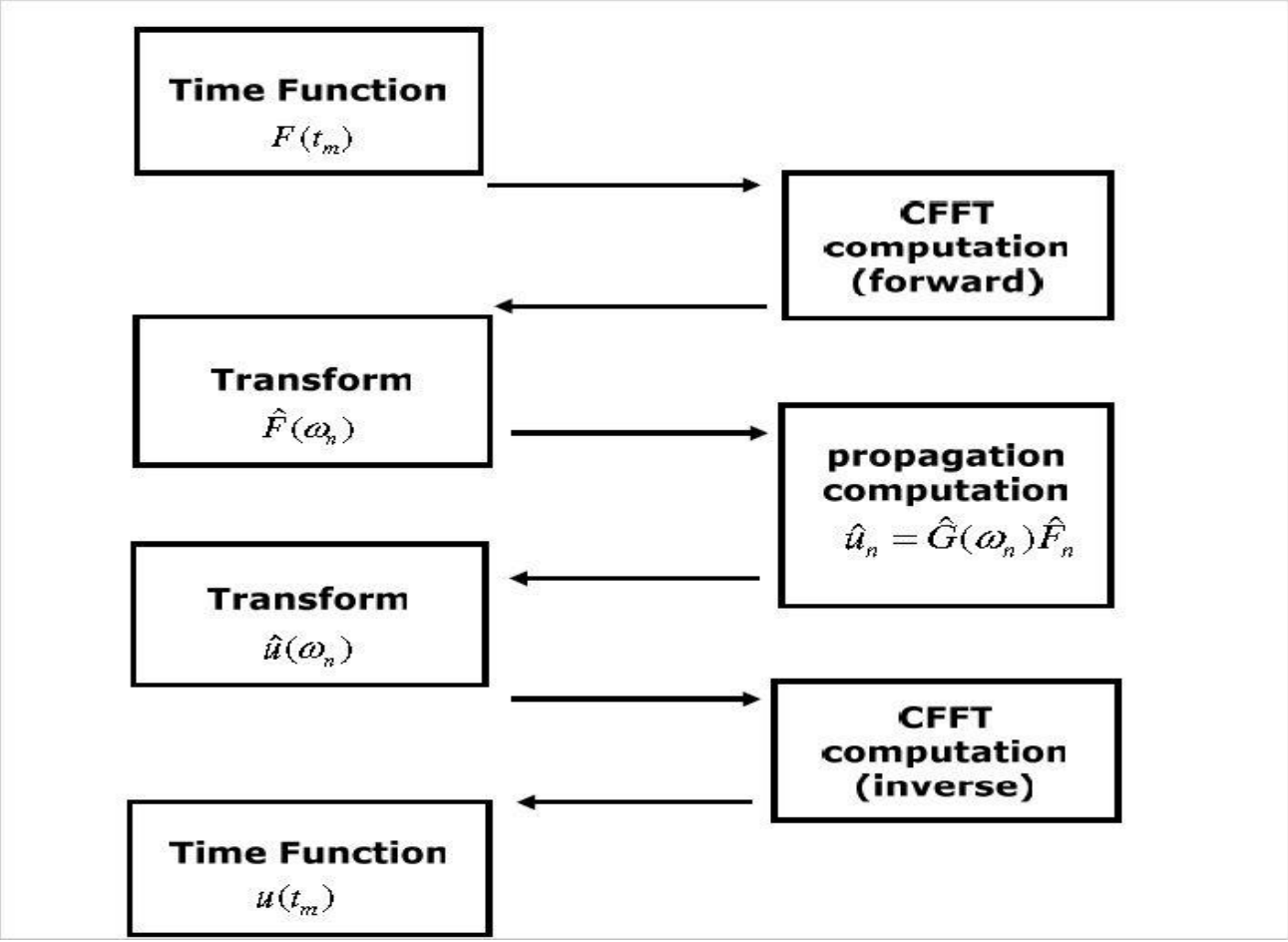

Figure 2.2: Flow diagram for wave reconstruction program [10]

This is finally reconstructed in the time domain by the use of the inverse FFT. In the process, it is necessary to realize (when using the FFT to perform the inversion) that F_n G is evaluated only up to the Nyquist frequency and the remainder is obtained by imposing that it must be complex conjugate of the initial part, This ensures that reconstructed time history is real only.

Limitations of Spectral element method

- Exact solutions for complex differential equations are difficult to obtain, hence this method becomes inefficient in this case.
- Non-linear problems are difficult to solve using this approach.

2.3.3 Finite Element Approach

One approach to modeling guided wave propagation phenomena is to solve the governing differential equations of motion and their associated boundary conditions analytically. However, these equations become intractable for complicated geometries. Another approach to this problem is a numerical solution; the main advantage of this approach is that the

difficulties associated with complicated geometries and defects are much easier to handle numerically. Many numerical tools have been used in the past to study wave propagation in structures; Finite Difference, Boundary Element, Finite Element [11], [12], [13].

The Finite Difference (FD) method simplifies the problem of the solution of the differential equations of wave motion in a continuum by discretizing them into a set of difference equations, in which the field variables are defined at the nodal intersections of the grid. The Boundary Element (BE) method converts volume integrals into surface integrals with the aid of the Green's functions. In the boundary element method elements are placed over the boundary of the solid under investigation and over defects within the structure. In the Finite Element (FE) method, the structure is divided into a finite number of elements of finite size, which are connected to the rest of the structure by the boundaries of the elements.

The most attractive feature of the Finite Difference method is that it is very easy to implement. The Finite Difference method in its basic form is restricted to handle rectangular shapes and simple alterations. Another practical problem in the Finite Difference formulation is the difficulty in defining stress free boundary conditions, which are very common in NDT. The BE method has the advantage that just the surface of the specimen needs to be discretised; the numerical problem itself is therefore reduced by one dimension. However, for many problems boundary element methods are significantly less efficient than volume-discretisation methods (Finite Element, Finite Difference, and Finite Volume). Handling of geometries in FEM is theoretically straightforward and another primary advantage of the FE method is that there are numerous commercial FE codes available, thus eliminating any need to develop actual code. These commercial FE codes have the additional advantages of being very user friendly, and providing sophisticated pre and post-processing options. Thus the FE method has been widely used in the past to study wave propagation.

2.3.4 Distributed Point Source Method (DPSM)

This method is used specifically well for modeling of ultrasonic field .The main originality of DPSM method is that it is not necessary to mesh the totality of the computation volume, but only the surface of interest, in the contrary to a classical finite elements method. The implementation of the model simply requires discretization of the active surface of the transducer or the interfaces to obtain an array of point sources, so that the initial complexity is changed into a superposition of elementary problems. The active surfaces like transducers, emitters, or interfaces reflecting a part of an incident field are discretized into a finite number

of elementary surfaces, a point source being placed at the centroid of every elemental surface. DPSM technique for ultrasonic field modeling was first developed by [14]. They successfully used this technique to model ultrasonic fields in a homogeneous fluid and for a non-homogeneous fluid. The interaction between two transducers, for different transducer arrangements and source strengths, placed in a homogeneous fluid has been studied by [15].

Figure 2.3 shows spherical waves generated by a point source in an infinite medium, cylindrical waves generated by a line source and plane waves generated by an infinite plane. The pressure field due to a finite plane source can be assumed to be the summation of pressure fields generated by a number of point sources distributed over the finite source as shown in **Figure 2.4**.

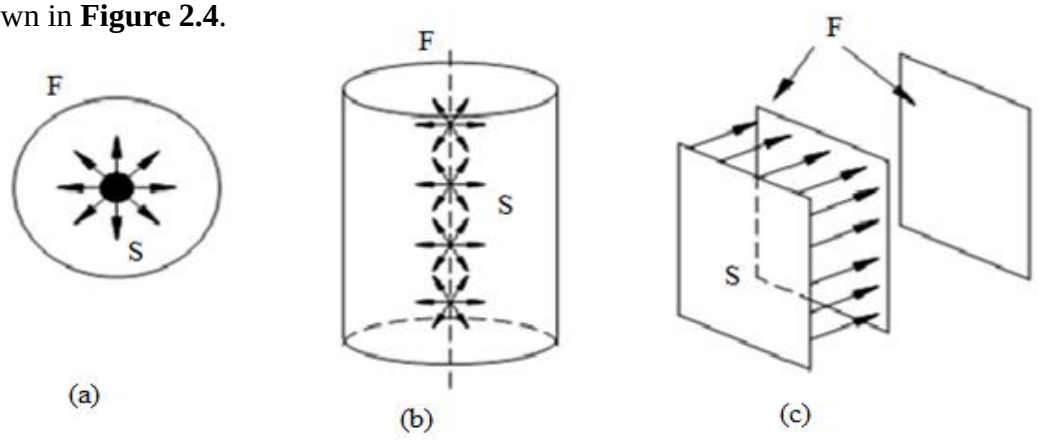

Figure 2.3: (a) Point source generating spherical wave front (b) Line source generating cylindrical wave front (c) Infinite plane source generating plane wave front [15]

The finite source can be the front face of the transducer. A harmonic point source, which expands and contracts alternately, can be represented by a point and a sphere as shown in **Figure 2.5a**.The point represents the contracted position and the sphere represents the expanded position. When a large number of point sources are placed side by side on a plane surface, then the contacted and expanded positions are shown in **Figure 2.5b**. The combined effect of a large number of point sources placed side by side is shown in **Figure 2.5c**. From this figure it is clear that the combined effect of a large number of point sources distributed on a plane surface is the vibration of particles in the direction normal to the plane surface. Non-normal components of motion at a point on the surface generated by neighbouring source points cancel each other as shown in **Figure 2.5d**. However, non-normal components do not vanish along the edge of surface. The particles not only vibrate normal to the surface but also expand to a hemisphere and contract to a point on the edge as shown

.

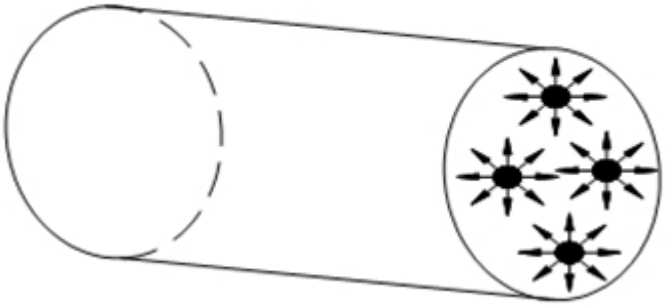

Figure 2.4: Four point sources distributed over a finite surface [15]

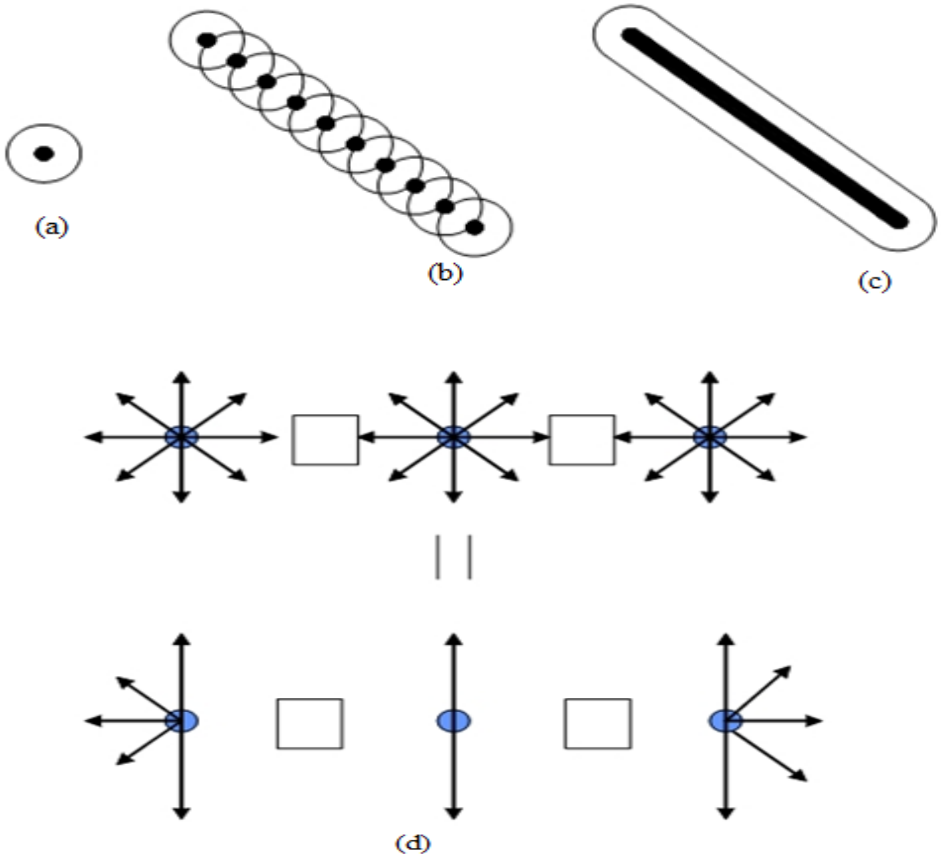

Figure 2. 5: Position of particles for (a) Point source (b) Distributed finite number of points (c) Large number of point sources (d) Components of motion of multiple point sources [15]

This DPSM technique was modeled by [14]. In this method the problem geometries is considered first with any number of interfaces with combination of non-homogeneous media or a homogeneous media. The source of the field is named as "transducer" or "sensor", and the interface between the two media is sometimes called "target". Observation points that are not necessarily on the interface are also called "target points". The transducer surface is discretized into number of points, these points are called source points and also called as the

active source points. If there is any interface in the homogeneous or non-homogeneous media the no of points are considered on the interface as well. And these points are called as passive source points. So, to calculate ultrasonic pressure field between transducer and interface, the number of points are considered in between them and these points are called ad target points. The pressure will be calculated on every single point on the target points. This process to calculate the pressure on every target point will be discussed in chapter four.

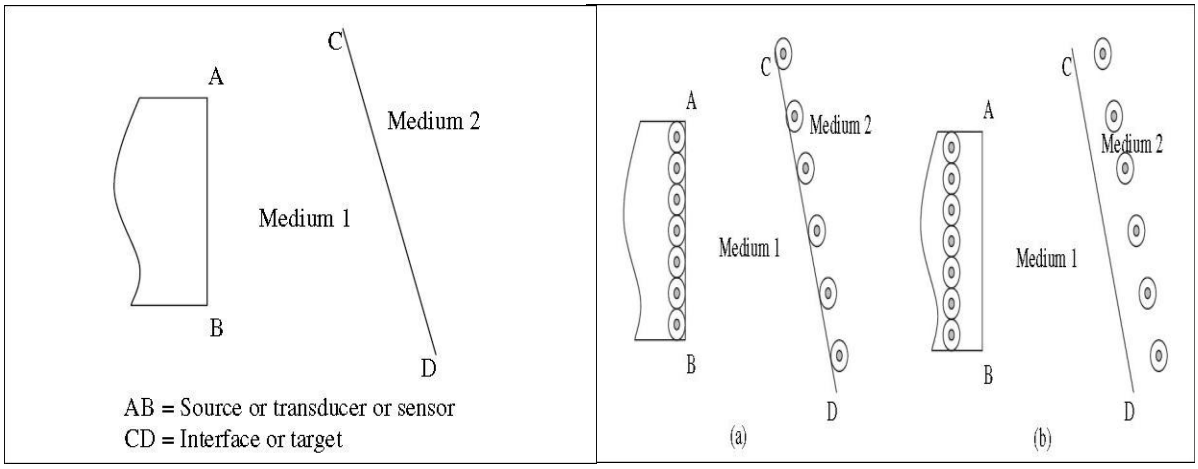

Figure 2.6: Problem geometry with interface and also showing the placing of source points [16]

In the DPSM modeling technique the transducer surface and interface are replaced by a distribution of point sources, as shown in **Figure 2.6**. One layer of sources is introduced near the transducer are called the "active" sources and those near the interface are called the "passive" sources. It should also be noted that a transducer generates a field and an interface alters that field by introducing reflected, transmitted and scattered fields. If the interface is removed, the active point sources should still be present. However, if the active sources are turned off, then the passive point sources must be turned off as well because in the absence of active sources, the passive sources do not exist. Active and passive point sources can be distributed very close to the transducer face and interface, respectively, as shown in **Figure 2.6.**

Like other numerical modeling schemes, accuracy of the computation using DPSM also depends on the number of point sources considered. This process of introducing a number of point sources can be called "mesh generation".

2.3.5 Semi-Analytical Finite Element (SAFE)

Several methods based on the superposition of bulk waves, including, for example, the transfer matrix method or the surface impedance matrix method, have been developed in the

past for the dispersion equation solution for simple geometries of waveguide such as plates or pipes. However, these methods cannot be used to find dispersion relations of guided modes in structures with arbitrary cross section.

A technique called the semi analytical finite element (SAFE) [17], [18], [29] method has been developed in the recent past to investigate waveguides of arbitrary cross section. This method is also referred as the spectral or waveguide finite element methods. This method uses a Finite Element representation of the cross-section of the waveguide, with a harmonic description along the propagation direction. The main advantage of the SAFE method is that only the cross section of the waveguide has to be meshed by finite elements. This greatly reduces the computational time and can be used to model large geometries. However the SAFE method is not capable of modeling discontinuities and therefore cannot be used to model defects. For plane structures of constant thickness, one dimensional SAFE (1D-SAFE) with one dimensional finite element is used. The use of a one-dimensional finite element mesh was first studied about 30 years ago to describe the cross-sectional deformation of a laminate and the characteristic equation for free wave propagation was expressed as a linear eigenvalue problem in frequency. The complex roots of the dispersion curves were obtained by writing the characteristic equation as an eigenvalue problem in wave number. The linear mesh has been used to investigate the dispersion curves in many cases. In a study of plate edge reflection of Lamb waves, the dispersion curves for elastic plates were determined using the same approach, fixing the wave number and formulating the eigenvalue problem in frequency. 1D-SAFE has also been used to investigate the wave propagation and damping in linear viscoelastic laminates. Two dimensional SAFE (2D-SAFE) has been used to study structures with arbitrary cross section. A rigorous solution of all the roots for waves in an elastic wave guide has been recently reported. The solution finds roots for both propagating and non-propagating modes in the wave guide, an important outcome being that necessary results are available for modal composition calculations, for example for the solution of scattering problems. The SAFE method has also been used for infinitely wide structures with periodic changes in geometry or material properties along the width of the model. Wave guides with damping properties have also been studied using the SAFE method. Some studies have reported on how the SAFE method may be applied easily using standard commercial Finite Element (FE) programs [19], thus avoiding the necessity to write special FE codes]. The SAFE method with absorbing regions has recently been applied to the case of

wave modes propagating along a guide of arbitrary cross-section, and radiating into a surrounding fluid or solid medium of infinite extent, the so-called "leaky" waves.

2.4 Concluding Remarks

The modeling contains number of techniques to work on and in this chapter those numerical techniques, which work for various software packages, have been discussed with their applications and limitations. Various techniques used for numerical modeling and softwares available have also been discussed such as FEM, DPSM, SAFE etc.

The following chapter deals with the literature review of the various modeling tools used for wave propagation in. The research work carried till date has been discussed.

CHAPTER THREE

LITERATURE REVIEW

3.1 General

The problem of wave propagation can be solved by several methods as discussed in previous chapter. Ray tracing method is limited to one dimension wave propagation and cannot be applied to 2 or 3 dimensions. Spectral approach is a frequency based method and involves decomposition of the applied impulse into its many sinusoidal components (Fourier components). This is affected by Fast Fourier Transform (FFT) Algorithm. But the disadvantage of this method is exact solutions for complex differential equations are difficult to obtain. The above two methods seem to be very useful to determine stress wave propagation in the 1-D models, however they prove to be futile when complex models are to be analysed. In order to analyse linear and non-linear problems, conventional FEM proves to be more useful but it has limitations regarding the mesh resolution required to cope with huge frequency content of the ultrasonic related problem. And also DPSM proves to be more efficient than FEM because this DPSM technique is a mesh free technique as compared to FEM.

This chapter presents a review of literature on propagation of elastic waves through various media like solid, fluid or both. This gives an idea of study carried out in this area up to this stage. This work can be classified based on the theoretical/analytical studies.

3.2 Review of latest works done

Daniulaitis & Barauskas [20] had used two different approaches on solid case problem. The two approaches were Finite Element and Boundary Integral Equation Approach. The problem, which was being formulated, was same for both these approaches but difference lied in the discretization.

The boundary element method often presented an alternative to the finite element method as it had advantages:

- Only the boundary of the structure had to be meshed.
- There was no need to define boundary conditions because they were naturally included into equation.
- The method was recommended when modeling areas with a high stress concentration.

Authors concluded that FEM provided better results of the signal to noise ratio thus enabled to obtain the finer wave pulse by means of the model. The boundary integral equation algorithm enabled to obtain the noise-free signals by means of the model. Consequently, the calculated displacements were in good agreement with exact displacements. Despite the precision of the technique the calculations were time consuming in comparison with the FE approach.

Barauskas & Daniulaitis [9] found ways for effective simulation of the signal propagation in the structure subjected to non-destructive testing. In most simplified methods (ray tracing) could be used, however they were not based upon the differential equation and presented only rough evaluation of the wave front propagation. On the other hand, finite element or finite difference methods enabled to get adequate representation of the process; however, computer resource requirements were usually too great for problems of a practical value.

The situation was improved by developing efficient algorithms of numerical modeling based on deeper analysis of the wave propagation. In this paper the authors had used quadrilateral finite element and free triangular finite element for meshing of short wave propagation modeling in NDT processes, shown

Authors concluded that conventional methods, including finite element method, finite difference method or even combination of these methods did not provide solution of short wave propagation problems for cases of practical value. All methods required refined meshing and small integration step size that lead to large models and huge amounts of computational resources. The improvement of the effectiveness of a numerical simulation could be achieved by using explicit time integration schemes in uniform finite element meshes.

Kundu et al. [21] studied the modeling of the ultrasonic field using two transducers, one acting as a transmitter and the other acting as a receiver at one time, plate immersed in a homogeneous fluid.

The modeling was done by using semi-analytical technique named distributed point source method DPSM. In that transducer surface is divided into number of points named as source points. The study concluded that this DPSM technique worked well. And as the source points were raised the accuracy was also raising but at the expense of computational time.

Kessler [19] studied the primary damage detection methods. They were frequency response methods and Lamb wave techniques. Frequency response methods relied on loss in stiffness in a structure causing a noticeable shift in the natural frequencies and a corresponding change in the normal mode shapes. These methods were easily applied and fairly sensitive to damage, however they were often more practical in detecting global loss of stiffness than localizing the degraded region. The overall goal of the project was to create analytical tools and procedures that were validated by experimentation, in order to make knowledgeable decisions in designing a reliable SHM system for composite structures using piezoelectric sensors.

Author concluded that using frequency response methods, good correlation was found between the model and the experimental results for low frequencies, however coalescing modes at higher frequencies made comparison impractical. The limitation of these methods was that they required an active driving mechanism to propagate the waves, however, Lamb wave methods had been found to be the most effective for the determination of the presence of damage in composite materials.

Bartoli et al. [17] presented a Semi-Analytical Finite Element (SAFE) method for modeling wave propagation in waveguides of arbitrary cross-section. The method required the finite element discretization of the cross-section of the waveguide by assuming harmonic motion along the wave propagation direction. The general SAFE technique was extended to account for viscoelastic material damping by allowing for complex stiffness matrices for the material. Phase velocity, energy velocity, attenuation, and cross-sectional mode shapes were obtained by solving an eigenvalue problem. The study extended the SAFE method for modeling dispersive solutions in waveguides of arbitrary cross-sections by accounting for material damping. The extension was particularly relevant for NDE/SHM applications on high-loss materials such as viscoelastic fibre-reinforced polymer composites. When accounting for damping, the energy velocity, rather than the conventional group velocity, was calculated along with the frequency-dependent attenuation of the modes.

Gomez et al. [11] found the most effective methods for damage detection in aeronautic structures using lamb waves. But the problem was, for a given frequency multiple modes could exist shown in **Figure 3.1**, making defect identification difficult. Therefore, it became necessary to choose the optimal frequency excitation, and the appropriate actuator location, to obtain the modes more adequate to defects detection. **Figure 3.1** shows a plot of the

wavenumber versus the frequency for the symmetric and antisymmetric Lamb wave modes. It was observed that the first six Lamb propagating modes were present. The branches corresponding to each Lamb mode were clearly identifiable. At low frequencies, below 1 MHz, only two Lamb modes were present: the A_0 mode and the S_0 mode. Frequency excitation ranges above 1.5 MHz would produce other modes making difficult lamb mode selection.

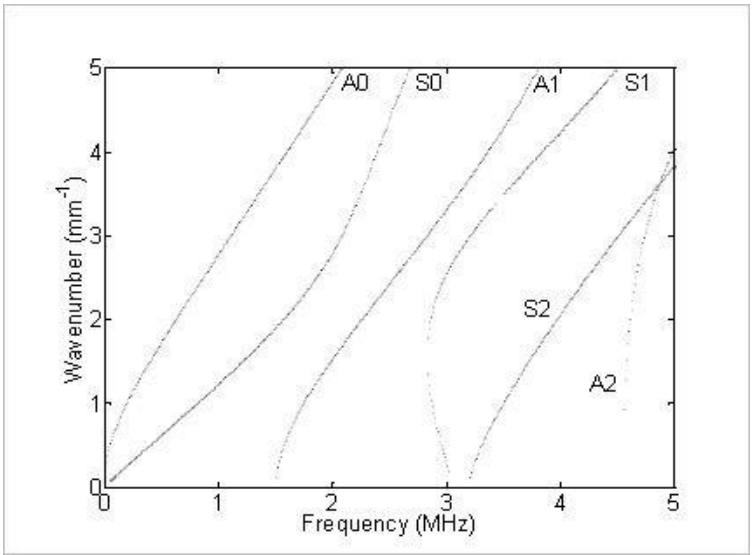

Figure 3.1: Analytical dispersion curves for aluminium plate [11]

In the end, the study and generation of the Lamb wave dispersion curves in thin aluminium plates was presented. Lamb waves were generated and received by using PZT actuators bonded onto the plate. The use of these piezoceramics had demonstrated to be an effective technique to generate Lamb waves. The experimental dispersion curves of an aluminium plate obtained with the 2D FFT algorithm showed a very good agreement with the analytical and FEM dispersion curves calculated. Bonding another piezoceramic in the appropriate location of the plate had demonstrated to be an easy and effective method to selectively filter individual Lamb modes. In that way, by filtering the appropriated Lamb modes, defects identification could be achieved easily.

Kundu et al. [22] presented that the DPSM study is to model ultrasonic fields in both solids and fluids generated by the leaky Rayleigh wave when finite size transducers are inclined at Rayleigh critical angles. This phenomenon had been correctly modelled by the technique. It should be mentioned here that techniques based on paraxial assumptions failed to model the critical reflection phenomenon.

Ray tracing and reflection/transmission coefficient computation become cumbersome in presence of multiple interfaces while such geometries can be relatively easily modeled by the

matrix inversion based DPSM technique. In this paper, a fluid–solid half-space structure with an interface was modeled for critical and non-critical angles of incidence. The theory behind two different techniques of DPSM was presented. The first one was based on the conventional Rayleigh–Sommerfield integral technique and the second one was newly developed Matrix inversion based DPSM technique. Traditional surface integral technique or Rayleigh–Sommerfield integral technique had been adopted here for comparison purposes only to validate the matrix inversion based DPSM technique. It was noted that the traditional Rayleigh–Sommerfield integral based DPSM technique was to some extent similar to other available techniques based on the point source superposition that required a number of point sources distributed near or on the transducer face and then transmission and reflection coefficients at the interface needed to be computed.

The computed results show how the finite size transducers inclined at the Rayleigh critical angle generate leaky Rayleigh waves at the fluid–solid interface.

Kundu & Banerjee [23] extended DPSM Technique to model the ultrasonic field generated in a homogeneous isotropic solid plate immersed in a fluid. The objective of the study was to model the generation of guided waves in a solid plate when ultrasonic beams from transducers of finite dimension strike the plate at different critical angles. And also to model the Lamb wave propagation phenomenon in the plate to see the energy leaking into the surrounding fluid, the symmetric and anti-symmetric modes were formed in the plate and the mode shapes for different Lamb modes vary as the distance of the observation point increases from the transducer position. That calculation required explicit expressions of stress and displacement Green's functions for fluid and solid media. The ultrasonic fields in a solid plate were calculated for critical angles of inclination to generate symmetric and anti-symmetric Lamb modes.

The results showed the strength of the propagating ultrasonic energy decayed along the length of the plate because of the energy leakage into the surrounding fluid. Qualitative agreement between the theoretical and experimental results assured the reliability of the computation. Comparison of DPSM and FEM predicted results established the superiority of the DPSM technique.

Kundu et al. [24] studied the Ultrasonic wave scattering in a solid half-space containing a circular cylindrical hole. The solid was struck by a bounded ultrasonic beam. Distributed Point Source Method (DPSM) was adopted to model the ultrasonic field. A finite size

transducer was used to generate the ultrasonic field. The circular hole in the solid was modeled by passive point sources. The point sources placed near the fluid–solid interface contribute to the scattered wave field in the solid, as shown in **Figure 3.2**, where A1 & A1* are the point sources which are considered as passive point sources, as these points are on the interface. A finite size transducer was immersed in an unbounded fluid medium near a fluid–solid interface. The solid half-space had a circular hole (see **Figure 3.2**). Different diameters (D) of the hole were considered for two different exciting frequencies of the transducer.

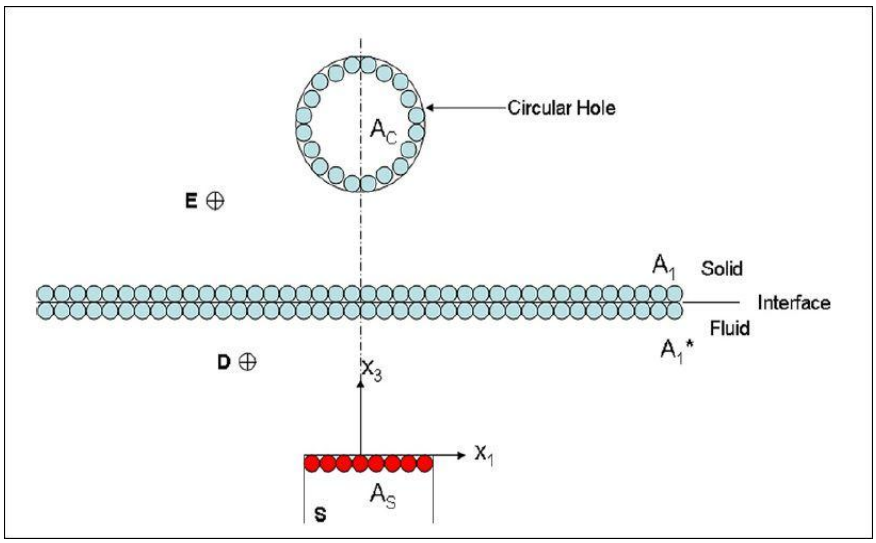

Figure 3.2: DPSM model for the solid half-space with a circular hole, S is the ultrasonic transducer [24]

In this research paper ultrasonic field scattering from a side-drilled circular hole in a solid half-space was investigated.

Tirukkavalluri [10] used Distributed Point Source Method (DPSM), which is a semi-analytical technique. And the author extended this technique to model the propagation of transient wave and its pressure tomo-grams generated both inhomogeneous fluid and non-homogeneous fluid having single interface.

It was concluded that the DPSM results were matched closely with the experimental work. It had been found that experimentally time taken by the wave to hit the interface was matching with the calculated time by DPSM technique. The advantage of DPSM method over traditional wave propagation method is that modeling of transducer (source) and discontinuity (interface) was sufficient to know the whole behaviours of wave propagation in fluids.

Vermani [13] discussed the use of two most commonly used ultrasonic techniques i.e. pulse echo and through transmission to detect the damage in reinforcing steel bars.

Pulse echo was used to locate the exact position of damage and through transmission was used to know the magnitude of damage in steel rod. Negative spike pulse was used as an input signal to sending transducer at one end of the rod through Pulser/Receiver system and transmitted pulse was received at the other end by receiving transducer. The wave signatures obtained were analysed using mixed-signal oscilloscope and digitizer card. A parametric study was carried out to see the effect of change in location of damage and magnitude of damage on wave propagation through steel rods of variable length. The final results obtained were reported in the form of voltage-time curves.

Observation from Pulse Echo method concluded that the measured amplitude and time of flight in that method could be used to find the exact location of the crack. The magnitude or amplitude of the peak received after reflecting from the crack boundary related the amount of defect. It was observed that the amplitude of first peak received from the crack increased with the increase in percentage of area reduction and the amplitude of first back wall echo (BWE) reduced with the increase in the amount of defect.

Observation from through transmission method said that in that method the amplitude of the second peak received after reflecting from the crack boundary could be used to define the amount of defect in the specimen. It was observed that amplitude of the second peak increased with the increase in percentage area reduction signifying the increase in the defect in the specimen.

Sharma [25] used Distributed Point Source Method also known as DPSM in his thesis work. The author adopted this technique to model elastic wave field in solid media with and without internal anomalies by using finite size transducer placed directly on solid fluid couplant interaction. Transient state analysis has also been carried out for the same. And the work also contains the wave propagation analysis for fluid (homogeneous and non-homogeneous) for transducer having non-normal incidence.

And for transient analysis, tone burst signal was used as input signal and response was observed at different target points and results were found to be matching with the wave velocities in specified media. Ultrasonic field in solid media had been modeled for circular and rectangular shapes of the transducer. And in the latter case, fluid-solid interface was

considered and was kept normal as well as non-normal angle to wave propagation direction. In both cases, Fast Fourier transformation (FFT) was used to convert time domain signal into frequency domain and inverse FFT was used to again transform results into time domain.

The DPSM modeling presented here outlines an efficient technique for modeling homogeneous fluid, layered fluids, homogeneous solids, submerged plates with cracks, cavities and inclusions in half-space and plate structure. The modeling of ultrasonic waves in the solids structures were generated by finite sized transducers directly attached in case of solid and immersed in the coupling fluids as in plates. Computed results showed that the propagating waves were significantly affected by the frequency, angle and diameter of the transducer. While modeling fluids (homogeneous and non-homogeneous the transducers were kept at non-normal incidence and its effects were calculated.

Kundu et al. [26] studied the interaction between a bounded ultrasonic beam and a liquid wedge over a solid half-space and analyzed the ultrasonic wave's partially immersed structures. It was also used for studying the effect of underwater ultrasonic or acoustic wave. The problem geometry considered a bounded acoustic beam striking a fluid–solid interface between a fluid wedge and a solid half-space at steady-state. The problem geometry is shown in **Figure 3.3**. A homogenous solid half space was partially immersed in a homogenous fluid

at an angle forming a fluid wedge. A finite size transducer immersed in the fluid acted as the ultrasonic energy source. The ultrasonic beam stroked the inclined fluid–solid interface.

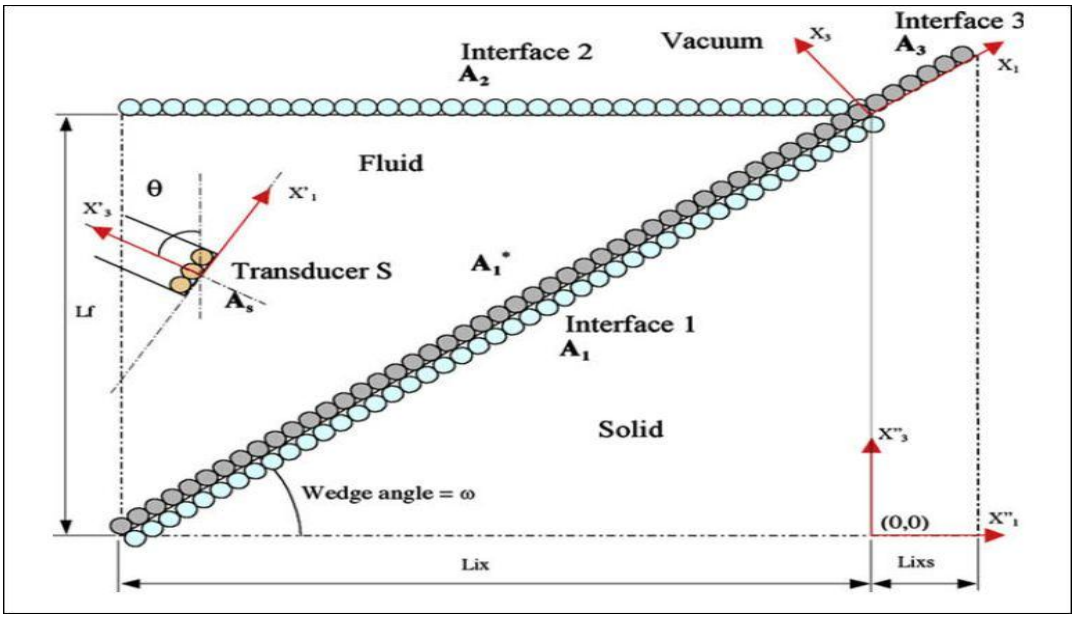

Figure 3.3: Geometry of the wedge problem with point sources [26]

On each side of the fluid–solid interface (Interface 1) 135 point sources were distributed on the central plane. Sources were placed in the illuminated region as well as well beyond the illuminated region of the interface. Therefore, to model the problem geometry with 3 planes of point source, a total of 405 point sources were necessary on each side of the fluid–solid interface. The technique was generalized in the paper to model traction-free fluid and solid boundaries and fluid wedges. Some theoretical predictions were compared with the experimental results and good qualitative matching between the two was observed. Experimental results showed that the trends predicted by the DPSM computation were in line with the experimental findings. Partially immersed and fully submerged solid half space cases were compared. Significant increase in the ultrasonic energy in the fluid wedge for the partially immersed solid half-space case was noticed.

Kundu et al. [27] studied that numerical modeling of the ultrasonic wave propagation was important for Structural Heath Monitoring and System Prognosis problems. In order to develop intelligent and adaptive structures with embedded damage detector and classifier mechanisms, detailed understanding of scattered wave fields due to anomaly in the structure was inevitably required.

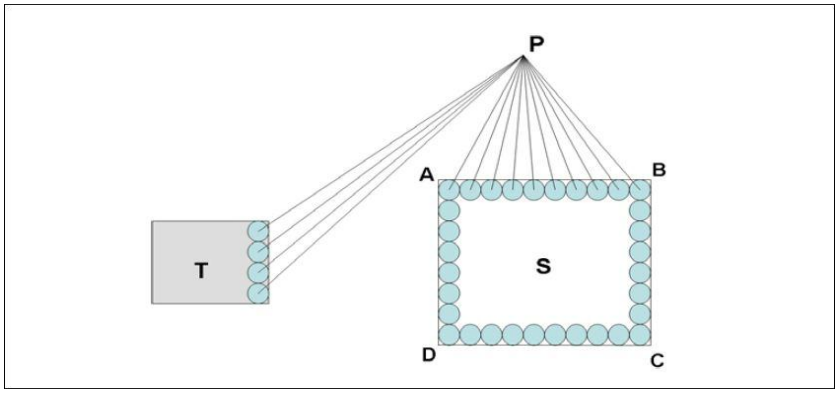

Figure 3.4: In CSR modeling showing point sources & boundaries [27]

A detailed understanding of the problem demanded a good modeling of the wave propagation in the problem geometry in virtual form. In the conventional DPSM approach point sources were placed along the transducer faces, problem boundaries and interfaces to model incident and scattered fields. Every point source emits energy in all directions uniformly. Source strengths of these 360° radiation sources were obtained by satisfying interface and boundary conditions of the problem. In conventional DPSM modeling approach it was assumed that the shadow zone did not require any special consideration. 360° Radiation point sources would be capable of properly modeling shadow zones because all boundary and interface conditions

were satisfied. In this paper it was investigated how good the assumption was by introducing the ‘shadow zone’ concept at the point source level and comparing the results generated by the conventional DPSM and by this modified approach where the conventional 360° radiation point sources were replaced by the Controlled Space Radiation (CSR) sources.

This **Figure 3.4** shows a rectangular scatterer S is placed in front of an ultrasonic transducer T. The total ultrasonic field at point P is the summation of contributions of point sources distributed at the transducer face and at the top surface AB of the scatterer. Since the scattered field from boundaries BC, CD and DA cannot see point P the point sources placed next to those boundaries should not be considered while computing the field at point P. However, in the DPSM formulation the contribution of every point source shown in **Figure 3.4** is considered to compute the field at point P. The DPSM formulation was modified in this paper by introducing the CSR (Controlled Space Radiation) sources such that only the point sources placed along the transducer surface and along the top boundary of the scatterer could contribute to the ultrasonic field at point P. CSR sources were conventional point sources with a superficial mask that made the point sources ineffective or non-radiating in certain directions. Non-radiating directions were different for different point sources that depend on the problem geometry. In this paper an isotropic solid half-space with and without an internal crack excited by an ultrasonic beam generated by a finite size transducer immersed in a fluid medium was modelled by the DPSM technique with CSR and with conventional point sources and the two sets of results were compared.

Fan [28] developed a Semi-Analytical Finite Element (SAFE) method, which used finite elements to represent the cross section of the waveguide and a harmonic description along the propagation direction, to investigate the modal properties of structures with irregular cross-section. Two attractive applications had been investigated with the SAFE method, and the results were encouraging.

The first application related to fluid characterization. Guided torsional waves in a bar with a non-circular cross-section had been exploited by previous researchers to measure the density of fluids. However, due to the complexity of the wave behaviour in the non-circular cross-sectional shape, the previous theory could only provide an approximate prediction; thus the accuracy of the measurement had been compromised. An experimental observation on a large welded plate found that the weld could concentrate and guide the energy of a guided wave traveling along the direction of the weld. That was attractive for NDE since it offered the

potential to quickly inspect for defects such as cracking or corrosion along long lengths of welds.

Kundu et al. [29] studied that the modeling ultrasonic fields in front of a transducer in the presence and absence of a scatterer was a fundamental problem that had been attempted by different techniques: analytical, semi-analytical, and numerical. However, a comprehensive comparison study among these techniques was missing in the literature. The objective of the paper was to make that comparison for different ultrasonic field modeling problems with various degrees of difficulty. Four fundamental problems were considered: a flat circular transducer, a flat square transducer, a circular concave transducer, and a point focused transducer (concave lens) in the presence of a cavity. The ultrasonic field in front of a finite-sized transducer could be obtained by Huygens-Fresnel superposition principle that integrated the contributions of several point sources distributed on the transducer face. The integral which is also known as the Rayleigh integral or Rayleigh-Sommerfeld integral (RSI) could be evaluated analytically for obtaining the pressure field variation along the central axis of the transducer for simple geometries, such as a flat circular transducer. The semi-analytical solution is a newly developed mesh-free technique called the distributed point source method (DPSM). The numerical solution was obtained from finite element analysis. Note that the first three problems studied the effect of the transducer size and shape, whereas the fourth problem computes the field in presence of a scatterer.

Ultrasonic pressure fields in front of transducers in the absence and presence of a scatterer were obtained by semi analytical DPSM, numerical FEM, and analytical techniques. The finite element technique worked very well for 2-D analyses, as in the axisymmetric cases. However, when a true 3-D analysis was needed (such as for a square transducer) the DPSM analysis was found to be more efficient. Solving some fundamental problems of ultrasonic transducer modeling in the presence and absence of a cavity type scatterer, it was concluded that, overall, the DPSM is the more efficient technique. However, for a few specific problems, analytical or 2-D FEM techniques might be more desirable.

Kundu et al. [30] studied the interaction between a cavity or void in a liquid and a converging ultrasonic beam generated by a point-focused acoustic lens. A semi-analytical technique called the distributed point source method (DPSM) was adopted because no analytical solution was available for the problem involving cavities of different size and the finite element method was not very efficient for modeling high-frequency ultrasonic

problems. The solution showed that if the cavity was placed very close to the focal point of the lens then it could be detected by the acoustic lens. The detectability of the cavity at the off-focus position depended on the distance of the cavity from the focal point. The variation of the distance as the cavity moves in horizontal and vertical directions from the focal point was also investigated.

The authors modeled the ultrasonic field in the presence of an a cavity, the point sources that needed to be distributed not only along the lens surface but also along the cavity surface, as shown in **Figure 3.5**. Source layers are denoted as A_S for the microscope lens surface and A_B for the cavity surface. The ultrasonic field at point P is obtained by superimposing the contributions of all point sources in layers A_S and A_B.

The authors concluded at the end that the interaction between a converging ultrasonic beam, generated by a point-focused transducer, and a cavity was modeled by the mesh-free DPSM technique. A simplified DPSM analysis for small cavities and the complete DPSM analysis that could handle cavities of any size were presented. Simplified analysis was faster because it did not need to solve a large system of equations. However, for large cavities the complete solution was necessary. Ultrasonic fields were given in presence and absence of the cavity.

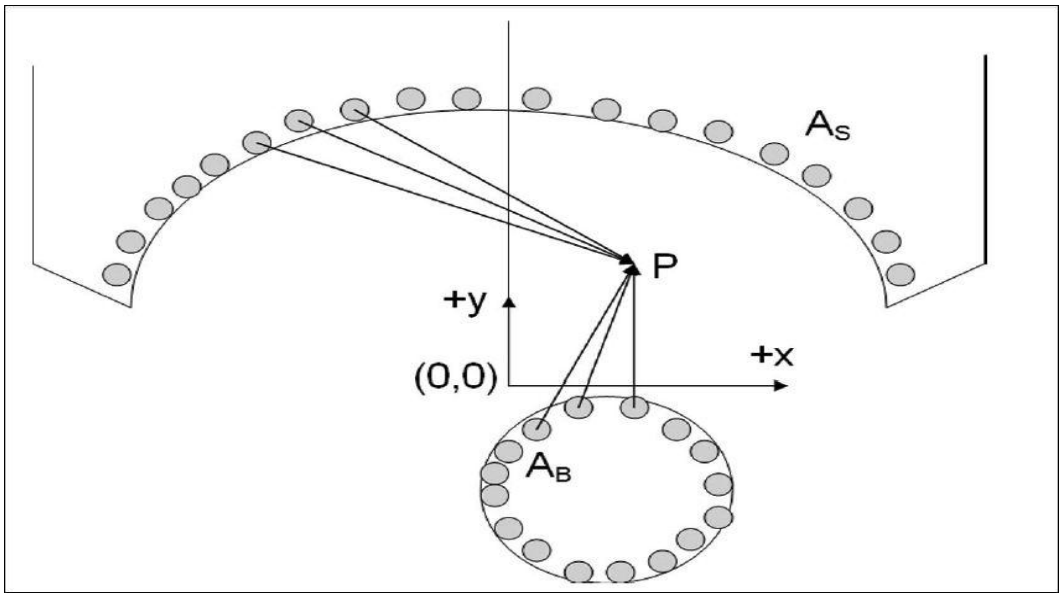

Figure 3.5: Problem geometry having the distribution of point sources (small circles) along the acoustic lens and the cavity [30]

Acoustic force on the transducer surface generated by the reflected energy from the cavity was calculated for different positions of the cavity near the focal point. Results generated by the single-point model and multi-point model of the cavity, ignoring and considering the

multiple reflection effects, were compared. As expected, it was found that for small cavities the simplified single-point model gave good results, but for larger cavities the complete DPSM analysis were needed.

Raisutis et al. [18] carried out investigations to review analytical and semi-analytic modeling methods to relate propagation of ultrasonic guided waves.
Analysis of the propagation of harmonic elastic waves in *n*-layered anisotropic plates and the solutions for each layer were obtained and expressed in the terms of the wave amplitudes using the transfer matrix method. The wave amplitudes were replaced by stresses and displacements at interlayer interfaces and the global transfer matrix was constructed. The expression for the transfer matrix was modified and taken into account the direction of propagation and the attenuation caused by anisotropic structure of the composite.

The limitation of the analytic methods was that those were applicable only for waveguides possessing relatively simple geometry: plates, cylindrical bars or pipes. The semi-analytic finite element (SAFE) method in general enabled to determine dispersion curves of the waveguides possessing arbitrary shaped cross-section. The only cross-section of the arbitrary shape was divided in the finite elements (finite element grid). Therefore, it was always a 2D task. SAFE method was applicable to a wide range of structures, starting from layered plates up to the bars with arbitrary cross-sections. The advantage of the SAFE method was that it was suitable for acquiring of dispersion curves for bars of arbitrary complicated cross-sectional geometries such as rail.

The authors concluded that the review of analytical and semi-analytical methods concerning simulation of ultrasonic guided waves propagation in the composite materials, structures of which were close to the multi-layered composite structures of power plants, had been performed. The advantages and limitations of each technique were clarified. The analytical techniques could be used just for very rough estimation in 1D approach and did not take into account the peculiarities of geometry. It was shown that the most suitable for the determination of the dispersion curves of guided waves propagating in the object under investigation was the semi-analytical finite element method. However, the main problem usually was caused by non-accurate definition of the elastic properties.

Kundu & Rahani [31] studied that transient ultrasonic wave in a fluid medium generated by a flat circular and a point-focused transducer of finite size and also modeled by the distributed point source method (DPSM). DPSM was extended to the time domain without

the fast Fourier transform (FFT) but using the Green's function in the time domain. That modified method was denoted t-DPSM. Harmonic point sources of DPSM were replaced by time-dependent point sources in t-DPSM. Generated t-DPSM results were compared with the finite element (FE) results for both focused and flat circular transducers. The developed method was used to solve the transient problem of wave scattering by an air bubble in a fluid as the bubble was moved horizontally or vertically from the focal point of the focused transducer. The received energy signal was compared for different eccentricities.

The authors considered a single point source, as shown **Figure 3.6**(b). The pressure value at the apex point caused by excitation of the point source is obtained as

$$P(t) = -\frac{1}{4\pi r_s} A\left(t - \frac{r_s}{c_f}\right) \qquad \text{Eq.3.1}$$

where A(t) is a time-dependent function defining the point source strength, r_s is the point source sphere radius . As shown in **Figure 3.6**(a), function A(t) is assumed to vary linearly

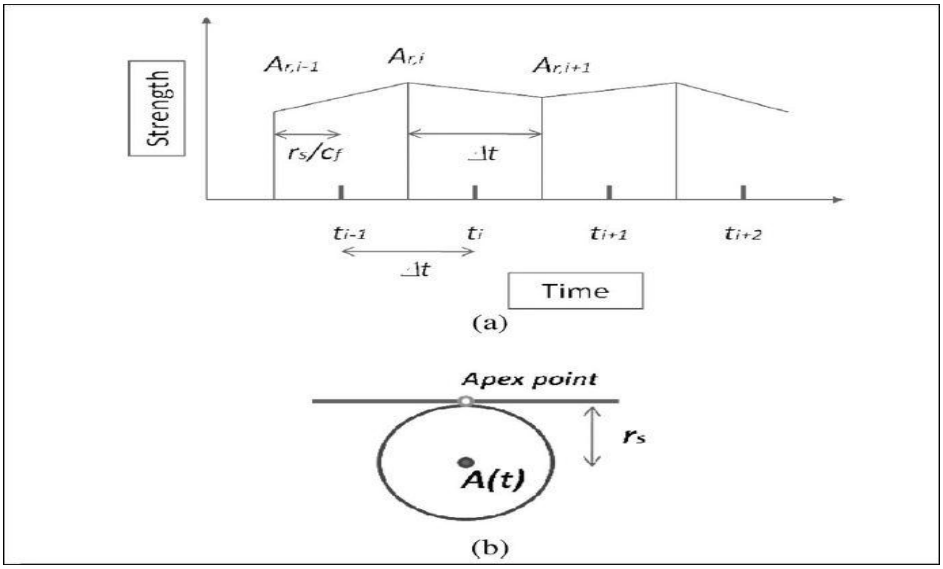

Figure 3.6: (a) A time-dependent point source strength function by linear interpolation, (b) point source schematic [31]

over a time step Δt. Now, the authors discretized the total time interval with time steps Δt. Because it would take a retarded time $\frac{r_s}{c_f}$ for any excitation to travel from the point source to

the apex point, their objective was to find the point source value at $t - \frac{r_s}{c_f}$ in which t is the ith time step at which the boundary condition should be satisfied

As shown in **Figure 3.6**, at each time step t_i, the point source strength $A_{r,i}$ was calculated and, by using a linear interpolation, the time-dependent excitation function for each point source was acquired.

A transient Green's-function-based method following the concepts of conventional DPSM was presented. The transient DPSM method or t-DPSM offers a significant advantage over the conventional numerical methods like FEM. Advantages of DPSM over FEM and BEM for solving ultrasonic wave propagation problems were established. The main advantage of DPSM was that computationally it was much faster than FEM for 3-D large domain problems because DPSM is a mesh-free technique. t-DPSM followed the same concepts and had similar advantages. t-DPSM generated results matched well with the FEM predictions for some sample problems. For more complex non-axisymmetric problems for which 3-D FEM analysis was too time consuming, t-DPSM was easy to implement. Unlike the steady state DPSM, the stiffness matrix generated in t-DPSM was sparsely populated and banded; it was also constant over time, making t-DPSM computationally very efficient.

3.3 Concluding Remarks

In this chapter the major literature related to contention for modeling wave propagation in solid and fluid media has been reviewed. Various techniques are available like Ray Tracing, Spectral Approach, FEM, DPSM etc. with each one having limitation, but DPSM is found more suitable for the study of steady state and transient state in multi-layered fluid and the following chapter discusses that in detail.

CHAPTER FOUR

ULTRASONIC FIELD MODELING USING DISTRIBUTED POINT SOURCE METHOD (DPSM)

4.1 General

The basic principle of DPSM method, which is based on the idea of using multiple point sources distributed over the active part of a sensor or an interface. Active sources synthesize the transducer-generated signals in a homogenous medium, whereas the passive point sources distributed along the interface generate signals to model the reflection and transmission fields. For a finite interface the passive sources model the total field, we call this method the "distributed point source method" or DPSM. It should be mentioned here that this technique is based on the analytical solutions of the basic point source problems. Therefore, it can be considered as a semi-analytical technique for solving sensor problems that include magnetic, ultrasonic, and electrostatic sensors.

4.2 Modeling Ultrasonic Transducer of Finite Dimension Immersed in a Homogenous Fluid: Homogenous fluid is fluid which is having same properties and they do not change from point to point. As mentioned earlier, in the DPSM technique, sources and boundaries of finite dimension are modeled by distributing a number of point sources along the ultrasonic transducer surface (active or primary sources) and the reflecting (or transmitting) boundaries (secondary or passive sources). Point source strengths are adjusted to satisfy the appropriate boundary conditions. The ultrasonic field produced by a single point source is given by

$$p(r) = A\frac{e^{ik_f r}}{r} \qquad \text{(Eq-4.1)}$$

Where $p(r)$ is the pressure at a radial distance r from the point source, A is the source strength, and k_f is the wave number in the fluid. The point source displacement oscillates with time dependence $e^{-i\omega t}$. As shown in **Figure 4.1**, the single point source alternatively expands and contracts giving a radial outward motion from the contracted position and inward motion from the expanded position.

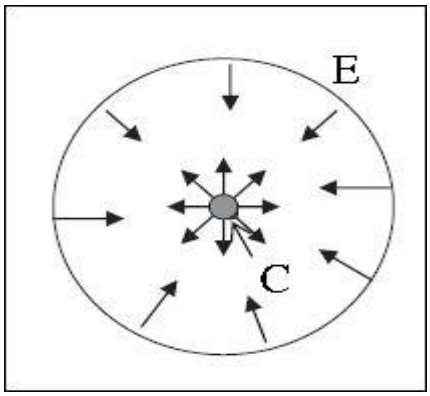

Figure 4.1: Schematic of a point source. Inward arrows show the displacement direction from the expanded position, and outward arrows show displacement direction from the contracted position [15]

Similarly, if there are N numbers of point sources distributed over a plane surface S, as shown in **Figure 4.2,** then the total pressure field at point x generated by all point sources is given by

$$p(x) = \sum_{m=1}^{N} P_m(r_m) = \sum_{m=1}^{N} A_m \frac{e^{ik_f r_m}}{r_m} \qquad \text{(Eq-4.2)}$$

Where A_m is the source strength and r_m is the distance of the observation point from *m*th point source located as y_m as shown in **Figure 4.2.**

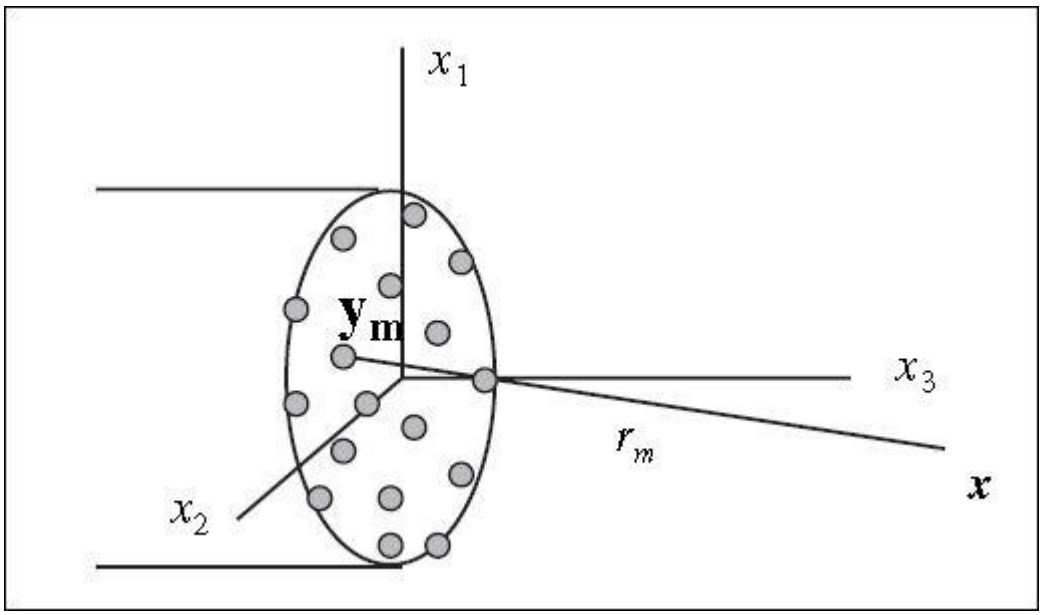

Figure 4.2: Pressure field at point x due to N number of point sources distributed over transducer face [15]

Source strength A_m can be obtained by satisfying the boundary conditions specified on the transducer surface. For example, if the pressure p_0 or the x_3 direction velocity v_0 on a specific point B (see **Figure 4.3**) on the transducer surface is specified, then for that point we can write the boundary conditions in the following form

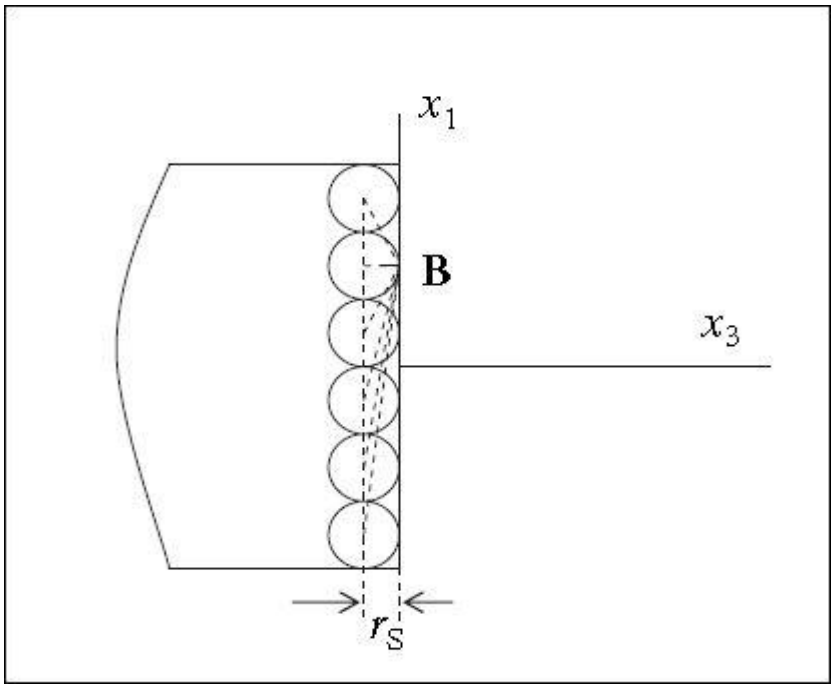

Figure 4.3: Side view of a transducer showing the point sources located at r_s behind the transducer front and a general point B on the transducer face [15]

$$P_0(x) = \sum_{m=1}^{N} P_m(r_m) = \sum_{m=1}^{N} A_m \frac{e^{ik_f r_m}}{r_m} \qquad \text{Eq-4.3}$$

$$v_0(x) = \sum_{m=1}^{N} \frac{A_m}{i\omega\rho} \frac{x_{3m}\, e^{ik_f r_m}}{r_m^2}\left(ik_f - \frac{1}{r_m}\right) \qquad \text{Eq-4.4}$$

Figure 4.3 shows the side view of a transducer whose front face is placed on the x_1x_2 plane. Point sources are distributed at a distance r_S behind the transducer face for avoiding the singularity problem.

4.2.1 Restriction on r_s for point source distribution

It can be observed from the **Figure 4.3,** that as the number of point sources used to model the transducer surface is increased, r_s is decreased. It is evident that with larger number of point sources, the computational time and accuracy both would increase. So, it is required to obtain the optimum number of point sources that should produce reliable results.

For a very small transducer of surface area *dS* vibrating with a velocity of amplitude v_0 in x_3 direction, the pressure at point *x* (at a distance r from the source at point *y*) cab be computed from Eq-4.2

$$p(x) = -\frac{i\omega\rho v_0}{2\pi}\frac{\exp(ik_f r)}{r}dS \qquad \text{Eq-4.5}$$

where, ω is the signal frequency, ρ is the fluid density, $v_0$is the transducer velocity, k_f is the wave number & *r* is the distance of the point source.

Now, the particle velocity in the radial direction can be computed from above pressure field.

$$v_r = \frac{1}{i\omega\rho}\frac{\partial p}{\partial r} = \frac{1}{i\omega\rho}\left(\frac{-i\omega\rho v_0}{2\pi}\right)\left(\frac{ik_f\exp(ik_f r)}{r} - \frac{\exp(ik_f r)}{r^2}\right)dS$$

$$= -\frac{v_0(ik_f r-1)}{2\pi r^2}\exp(ik_f r)dS \qquad \text{Eq-4.6}$$

And the velocity in the x_3 direction

$$v_3 = -\frac{v_0(ik_f r-1)}{2\pi r^2}\exp(ik_f r)dS\frac{x_3-y_3}{r} \qquad \text{Eq-4.7}$$

where, x_3 & y_3 are the x_3 coordinate value of points x & y, respectively

If the point x is taken on the surface of the sphere of radius r_s as shown in **Figure 4.3**, then r = $r_s = x_3 - y_3$, & v_3 of Eq-4.7 is simplified to

$$v_3 = -\frac{v_0(ik_f r-1)}{2\pi r^2}\exp(ik_f r)dS$$

$$\approx v_0\left(1 + k_f^2 r_s^2\right)\frac{dS}{2\pi r_s^2} \qquad \text{Eq-4.8}$$

And also dS should be the surface area of a hemisphere of radius r_s, and the condition implies the following:

$$k_f^2 r_s^2 = \left(\frac{2\pi f}{c_f}r_s\right)^2 \ll 1$$

$$r_s \ll \frac{c_f}{2\pi f}$$

$$r_s \ll \frac{\lambda_f}{2\pi} \qquad \text{Eq-4.9}$$

where, c_f & λ_f are the wave speed and wavelength respectively

In this way the restriction on r_s is implied to get the optimum number of the source points on the transducer surface in accordance with its frequency the size of $r_s$can be varied.

It can be observed in the **Figure 4.3,** r_s, radius of source point is taken at -r_s from the transducer surface, because if the source points are taken on the surface of the transducer then the pressure, suppose a target point is very close to the transducer surface, can't be calculated accurately also it has been calculated using Eq-4.4 if the value of r_s is taken as zero it will produce the singularity problem. So to avoid this phenomenon to occur the source points are taken at -$r_s$position from the transducer surface.

4.3 Computation of Velocity, Pressure and Displacement Fields in a fluid generated by a group of point sources: For a flat surface transducer, where all point sources are excited at the same time, the pressure field generated at a point x (see **Figure. 4.4**(a)) by the transducer can be obtained by integrating the spherical waves, as done in the conventional surface integral technique. The combined effect of a large number of point sources distributed over a plane surface such as the transducer face is the vibration of particles in a direction normal to the plane surface.

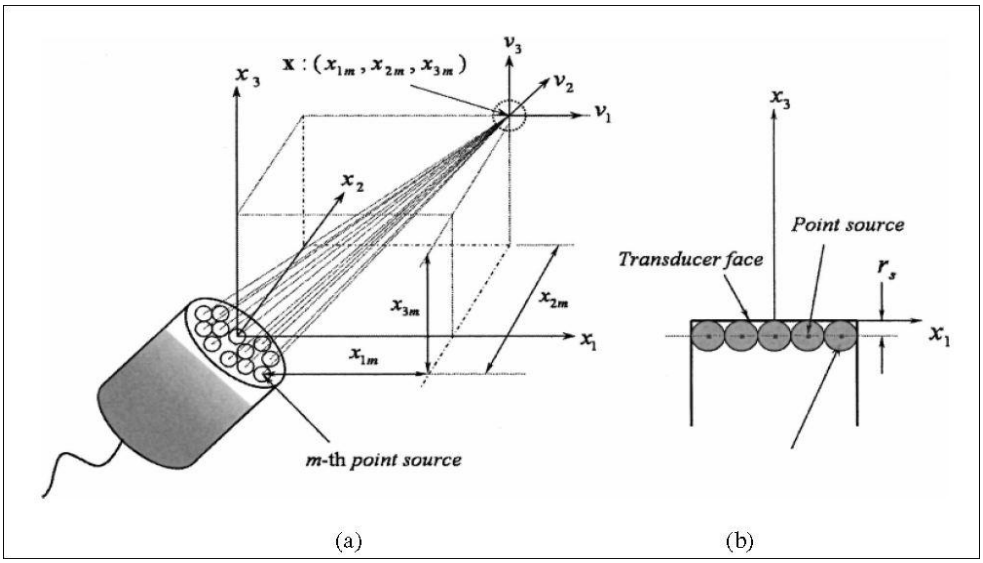

Figure 4.4: (a) Position of an observation point (target point) and its distance from the nth point source on the transducer surface, (b) Side view of a transducer and actual positions of the point sources [23]

From the surface integral technique, the pressure field at point x in front of a group of point sources at y can be written as

$$p(\mathrm{x}) = \int B \frac{e^{ik_f r}}{r} ds(y) \qquad \text{Eq-4.10}$$

where B represents the source strength of the point sources. This integral can also be written in the summation form

$$p(\mathrm{x}) = \sum_{m=1}^{n} \left(\frac{B}{4} \nabla Sm\right) \frac{e^{ik_f r_m}}{r_m} = A_m \frac{e^{ik_f r_m}}{r_m} \qquad \text{Eq-4.11}$$

In the DPSM technique it has been assumed that each point source distributed over the surface has different source strengths as specified by A_m , where m designates the m^{th} point source and r_m is the distance of the target point x from the m^{th} point source. Hence, pressure at any point at a distance r_m from the m^{th} point source with source strength A_m can be written as

$$\hat{p}_m(r) = A_m \frac{e^{ik_f r_m}}{r_m} \qquad \text{Eq-4.12}$$

For 'N' number of point sources distributed on a surface, the pressure at the target point is given by

$$\hat{p}\,(x) = \sum_{m=1}^{N} P_m(r_m) = \sum_{m=1}^{N} A_m \frac{e^{ik_f r_m}}{r_m} \qquad \text{Eq-4.13}$$

Therefore, the velocity in the radial direction, at a distance r from the m^{th} point source, is given by

$$\hat{v}_m(r) = \frac{A_m}{i\omega\rho} \frac{\partial}{\partial r}\left(\frac{e^{ik_f r_m}}{r_m}\right) \qquad \therefore \hat{v}_m(r) = \frac{A_m}{i\omega\rho} \frac{e^{ik_f r_m}}{r_m}\left(ik_f - \frac{1}{r}\right) \qquad \text{Eq-4.14}$$

and the three components of velocity are

$$\hat{v}_{1m}(r) = \frac{A_m}{i\omega\rho} \frac{x_1\, e^{ik_f r}}{r^2}\left(ik_f - \frac{1}{r}\right) \qquad \text{Eq-4.15}$$

$$\hat{v}_{2m}(r) = \frac{A_m}{i\omega\rho} \frac{x_2\, e^{ik_f r}}{r^2}\left(ik_f - \frac{1}{r}\right) \qquad \text{Eq-4.16}$$

$$\hat{v}_{3m}(r) = \frac{A_m}{i\omega\rho}\,\frac{x_3\, e^{ik_f r}}{r^2}\left(ik_f - \frac{1}{r}\right) \qquad \text{Eq-4.17}$$

When the contributions of all M sources are added, the total velocity in x_1, x_2 and x_3 directions at point x can be written as

$$v_1(x) = \sum_{m=1}^{N} \frac{A_m}{i\omega\rho}\,\frac{x_{1m}\, e^{ik_f r_m}}{r_m^2}\left(ik_f - \frac{1}{r_m}\right) \qquad \text{Eq-4.18}$$

$$v_2(x) = \sum_{m=1}^{N} \frac{A_m}{i\omega\rho}\,\frac{x_{2m}\, e^{ik_f r_m}}{r_m^2}\left(ik_f - \frac{1}{r_m}\right) \qquad \text{Eq-4.19}$$

$$v_3(x) = \sum_{m=1}^{N} \frac{A_m}{i\omega\rho}\,\frac{x_{3m}\, e^{ik_f r_m}}{r_m^2}\left(ik_f - \frac{1}{r_m}\right) \qquad \text{Eq-4.20}$$

Where, x_{im} is the shortest distance along x_i direction between the m^{th} point source and the target point, as shown in **Figure 4.4**(a). If the transducer surface is parallel to the x_1x_2 - plane and its velocity in the x_3 direction is given by v_0 then for all x values on the transducer surface the velocity should be equal to v_0. Therefore,

$$v_3(x) = \sum_{m=1}^{N} \frac{A_m}{i\omega\rho}\,\frac{x_{3m}\, e^{ik_f r_m}}{r_m^2}\left(ik_f - \frac{1}{r_m}\right) = v_0 \qquad \text{Eq-4.21}$$

Special Case: When the transducer face is inclined at an Angle θ:

If the transducer face is inclined at an angle θ, measured from x_3 -axis when rotated about the x_2 axis (**Figure 4.5**), the velocity of the transducer face can be expressed as

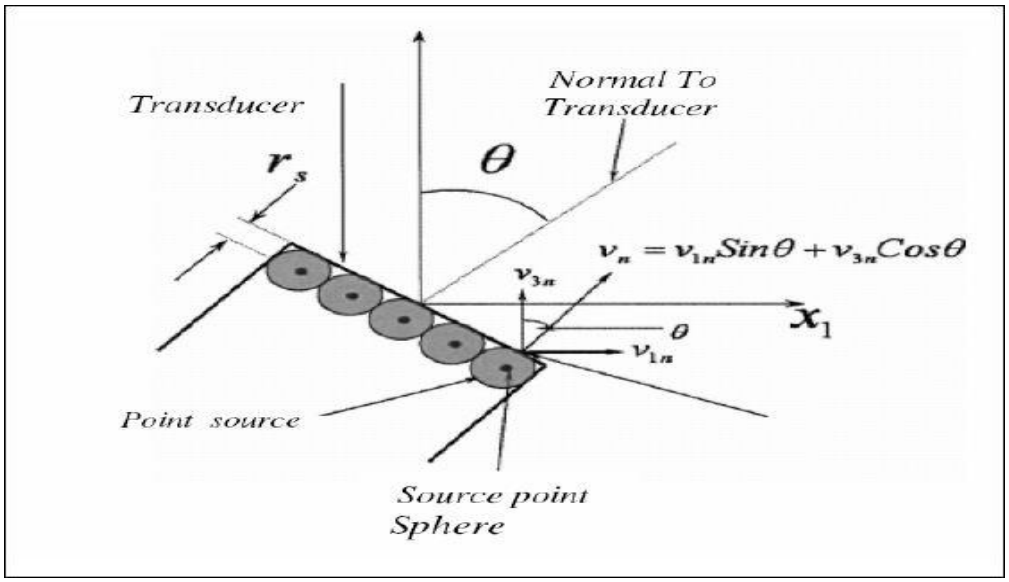

Figure 4.5: Rotation of the transducer with respect to x3-axis and velocity of the nth observation point adjacent to the transducer face [16]

$$v_3(x) = v_1(x)sin\theta + v_3(x)cos\theta$$

$$= \sum_{m=1}^{N} \frac{A_m}{i\omega\rho}\left(ik_f - \frac{1}{r_m}\right)\left(\frac{x_{1m}\exp(ik_f r_m)}{r_m^2}sin\theta + \frac{x_{3m}\exp(ik_f r_m)}{r_m^2}cos\theta\right) = v_0$$

Eq-4.22

4.4 Matrix Formulation: Velocity of the N target points placed on the transducer face due to point sources distributed just below the transducer surface at a distance r_s , can be written in matrix form as

$$V_S = M_{SS}A_S \qquad \text{Eq-4.23}$$

where, V_S is the (Nx1) vector of the velocity components, perpendicular to the transducer surface. If the velocity of the transducer face is given by v_0, then V_S can be written as:

$$\{V_s\}^T = [v_0^1 \quad v_0^2 \quad v_0^3 \quad \dots \quad \dots \quad \dots \quad v_0^{N-1} \quad v_0^N \quad]^T_{N\times 1} \qquad \text{Eq-4.24}$$

where, v_0^N is the velocity of the n^{th} target point. If A_S is the (Nx1) vector of the source strengths, then

$$\{A_s\}^T = [A_1 \quad A_2 \quad A_3 \quad A_4 \quad \dots \quad \dots \quad \dots \quad A_{N-2} \quad A_{N-1} \quad A_N]^T \qquad \text{Eq-4.25}$$

From the earlier discussion, we know that each point source is placed inside a sphere and hence, the number of apex points of the spheres touching the transducer surface will be the same as the number of point sources. When the target points are placed at the apex of the spheres of the point sources, then M is equal to N. Therefore, for the target points at the apex of the spheres of the point sources, the square matrix M_{SS} can be written as:

$$M_{SS} = \begin{bmatrix} f(x_{t1}^1, r_1^1) & f(x_{t1}^2, r_1^2) & f(x_{t1}^3, r_1^3) & \dots\dots & \dots\dots & f(x_{t1}^{N-1}, r_1^{n-1}) & f(x_{t1}^N, r_1^N) \\ f(x_{t1}^2, r_1^2) & f(x_{t2}^2, r_2^2) & f(x_{t2}^3, r_2^3) & \dots\dots & \dots\dots & f(x_{t2}^{N-1}, r_2^{n-1}) & f(x_{t2}^N, r_2^N) \\ f(x_{t1}^3, r_1^3) & f(x_{t3}^2, r_3^2) & f(x_{t3}^3, r_3^3) & \dots\dots & \dots\dots & f(x_{t3}^{N-1}, r_3^{n-1}) & f(x_{t3}^N, r_3^N) \\ \dots\dots & \dots\dots & \dots\dots & \dots\dots & \dots\dots & \dots\dots & \dots\dots \\ \dots\dots & \dots\dots & \dots\dots & \dots\dots & \dots\dots & \dots\dots & \dots\dots \\ f(x_{t1}^N, r_1^N) & f(x_{t2}^N, r_2^N) & f(x_{t3}^N, r_3^N) & \dots\dots & \dots\dots & f(x_{tN-1}^N, r_{N-1}^N) & f(x_{tN}^N, r_N^N) \end{bmatrix}_{N\times N} .$$

Eq-4.26

where ,

$$f(x_{tm}^n, r_m^n) = \frac{x_{tm}^n \exp(ik_f r_m^n)}{i\omega\rho\cdot(r_m^n)^2}\left(ik_f - \frac{1}{r_m^n}\right) = \frac{\exp(ik_f r_m^n)}{i\omega\rho\cdot(r_m^n)^2}\left(ik_f - \frac{1}{r_m^n}\right)(x_{3m}^n \cos\theta + x_{1m}^n sin\,\theta)$$

and r_m^n is the distance between the m[th] point source and the n[th] target point. Eq-4.27

Special Case: For large number of point sources

In Eq.(4.27) r_m^n appears in the denominator .Therefore for small values of r_m^nEq.(4.27) can be simplified in the following manner.

$$f(x_{tm}^n, r_m^n) = \frac{x_{tm}^n \exp(ik_f r_m^n)}{i\omega\rho\cdot(r_m^n)^2}\left(ik_f - \frac{1}{r_m^n}\right) = \frac{x_{tm}^n \exp(ik_f r_m^n)}{i\omega\rho\cdot(r_m^n)^2}\left(-\frac{1}{r_m^n}\right) = -\frac{x_{tm}^n \exp(ik_f r_m^n)}{i\omega\rho\cdot(r_m^n)^3} \quad \text{Eq-4.28}$$

Note that all spheres have the same radius $r_m = r_s = r$, and therefore $x_{tm}^n = r$ .substituting in the above expression and expanding the exponential term in the series expansion we get

$$f(x_{tm}^n, r_m^n) = -\frac{x_{tm}^n \exp(ik_f r_m^n)}{i\omega\rho\cdot(r_m^n)^3} = -\frac{r}{i\omega\rho\cdot(r_m^n)^3}\left(1 + ik_f r_m^n + \cdots\right) = -\frac{r}{i\omega\rho\cdot(r_m^n)^3} \quad \text{Eq-4.29}$$

For m = n, $r_m^n = r_m^m = r$, substituting it in above equation, we get

$$f(x_{tm}^n, r_m^n) \approx -\frac{r}{i\omega\rho\cdot(r_m^n)^3} \approx -\frac{r}{i\omega\rho r^3} \approx -\frac{1}{i\omega\rho r^2} \quad \text{Eq-4.30}$$

Substitution of above two equations yields

$$M_{SS} = -\frac{1}{i\omega\rho r^2}\begin{bmatrix} 1 & \left(\frac{r}{r_2^1}\right)^3 & \left(\frac{r}{r_3^1}\right)^3 & \cdots & \left(\frac{r}{r_N^1}\right)^3 \\ \left(\frac{r}{r_1^2}\right)^3 & 1 & \left(\frac{r}{r_3^2}\right)^3 & \cdots & \left(\frac{r}{r_N^2}\right)^3 \\ \left(\frac{r}{r_1^3}\right)^3 & \left(\frac{r}{r_2^3}\right)^3 & 1 & & \\ \cdots & \cdots & \cdots & \cdots & \left(\frac{r}{r_N^3}\right)^3 \\ \left(\frac{r}{r_1^N}\right)^3 & \left(\frac{r}{r_2^N}\right)^3 & \left(\frac{r}{r_3^N}\right)^3 & \cdots & \cdots \\ & & & & 1 \end{bmatrix}_{N\times N} \quad \text{Eq-4.31}$$

For a general set of target points located on any surface, the velocity due to the transducer sources can be written as:

$$V_T = M_{TS} A_S \quad \text{Eq-4.32}$$

where V_T, the velocity vector (Nx1) contains the normal velocity components of the target points distributed on the surface. The matrix M_{TS} has elements that are similar to those of M_{SS}, with different x_{tm}^n values and the size of the matrix is (MxN), where N is the number of target points and M is the

number of source points. Following the same concept, the pressure at any N number of target points due to M number of source points can be written as:

$$PR_T = Q_{TS}A_S \qquad \text{Eq-4.33}$$

Where, PR_T is the (Nx1) vector of pressure values at N target points, and Q_{TS} is a (NxM) matrix given below

$$Q_{TS} = \begin{bmatrix} \frac{exp(ik_f r_1^1)}{r_1^1} & \frac{exp(ik_f r_2^1)}{r_2^1} & \frac{exp(ik_f r_3^1)}{r_3^1} & \cdots & \cdots & \cdots & \cdots & \frac{exp(ik_f r_{M-1}^1)}{r_{M-1}^1} & \frac{exp(ik_f r_M^1)}{r_M^1} \\ \frac{exp(ik_f r_1^2)}{r_1^2} & \frac{exp(ik_f r_2^2)}{r_2^2} & \frac{exp(ik_f r_3^2)}{r_3^2} & \cdots & \cdots & \cdots & \cdots & \frac{exp(ik_f r_{M-1}^2)}{r_{M-1}^2} & \frac{exp(ik_f r_M^2)}{r_M^2} \\ \cdots & \cdots & \cdots & \cdots & \cdots & \cdots & \cdots & \cdots & \cdots \\ \cdots & \cdots & \cdots & \cdots & \cdots & \cdots & \cdots & \cdots & \cdots \\ \cdots & \cdots & \cdots & \cdots & \cdots & \cdots & \cdots & \cdots & \cdots \\ \cdots & \cdots & \cdots & & & & \cdots & \cdots & \cdots \\ \frac{exp(ik_f r_1^N)}{r_1^N} & \frac{exp(ik_f r_2^N)}{r_2^N} & \frac{exp(ik_f r_3^N)}{r_3^N} & \cdots & \cdots & \cdots & \cdots & \frac{exp(ik_f r_{M-1}^N)}{r_{M-1}^N} & \frac{exp(ik_f r_M^N)}{r_M^N} \end{bmatrix}_{N\times N}$$

Eq-4.34

When the target points are located at the apex of the spheres of the point sources, Eq-4.33 takes the form,

$$PR_S = Q_{SS}A_S \qquad \text{Eq-4.35}$$

where, Q_{SS} is a (NxN) matrix. The definition of r_m^n is identical to that given in Eq-4.28. It is the distance between the m^{th} point source and the n^{th} target point.

4.5 Modeling Ultrasonic Transducer of Finite Dimension Immersed in a Non-Homogenous or Multi Layered Fluid: We are interested in computing the ultrasonic field in multi-layered fluid systems. In the multi-layered problem geometry several interfaces may be present. When fluids with different densities and acoustic properties form a multi-layered system, the fluid density should monotonically vary from top to bottom. If we have 'n' number of fluids in the system, we should have (n-1) number of interfaces.

Each interface acts as a transmitter as well as a reflector of elastic wave energy generated by the ultrasonic transducers. When the entire system is considered, several continuity conditions across the interfaces and boundary conditions at the transducer surface are to be satisfied.

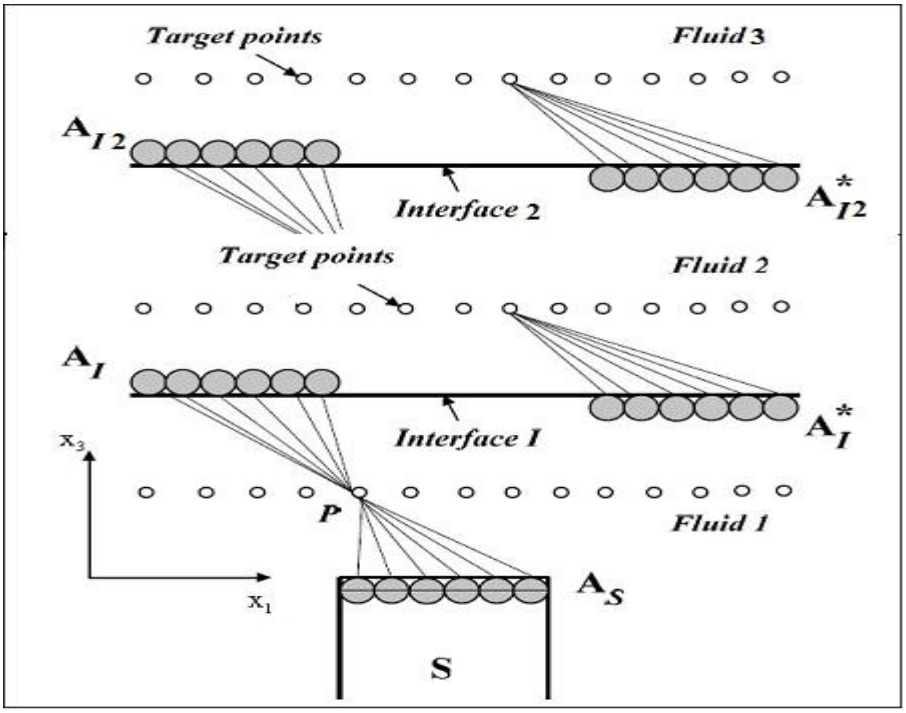

Figure 4.6: Distribution of point sources in the layered fluid system [15]

Let the transducer be immersed in a fluid medium consisting of two fluids, with a plane interface between two fluids located in front of the transducer, as shown in **Figure.4.6**. We can introduce five layers of point sourcesA_S ,A_I, A_I^* , A_{I2}, A_{I2}^*as shown in the **Figure.4.6** to model the incident field, reflected field and transmitted field, respectively. The sources with source strength A_I generate the ultrasonic field in the fluid1 below it and the sources with source strength A_I * generate the ultrasonic field in the fluid2 above it. Similarly, the sources with source strengths A_{I2} generate the ultrasonic field in the fluid2 below it and the sources with source strengths A_{I2}^* generate the ultrasonic field in the fluid3 above it. Observation points or target points are shown by open small circles in the **Figure.4.6**.The total ultrasonic field in each medium is obtained by superimposing the fields generated by three sets of sources as listed below:

Fluid 1: Summation of fields generated by A_S and A_I

$$P_T = Q_{TS}A_S + Q_{TI}A_I \quad \text{Eq-4.36}$$

$$V_T = M_{TS}A_S + M_{TI}A_I \quad \text{Eq-4.37}$$

Fluid 2: Summation of fields generated by A_I^* and A_{I2}

$$P_T = Q_{TI}^*A_I^* + Q_{TI2}A_{I2} \quad \text{Eq-4.38}$$

$$V_T = Q^*_{TI} A^*_I + Q_{TI2} A_{I2} \quad \text{Eq-4.39}$$

Fluid 3: Summation of fields generated by A_{I2}^*

$$P_T = Q^*_{TI2} A^*_{I2} \quad \text{Eq-4.40}$$

$$V_T = Q^*_{TI2} A^*_{I2} \quad \text{Eq-4.41}$$

4.5.1 Strength Determination from Boundary and Interface Conditions:

Certain boundary and interface continuity conditions must be satisfied for this problem geometry. On the transducer surface *T*, the velocity fields are specified as V_0. Across the interface, the pressure (PR) and the x_3-direction velocity must be continuous.

Since any set of sources and target points the velocity and pressure fields are given by V= M.A and PR = Q.A (refer to Eq.4.27 & 4.28), the boundary and continuity conditions give rise to the following equations:

$$M_{SS} A_S + M_{SI} A_I = V_0 \quad \text{Eq-4.42}$$

$$M_{IS} A_S + M_{II} A_I = M^*_{II} A^*_I + M_{II2} A_{I2} \quad \text{Eq-4.43}$$

$$Q_{IS} A_S + Q_{II} A_I = Q^*_{II} A^*_I + Q_{II2} A_{I2} \quad \text{Eq-4.44}$$

$$M^*_{I2I} A^*_I + M_{I2I2} A_{I2} = M^*_{I2I2} A^*_{I2} \quad \text{Eq-4.45}$$

$$Q^*_{I2I} A^*_I + Q_{I2I2} A_{I2} = Q^*_{I2I2} A^*_{I2} \quad \text{Eq-4.46}$$

These above Eq-4.37 to Eq-4.41 can be written in the matrix form as

$$\begin{bmatrix} M_{SS} & M_{SI} & 0 & 0 & 0 \\ M_{IS} & M_{II} & -M^*_{II} & -M_{II2} & 0 \\ Q_{IS} & Q_{II} & -Q^*_{II} & -Q_{II2} & 0 \\ 0 & 0 & M^*_{I2I} & M_{I2I2} & -M^*_{I2I2} \\ 0 & 0 & Q^*_{I2I} & Q_{I2I2} & -Q^*_{I2I2} \end{bmatrix}_{5\times5} \begin{bmatrix} A_S \\ A_I \\ A^*_I \\ A_{I2} \\ A^*_{I2} \end{bmatrix}_{5\times1} = \begin{bmatrix} V_{S0} \\ 0 \\ 0 \\ 0 \\ 0 \end{bmatrix}_{5\times1} \quad \text{Eq-4.47}$$

Or can also be written in this form

$$[MAT]\{A\} = \{V\} \quad \text{Eq-4.48}$$

The vector of source strengths of the total system can be calculated by taking inverse of [MAT] and multiplying it with the vector {V}

$$\{A\} = [MAT]^{-1}\{V\} \qquad \text{Eq-4.49}$$

4.6 Concluding Remarks

In this chapter this DPSM technique has been discussed for both homogeneous and non-homogeneous fluids and its formulation has been discussed to its fullest. The restriction on the size of r_s of source point's equation has been derived to show the effect of transducer frequency to the number of source points. The non-homogenous fluid is explained for three different fluids with two interfaces and to find the source strength of the transducer the formula has been mentioned

The Implementation & Discussions on the results are explained in the next chapter using the DPSM Methodology

CHAPTER FIVE

NUMERICAL RESULTS AND DISCUSSIONS

5.1 General

MATHCAD & MATLAB programs were developed to model the ultrasonic field in fluids. Modeling of ultrasonic field in homogeneous and triple layered non-homogeneous field having two interfaces was done in both steady and transient state where transducer was considered both at normal and at non-normal to the interfaces. Present work includes the modeling of ultrasonic field in both homogeneous and non-homogenous fluid where the transducer was placed at both normal and non-normal incidence. And also the non-homogeneous fluid was made up of three different fluids with two interfaces between them. The numerical results clearly showed that as the distance of the target points was increased from the transducer surface the pressure field started decaying with the increase in distance. Near Field zone and angle of Divergence have also came into effect as the frequency of the transducer increased. Programming codes were generated for different cases for both steady and transient state. Before that some assumptions for both steady and transient state needed to be studied. In all the cases the diameter was assumed to be 0.254 cm. The axis nomenclature for the transducer was assumed shown in **Figure 5.1.** For the precise modeling of the field while using DPSM, discretization of the transducer surface was utmost importance. Discretization routines were developed in both MATHCAD & MATLAB for both source and target points as shown in **Figure 5.2.** This chapter contains the detailed discussion on results for the each case considered

5.2 Basic Assumptions and conventions used for programing codes

The most basic element of the ultrasonic testing is a finite dimension transducer. In all following cases discussed in this chapter the transducer size was assumed to be 0.254cm. Following **Figure 5.1** shows the axis pattern that was considered while modeling ultrasonic field using MATCAD & MATLAB routines.

Transducer Axis Definition:-The three axes that are shown in **Figure 5.1** are used in all cases for modeling field using DPSM technique.

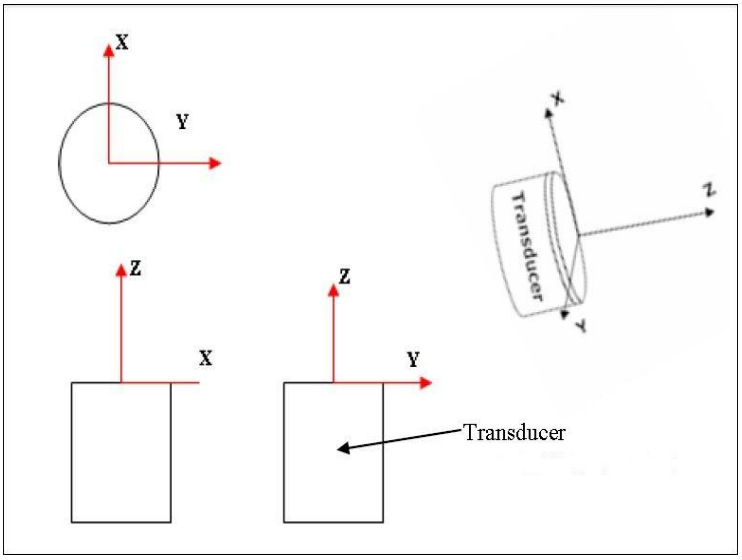

Figure 5.1: Circular Transducer axis definition

Discretization of transducer surface (source points):

To model the field accurately the discretization of the source points was utmost importance. A programming code was developed to discretize the surface of the circular transducer to find out the coordinates of the source point. This has been achieved by making a library function **Dcircle** (with Diameter of the transducer and the radius of the source point) as its arguments. For source point grid the following check (refer to Chapter Four) were placed in every routine of programming before the calculation of the source points.

$$r_s <<< \frac{\lambda}{2\pi}$$

where,

r_s, is radius of single source point

λ, wavelength of propagating wave

The programming routine, **Dcircle,** for the discretization of the transducer surface does its calculation on a step by step process that is explained as follow in the developed program. The source points has been calculated and placed on the transducer surface as shown in **Figure 5.2.**

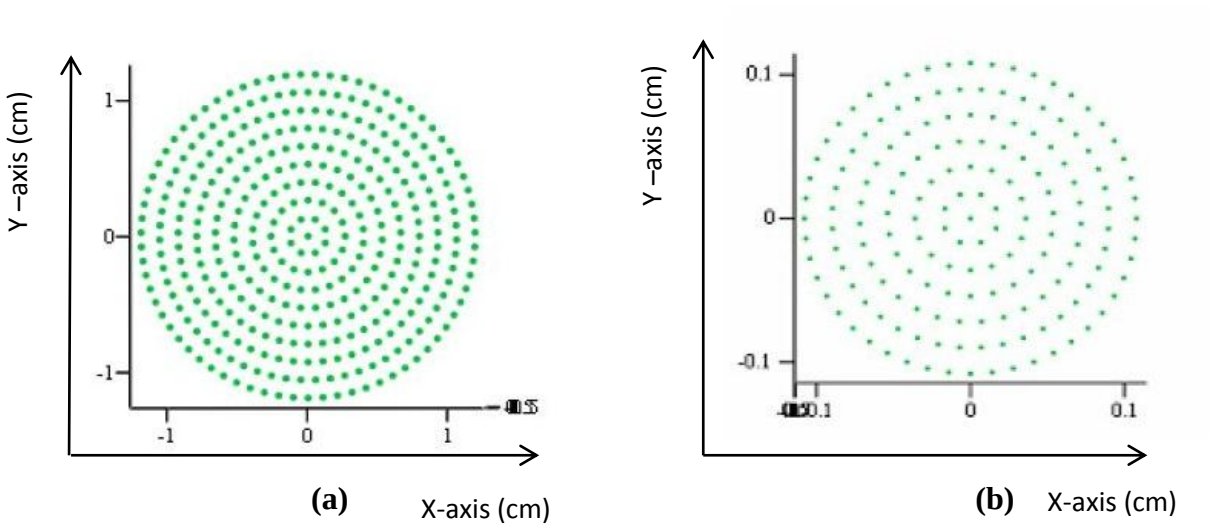

Figure 5.2: Discretized Transducer face of Dia = 0.254cm (a) At Freq=2MHz N = 225 (b) At Freq=1MHz N = 80, where, N = no. of source points

From the above **Figure 5.2** it was concluded that when the radius of the source increases the number of source point decreases to larger extent. Hence the check mentioned above needed to be put in all of the routines because it varies the number of source points and also connects the frequency of the transducer with source point grid.

Discretization for developing target grid point

In order to calculate pressure field in various fluids, number of target points were needed to calculate the ultrasonic field in between the fluid and transducer surface. So, for target point's grid generation the area of interest was divided into number of target points using a developed programme routine. This was done by making a library function **K** (on which plane, no. of points in X-direction, no. of points in Y-direction, minimum value of X, maximum value of X, minimum value of Y, maximum value of Y) as its argument. When the grid mesh was coarse the number of target points was lesser which lead to reduction in calculation and time but accuracy suffered. But when the target grid was finer the number of points increased to the expense of computational time and accuracy. Following plots shows the target grid at different planes, which were used while developing various programming routines. The programming routine, **K,** for the discretization of the target points does its calculation on a step by step process.

The **Figure 5.3** shows the target points made on different planes with points 25*25 in two directions

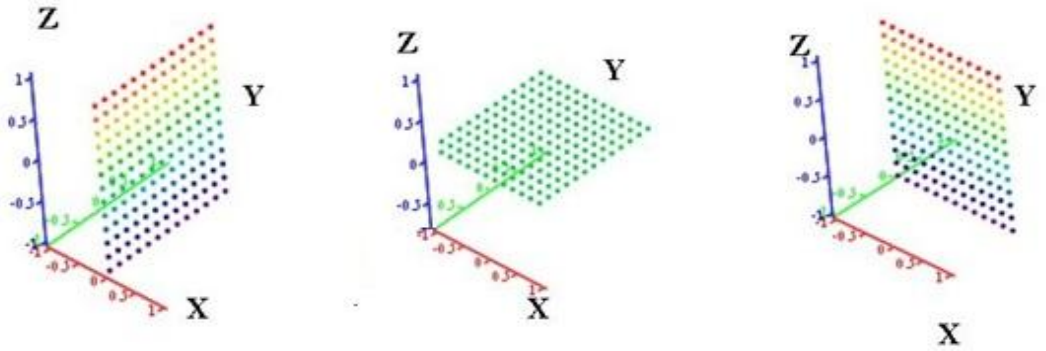

a) YZ Plane **b) XY Plane** **c) XZ Plane**

Figure 5.3: Target Points Discretization in Different Planes

Transient Analysis (Input and Flow Chart)

Fast Fourier Transform (FFT) was used to convert time domain impulse into frequency domain pulse. Then for each frequency, DPSM method was applied and obtained response has been transformed to time domain using Inverse Fourier Transforms (IFFT). Frequencies up to Nyquist frequencies were used for analysis and effect of remaining frequencies were taken care by superimposing anti-symmetry behaviour of the imaginary part about Nyquist Frequency. **Figure 5.4** shows the flowchart for reconstruction of transient wave program in Homogenous fluid using DPSM techniques.

Input Signal used for Transient Analysis;

Input signal that was used throughout the transient analysis was a five cycle tone burst. **Figure 5.5** shows the time distribution of the harmonic function and it's FFT in frequency domain.

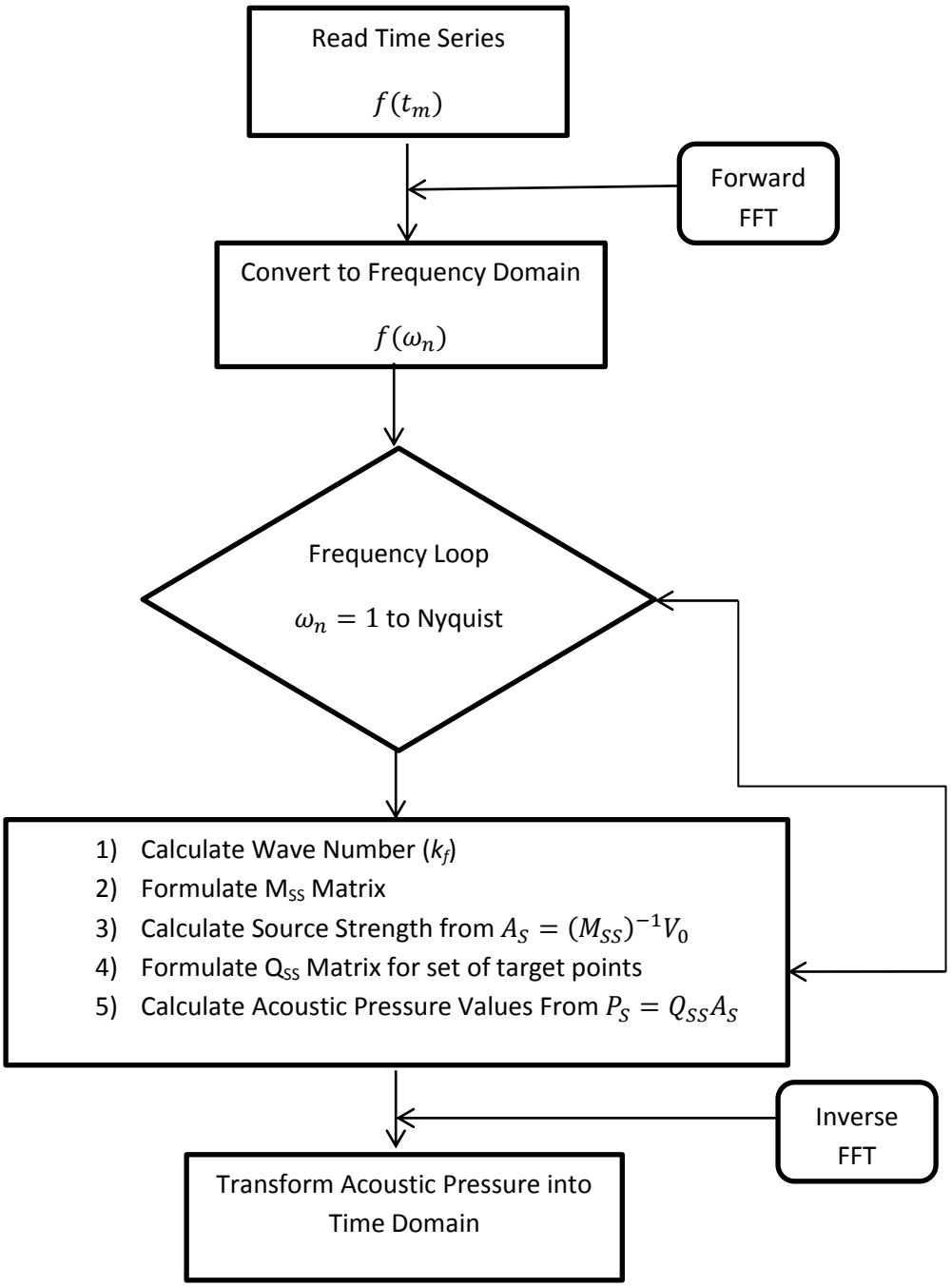

Figure 5.4: Flow Chat for Transient Analysis

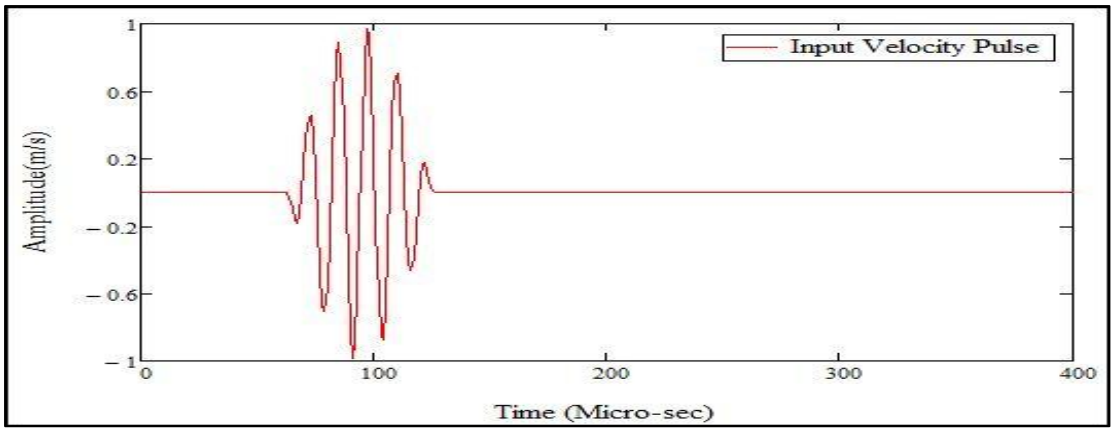

(a)

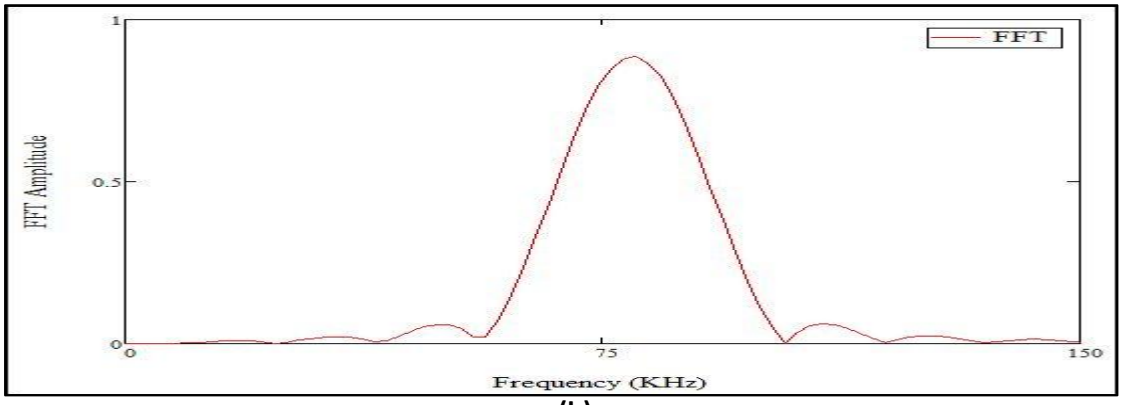

(b)

Figure 5.5: Tone burst Signal as (a) Input and (b) its FFT Signal

Now as all the basic assumptions have been discussed which were used extensively in all the developed routines. In next sections the modeling results will be discussed for each separate cases of fluids.

5.3 Wave Propagation in Homogenous Fluid

5.3.1 Steady wave propagation in Homogenous Fluid:

Following the DPSM technique described in previous chapters, have been implemented to compute the ultrasonic field generated in a homogeneous fluid (water) by a flat circular transducer as shown in **Figure 5.6**, the arrangement has been shown, having transducer at one end with number of source points and homogeneous fluid having number of target points placed at random position. For such simple problem geometry the expression of the near field zone length and the divergence angle of the emitted beam were calculated in closed form [].Numerically computed values (Eq-5.2) of these two parameters have been compared with the closed form analytical values to check the accuracy of the numerical results. From [].

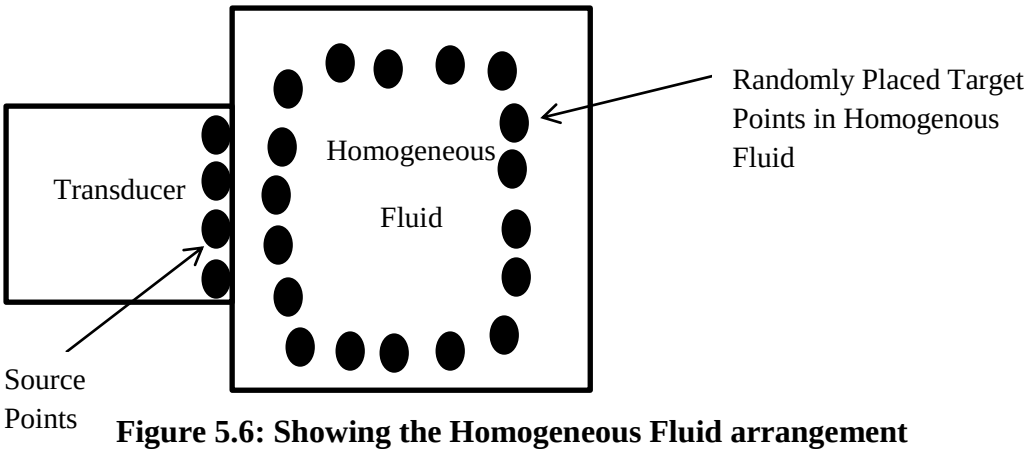

Figure 5.6: Showing the Homogeneous Fluid arrangement

$$N_f = \frac{D^2-\lambda^2}{4\lambda} \approx \frac{D^2}{4\lambda} \quad \text{for } \lambda << D \qquad \text{Eq-5.1}$$

where, N_f is the near field length. It has been explained in Chapter one .The analytical expression of the pressure in a homogeneous fluid along the central axis of a circular transducer is [].

$$p(x_3) = \rho c_f v_0 \left[\exp\left(ik_f x_3\right) - \exp\left(ik_f\sqrt{x_3^2 + a^2}\right)\right] \qquad \text{Eq-5.2}$$

where, c_f is the wave speed, ρ is the fluid density, $v_0$is the transducer velocity, x_3 is the transducer axis, a is the area of the transducer, k_f is the wave number & *r* is the distance of the point source.

Figure 5.7 and **Figure 5.8** showed acoustic pressure variations for the DPSM model using 133 point sources (1 MHz and 5 MHz signal frequencies) and 348 point sources (1 MHz and 5 MHz signal frequencies) along the central axis (Z axis) of a circular transducer computed by the DPSM technique described above and the analytical expression Eq-5.2. Coordinate Z was measured from the transducer face. The transducer area is 5.02mm^2, its diameter (D) = 2.54 mm. For example DPSM modeling for 356 sources was made by locating all of them at Z= - rs, while the transducer face was at Z = 0. For this problem geometry the point source, transducer surface distance has been calculated as

$$r_s = \sqrt{\frac{\pi D^2}{4\times 2\pi N}} = \frac{D}{\sqrt{8N}} = \frac{2.54}{\sqrt{8\times 348}} = 0.048139mm \qquad \text{Eq-5.3}$$

It has been calculated in Eq-5.3 that the radius of the point source is 0.048139mm for 348 number of source points.

Figure 5.7 showed that for 133 point sources DPSM curve is closely moving above the EXACT curve but there is no well match with it. **Figure 5.8** shows that with 348 point sources DPSM result match well with exact solution. Hence it was concluded that as the number of point sources increases accuracy of DPSM increases. As the waves speed in the surrounding fluid is 1.49 km/sec, wave length is equal to 0.298 mm for 5 MHz signal. From Eq.5.1 N_f is found to be 5.3mm that matched with last peak obtained numerically as shown in **Figure 5.8.**

Similar results were calculated for other fluids such as for glycerine (ρ = 1.26, c_f =1.92km/sec) and mobil oil (ρ = 0.87, c_f =1.72km/sec). And their solutions have been shown in **Figure 5.8 to Figure 5.12** respectively. The variation in the Near field can be seen varying because the wave speed is different in both glycerine and mobil oil (Eq-5.1)

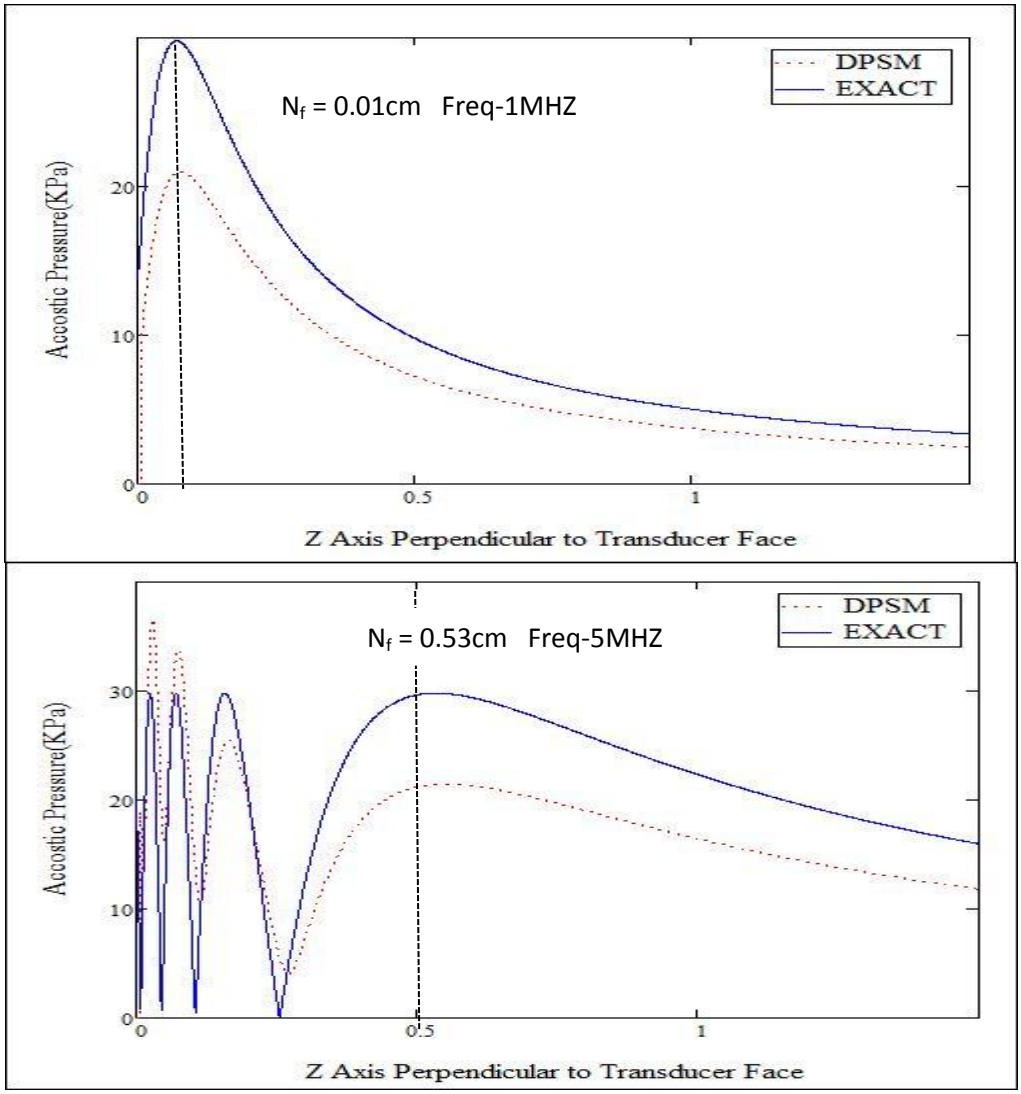

Figure 5.7: : Acoustic Pressure Variation for 133 source points along Z-axis perpendicular to Transducer Face in Case of Water with Freq-1MHz & 5 MHz

In the **Figure 5.8,** the two frequencies 1 & 5 MHz are shown with 133 source points and the variations in the length of Near Field. In 1 MHz the Near Field is very close to the transducer surface and in 5 MHz it has been shifted up to 0.53cm as calculated theoretically. These plots are following the Near Field formula Eq-5.1 as the frequency of the transducer face is increasing the Near Field length is also increasing.

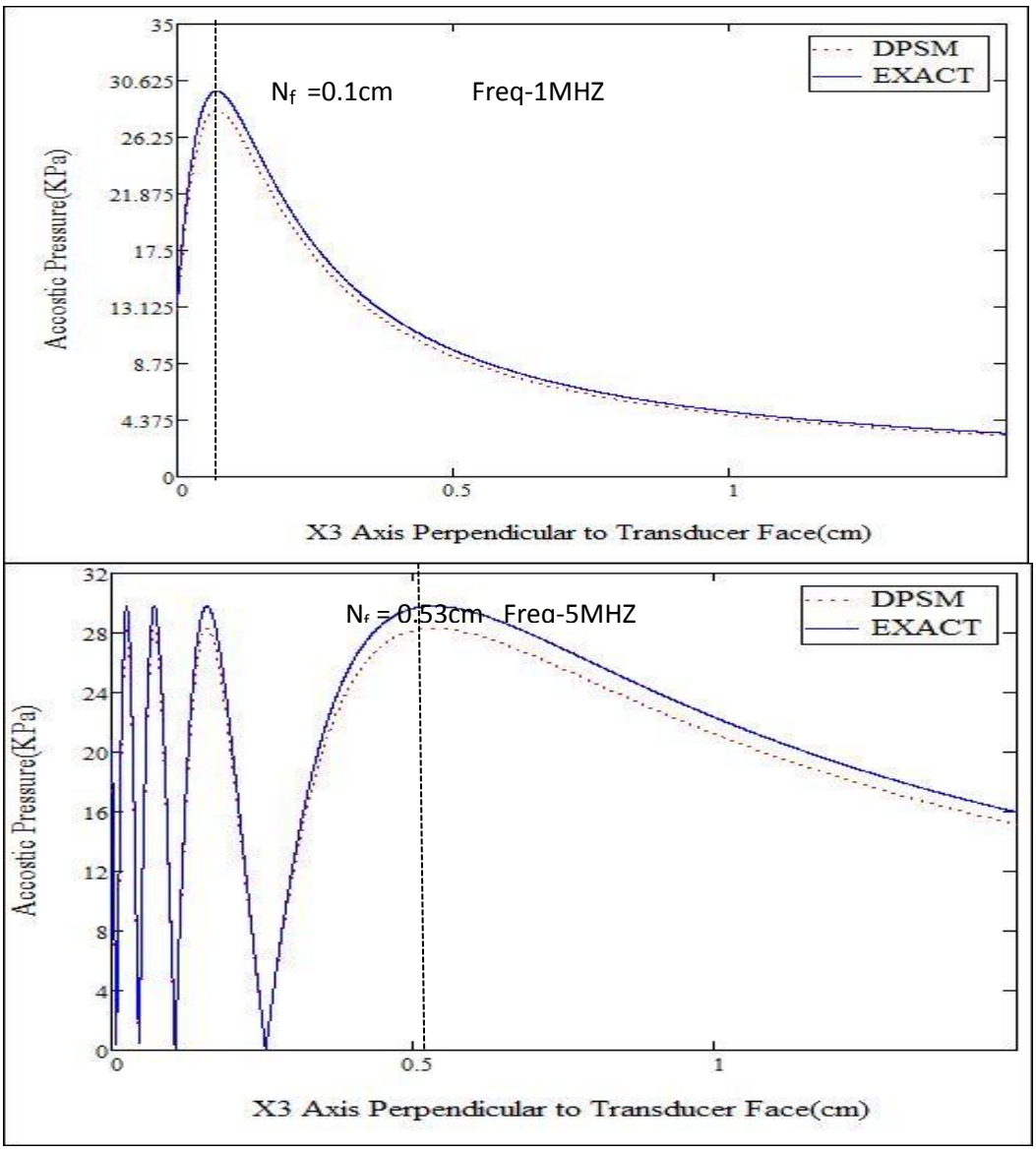

Figure 5.8: : Acoustic Pressure Variation for 348 source points along Z-axis perpendicular to Transducer Face in Case of Water with Freq-1MHz & 5 MHz

The **Figure 5.8,** the two frequencies 1 & 5 MHz are shown with 348 source points and the variations in the length of Near Field. In 1 MHz the Near Field is very close to the transducer surface 0.1cm as calculated and in 5 MHz it has been shifted up to 0.53cm as calculated theoretically. These plots are following the Near Field formula Eq-5.1 as the frequency of the

transducer face is increasing the Near Field length is also increasing. The source points are more and the DPSM curve is following Exact solution curve.

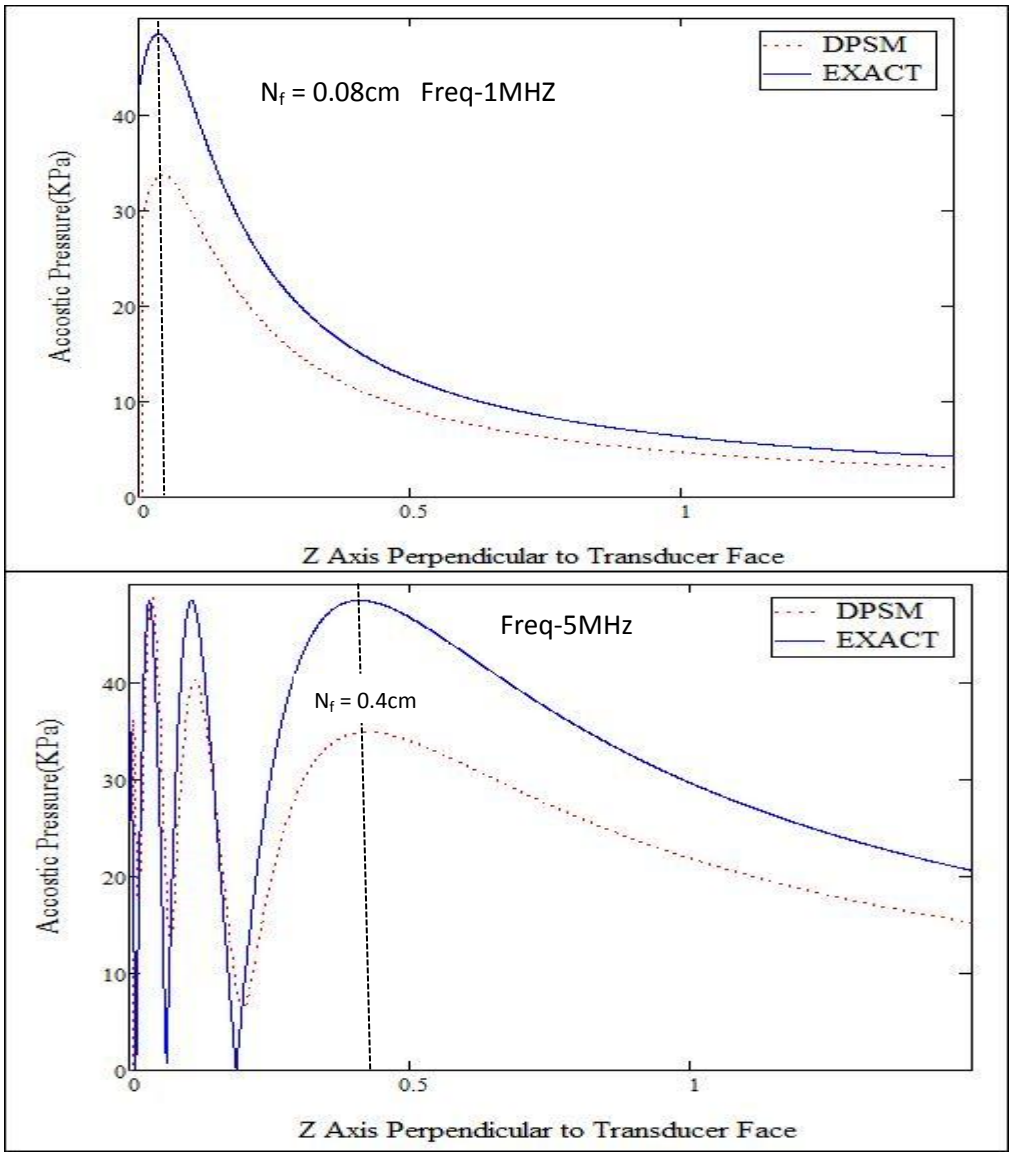

Figure 5.9: Acoustic Pressure Variation for 133 source points along Z-axis perpendicular to Transducer Face in Case of Glycerine with Freq-1MHz & 5 MHz

The **Figure 5.9,** the two frequencies 1 & 5 MHz are shown with 133 source points and the variations in the length of Near Field. In 1 MHz the Near Field is very close to the transducer surface 0.08cm as calculated and in 5 MHz it has been shifted up to 0.4cm as calculated theoretically. These plots are following the Near Field formula Eq-5.1 as the frequency of the transducer is increasing the Near Field length is also increasing.

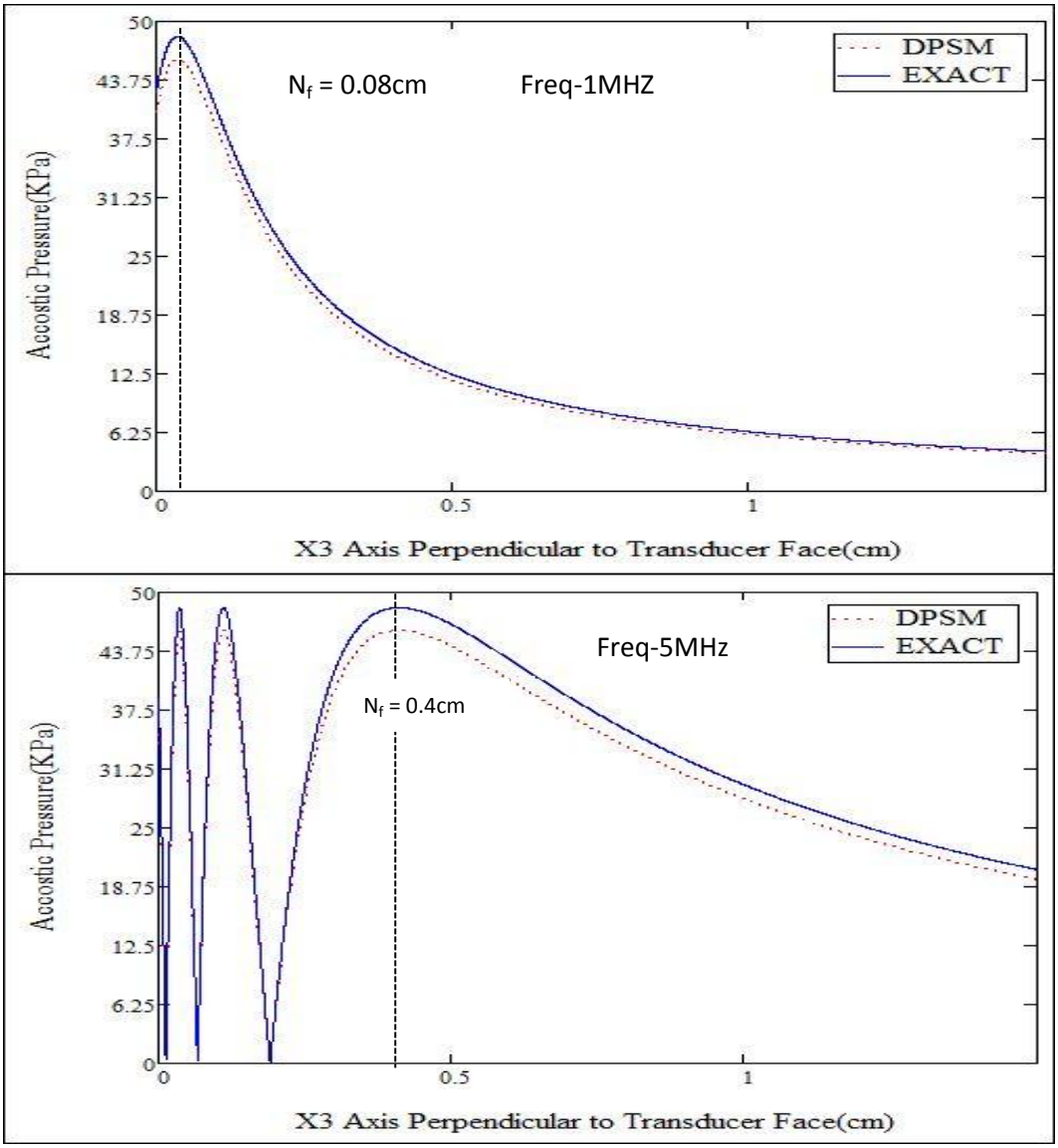

Figure 5.10: Acoustic Pressure Variation for 348 source points along Z-axis perpendicular to Transducer Face in Case of Glycerine with Freq-1MHz & 5 MHz

The **Figure 5.10,** the two frequencies 1 & 5 MHz are shown with 348 source points and the variations in the length of Near Field. In 1 MHz the Near Field is very close to the transducer surface 0.08cm as calculated and in 5 MHz it has been shifted up to 0.4cm as calculated theoretically. These plots are following the Near Field formula Eq-5.1 as the frequency of the transducer is increasing the Near Field length is also increasing.

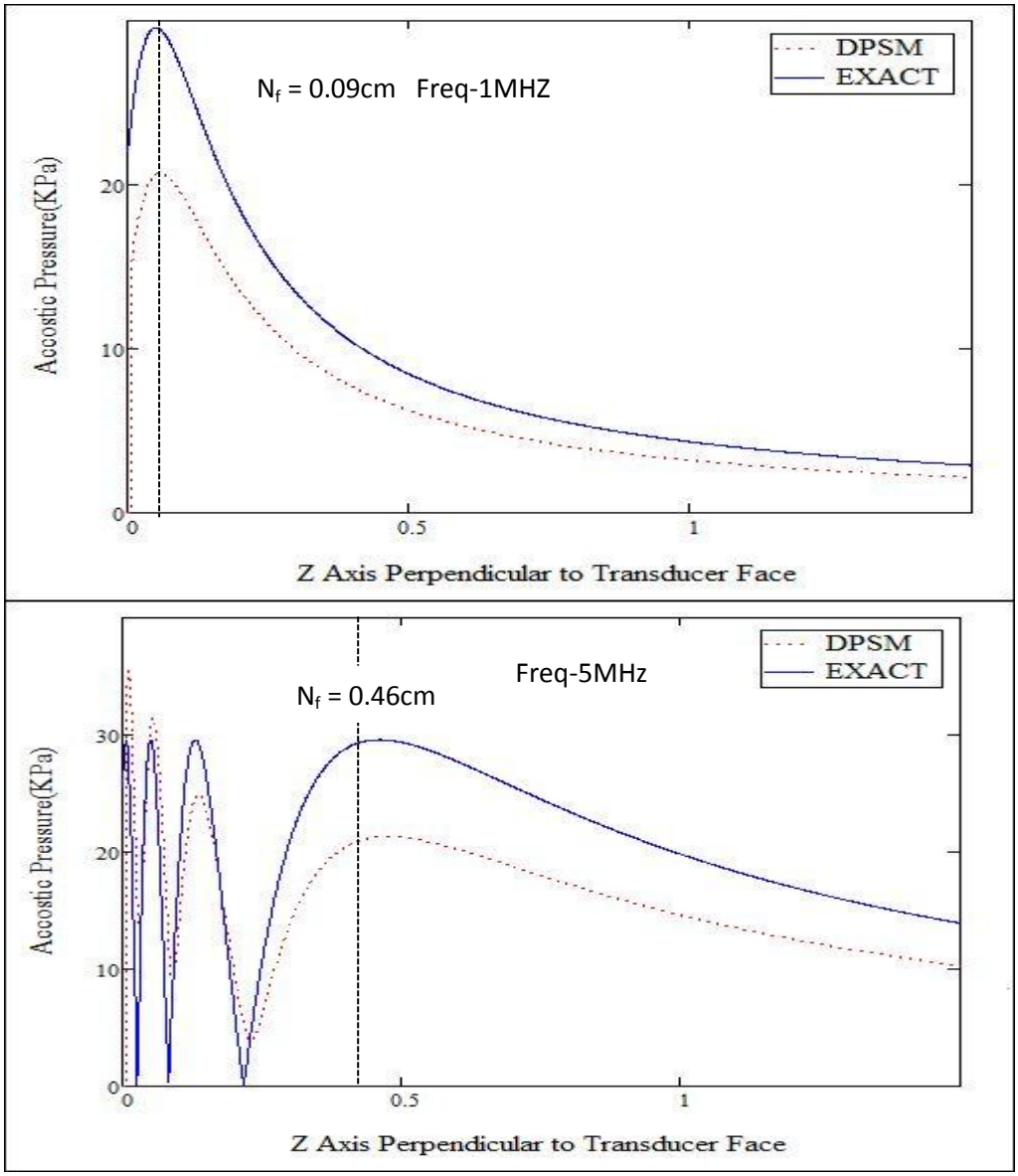

Figure 5.11: Acoustic Pressure Variation for 133 source points along Z-axis perpendicular to Transducer Face in Case of Mobil Oil with Freq-1MHz & 5 MHz

The **Figure 5.11,** the two frequencies 1 & 5 MHz are shown with 133 source points and the variations in the length of Near Field. In 1 MHz the Near Field is very close to the transducer surface 0.09cm as calculated and in 5 MHz it has been shifted up to 0.46cm as calculated theoretically. These plots are following the Near Field formula Eq-5.1 as the frequency of the transducer is increasing the Near Field length is also increasing.

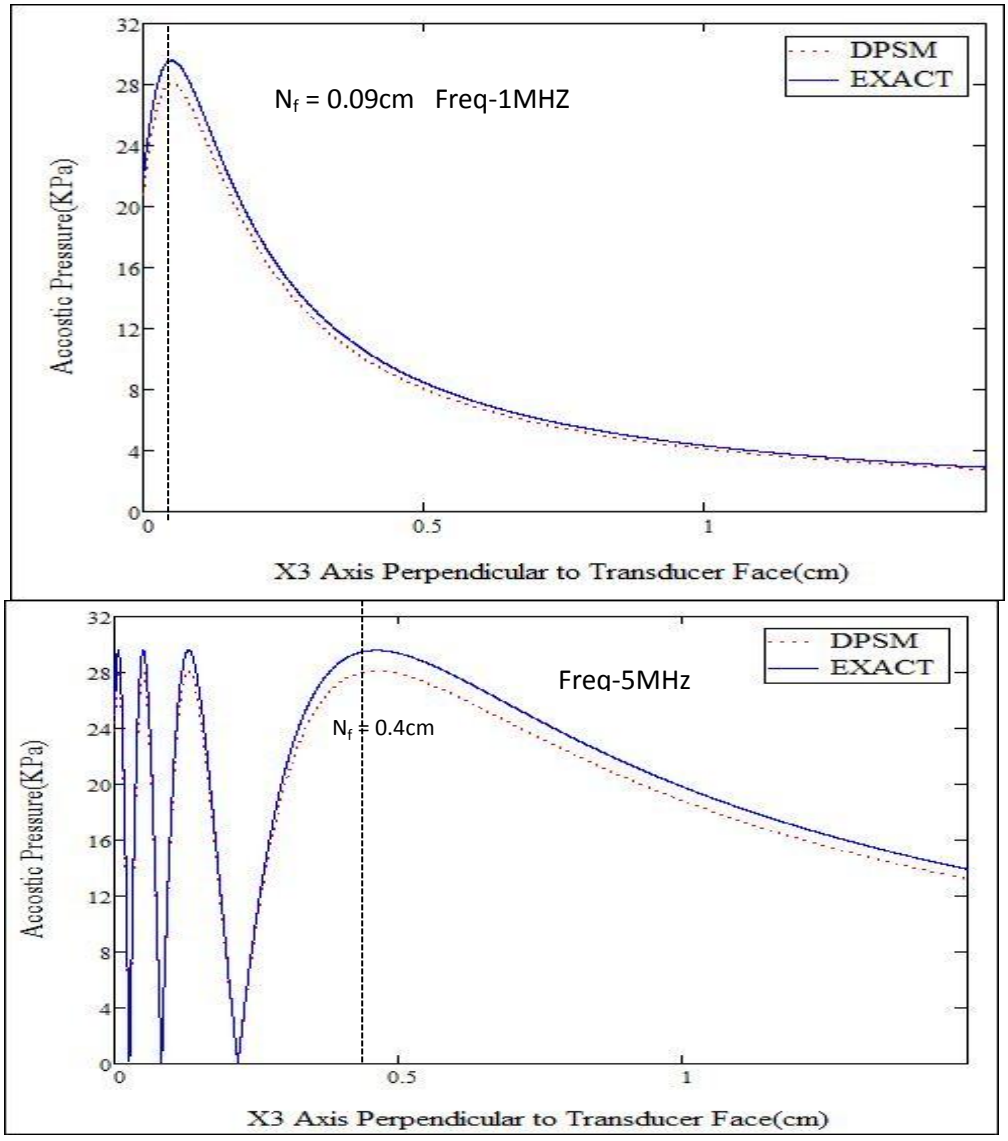

Figure 5.12: Acoustic Pressure Variation for 348 source points along Z-axis perpendicular to Transducer Face in Case of Mobil Oil with Freq-1MHz & 5 MHz

The **Figure 5.12,** the two frequencies 1 & 5 MHz are shown with 348 source points and the variations in the length of Near Field. In 1 MHz the Near Field is very close to the transducer surface 0.09cm as calculated and in 5 MHz it has been shifted up to 0.46cm as calculated theoretically. These plots are following the Near Field formula Eq-5.1 as the frequency of the transducer is increasing the Near Field length is also increasing.

After considering all of the above cases, it was observed that when the fluid properties were changed so did the Near Field length changed. In water, Glycerine & Mobil Oil fluids all have different Near Field Zone as calculated also.

5.3.1.1 Ultrasonic Pressure Variation in Homogeneous Fluid by Varying the Diameter of the Transducer: In this case the value of the diameter used for modeling of transducer surface was varied and the output was observed and the transducer was kept normal. And the plots were formed with the help of Eq-4.31 & Eq-4.32 where on target point grid, the pressure was calculated on every single point and that pressure variation was seen in both the plots, surface & contour plots.

(a) For Transducer Diameter = 0.254cm homogeneous fluid (water) was used with 1 MHz Frequency

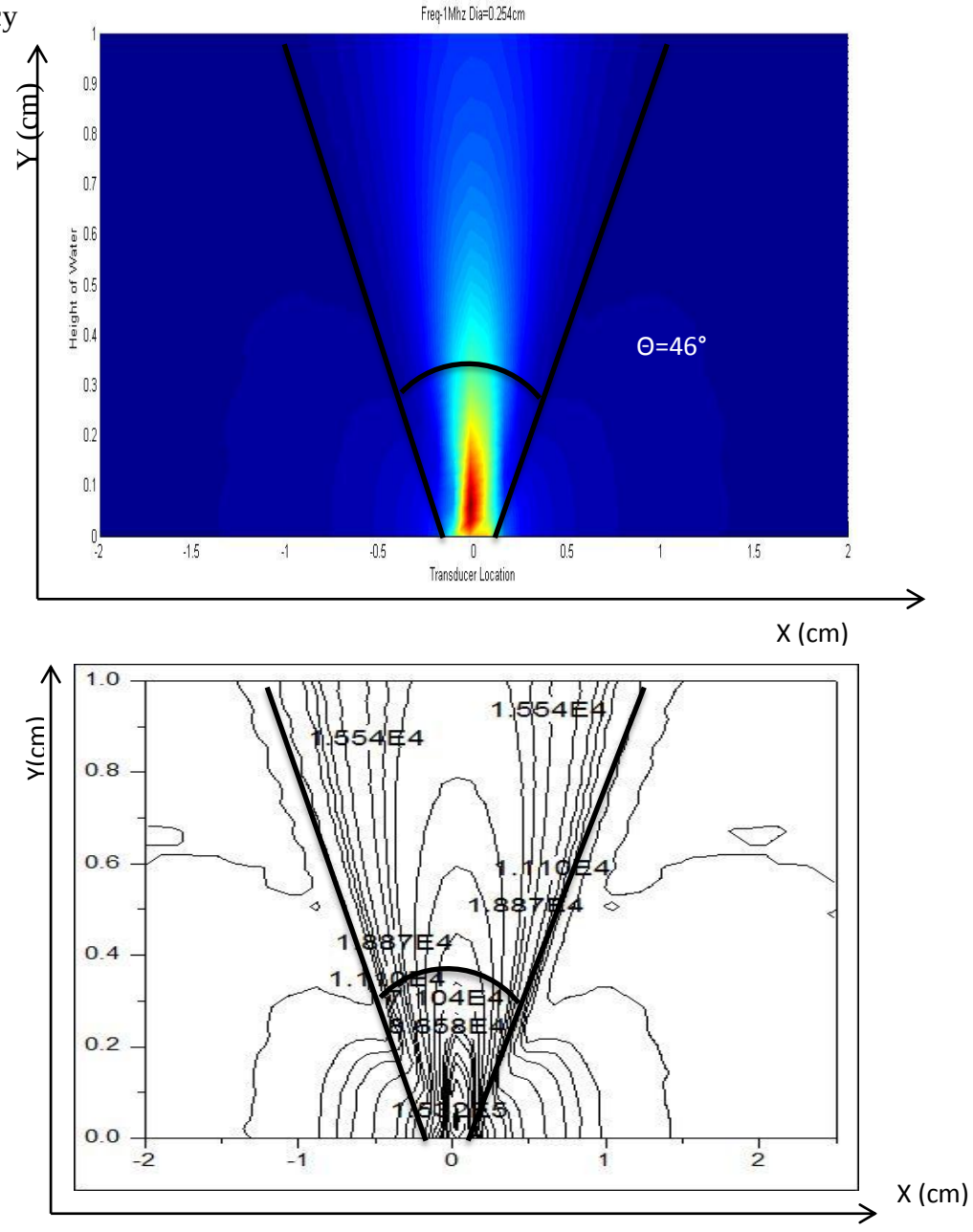

Figure 5.13: Pressure variation for 1 MHz Freq for Dia= 0.254cm

In the **Figure 5.13**, the plot is drawn with the diameter of the transducer as 0.254cm and in the contour plot the beam spread and angle of divergence is shown. The angle of divergence, which is half the value of beam spread, is calculated using the Eq-1.2, comes out to be 44.74° and it matched the measured angle. The pressure values at different locations have been shown by labelling them on the plots. The pressure is maximum at the bottom near the transducer face and keeps on decreasing as it has been moving from the transducer face. And also there is no Near Field Zone in this frequency and size of the transducer.

(b) For Transducer Diameter 0.508cm water was considered with same frequency of 1MHz but with increase in diameter of the transducer

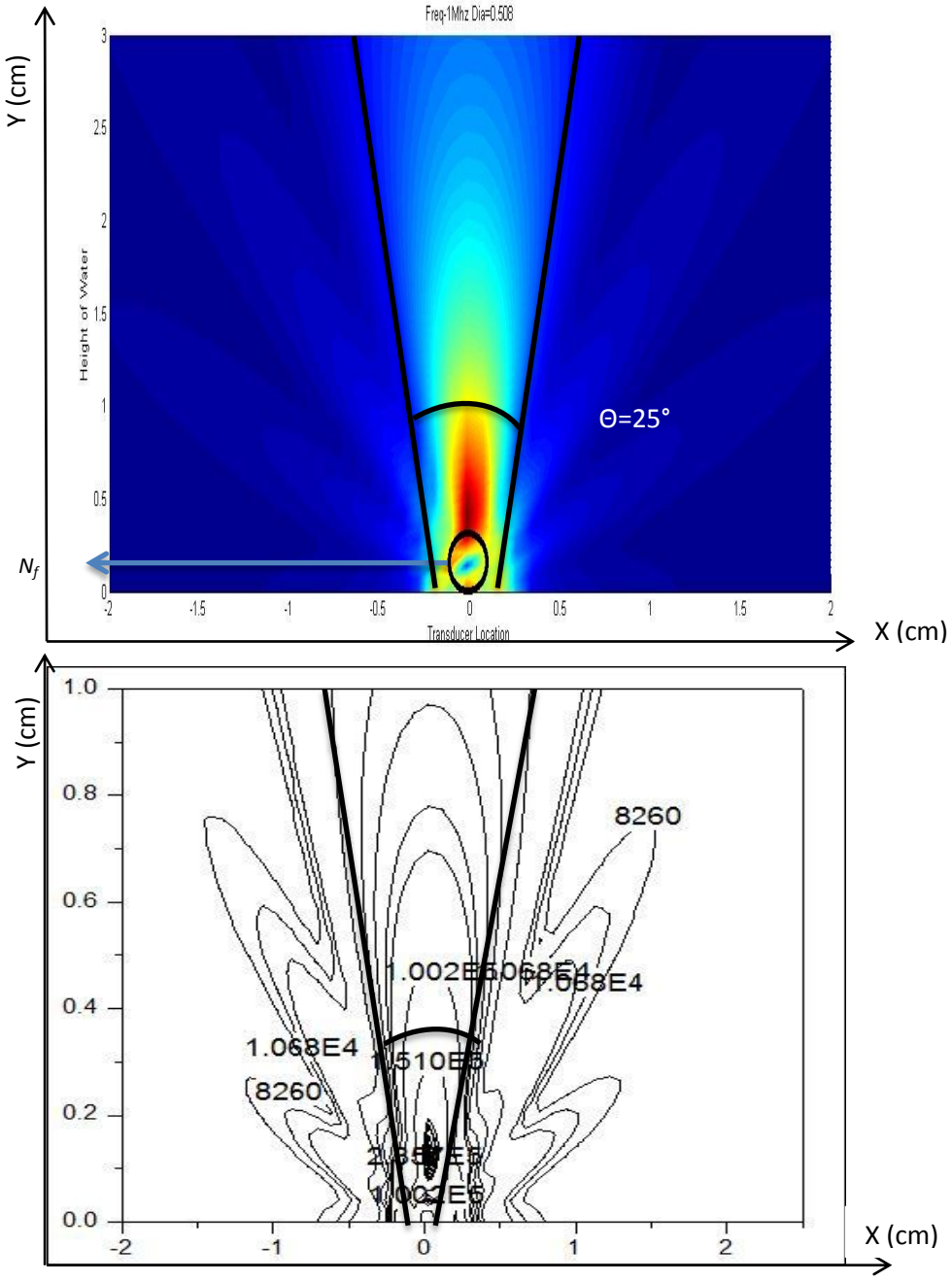

Figure 5.14: Pressure variation for 1 MHz Freq for Dia= 0.508cm

In the **Figure 5.14**, the plot is drawn with the diameter of the transducer as 0.508cm and in the contour plot the beam spread and angle of divergence is shown. The angle of the beam, calculated using the Eq-1.2, comes out to be 20.60° and it matched the calculated and it matched the measured angle. The pressure values at different locations have been shown by labelling them on the plots. The pressure is maximum at the bottom near the transducer face and keeps on decreasing as it has been moving from the transducer face. And it can be seen that there have been Near Field Zone appeared in this frequency and size of the transducer.

(c) For Transducer Diameter = 0.762cm water was considered with same frequency of 1MHz but with increase in diameter of the transducer

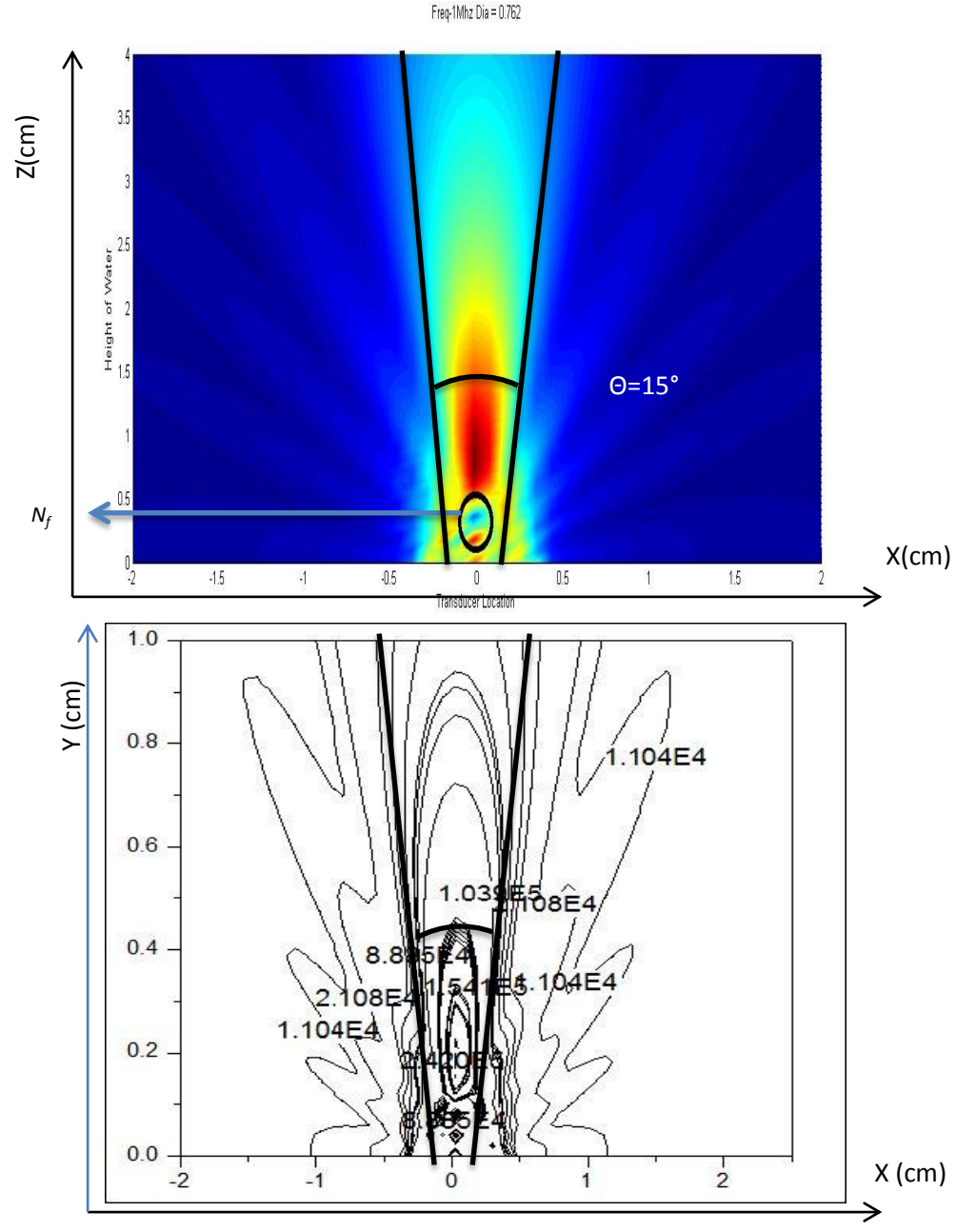

Figure 5.15: Pressure variations for 1 MHz Freq for Dia= 0.762cm

In the **Figure 5.15**, the plot is drawn with the diameter of the transducer as 0.762cm and in the contour plot the beam spread and angle of divergence is shown. The angle of the beam, calculated using the Eq-1.2, comes out to be 13.57° and it matched the measured angle. The pressure values at different locations have been shown by labelling them on the plots. The pressure is maximum at the bottom near the transducer face and keeps on decreasing as it has been moving from the transducer face. And it can be seen that there have been Near Field Zone appeared in this frequency and also it is at a distance as compared to the previous case of size of the transducer.

It has been seen from the **Figure 5.13 , 5.14, 5.15,** as the value of the diameter of the transducer is increased, the ultrasonic pressure variation keep on focusing. In the first case the diameter was 0.254cm the pressure across the fluid was diverging. But as the diameter of the transducer was increased the pressure started to collimate, because of increase in the number of source points as the diameter was increased. After that there was changes in the angle of divergance as the diameter was increasing the angle of divengence was also decreasing. Also as the diameter was increased the Near field Zone started to appear in the output. As discussed in the previous section the Near field Zone will increase in its Field length as stated in the Eq-5.1. And the diameter of the transducer was increased further to 0.762cm, the Near field Zone length had also increased. So it was following the Eq-5.1. The ultrasonic pressure variation was collimated when diameter was 0.762cm, can be seen in the **Figure 5.16.**

5.3.1.2 Ultrasonic Pressure Variation in Homogeneous Fluid by Varying the Frequency of the Transducer: In this case the value of the frequency used for modeling of transducer surface was varied and the output was observed and the transducer was kept at normal. Similarly the pressure was calculated on every point of the target point grid and was shown in the contour and surface plots. The process has been shown on the next page.

(a) For 1MHz Frequency of the Transducer homogeneous fluid (water) was used for 1MHz Frequency

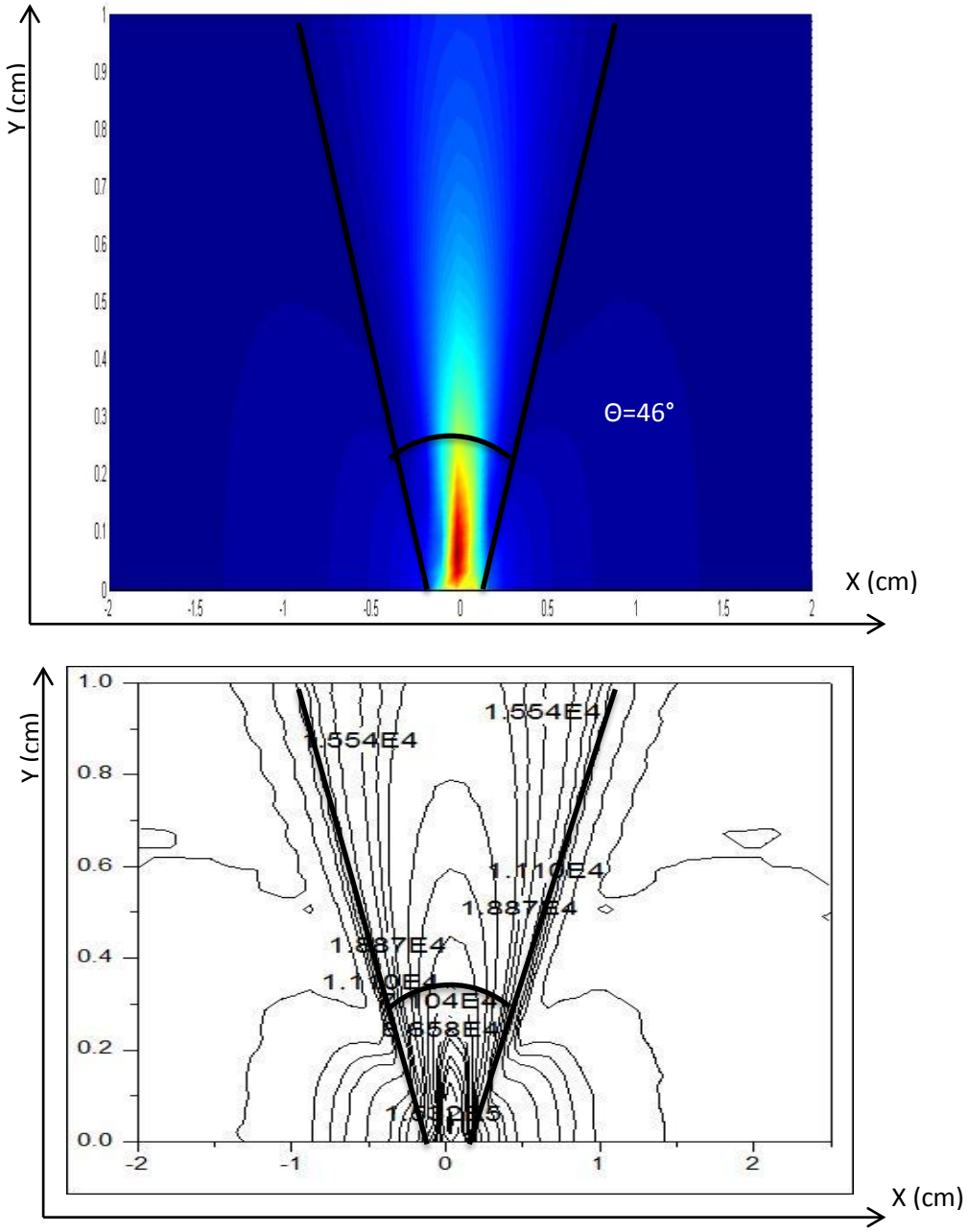

Figure 5.16: Pressure variation for 1 MHz Freq

In the **Figure 5.16**, the plot is drawn with the frequency of the transducer as 1MHz and in the. The angle of divergence, calculated using the Eq-1.2, comes out to be 44.74° and it matched the measured angle. The pressure values at different locations have been shown by labelling them on the plots. The pressure is maximum at the bottom near the transducer face and keeps on decreasing as it has been moving from the transducer face. And it can be seen that there have been no Near Field Zone in this frequency.

(b) For 2.25 MHz Frequency of the Transducer homogeneous fluid (water) was used for 2.25 MHz Frequency

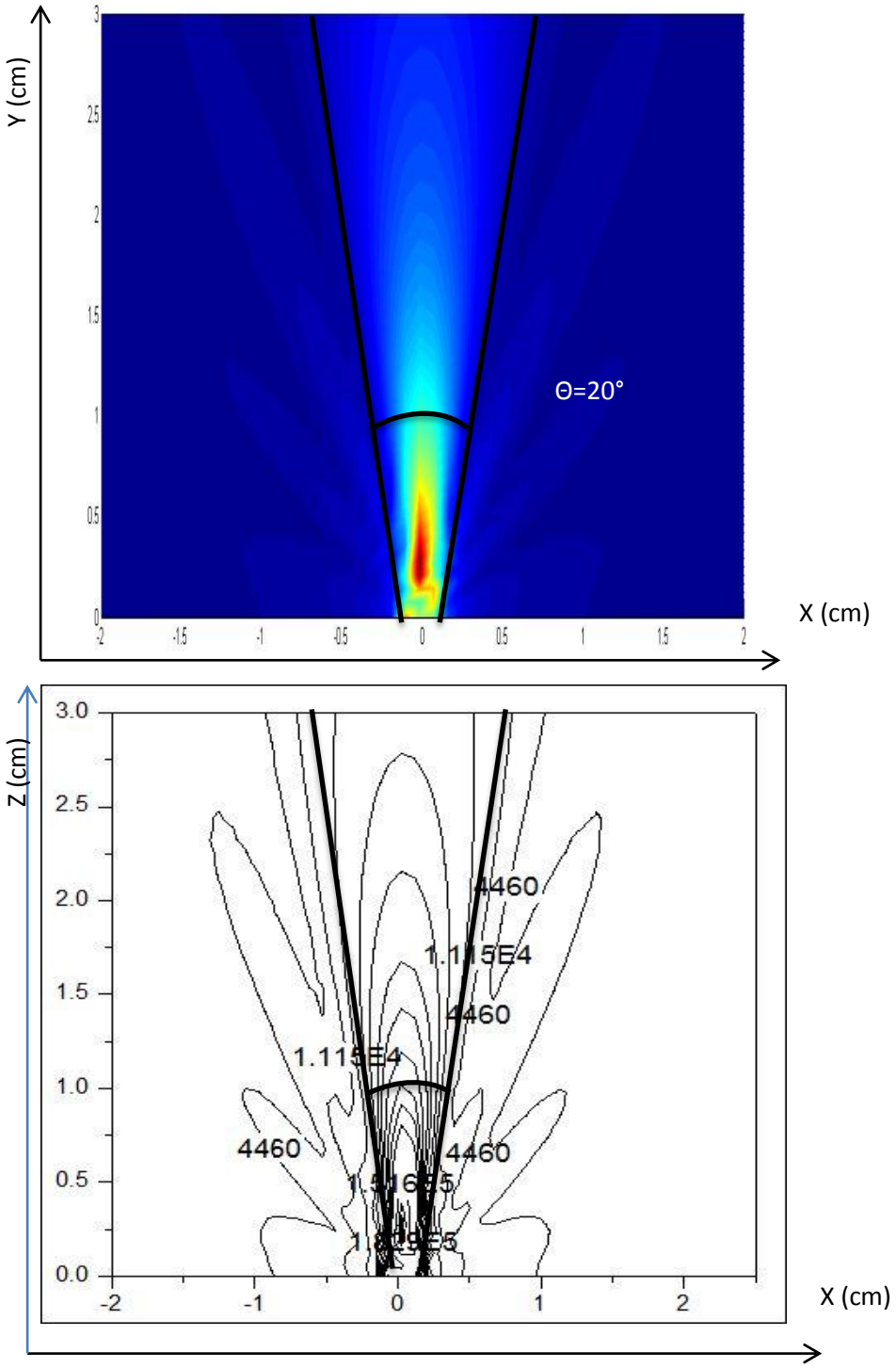

Figure 5.17: Pressure variations for 2.25 MHz Freq

In the **Figure 5.17**, the plot is drawn with the frequency of the transducer as 2.25 MHz and in the. The angle of divergence, calculated using the Eq-1.2, comes out to be 18.74° and it matched the measured angle. The pressure values at different locations have been shown by labelling them on the plots. The pressure is maximum at the bottom near the transducer face and keeps on decreasing as it has been moving from the transducer face. And it can be seen that there has appeared a Near Field Zone in this frequency. Angle of divergence had started to decrease as the frequency was increased.

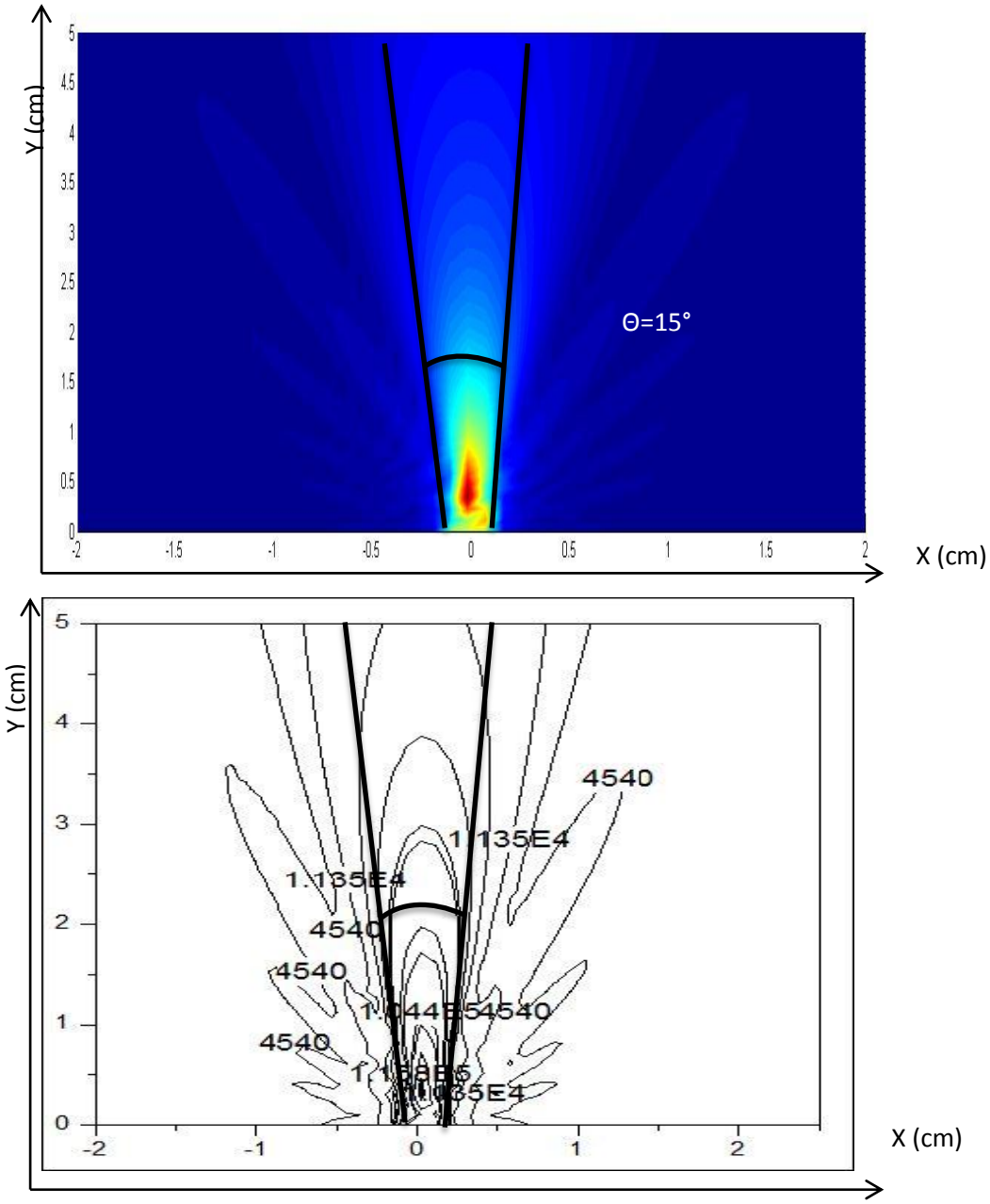

Figure 5.18: Pressure variations for 3.5 MHz Freq

In the **Figure 5.18**, the plot is drawn with the frequency of the transducer as 3.5 MHz The angle of divergence, calculated using the Eq-1.2, comes out to be 12.52° and it matched the

measured angle. The pressure values at different locations have been shown by labelling them on the plots. The pressure is maximum at the bottom near the transducer face and keeps on decreasing as it has been moving from the transducer face. And it can be seen that there has appeared a Near Field Zone in this frequency also. Angle of divergence had started to decrease as the frequency was increased.

So, it was concluded that by varying the diameter of the transducer, the angle of divergence was controlled. And it was also controlled by varying the transducer frequency as both the previous cases shown in the plots and sections.

5.3.1.3 Transducer Inclined at Non-Normal incidence: In the previous section the transducer has been placed at normal angle of incidence and the transducer can be kept at location other than normal. So the transducer is placed at non normal angles to check if there is any variation in the Near field Zone & angle of divergence While modeling field of an inclined transducer in homogenous fluid the point of strike and the initial velocity of transducer changed. The transducer was inclined by multiplying the rotation matrix about Y-axis and the coordinates of the source points on the transducer's face. As discussed in the previous chapter, it is clear that for considering the M_{SS} matrix was modified **Figure 5.19** showed the results for the same in steady state. These results were evaluated at different angle of incidences and frequencies. It was seen that when the frequency increased the scattering of wave decreased and the wave behaved as if the whole energy was concentrated in middle core.

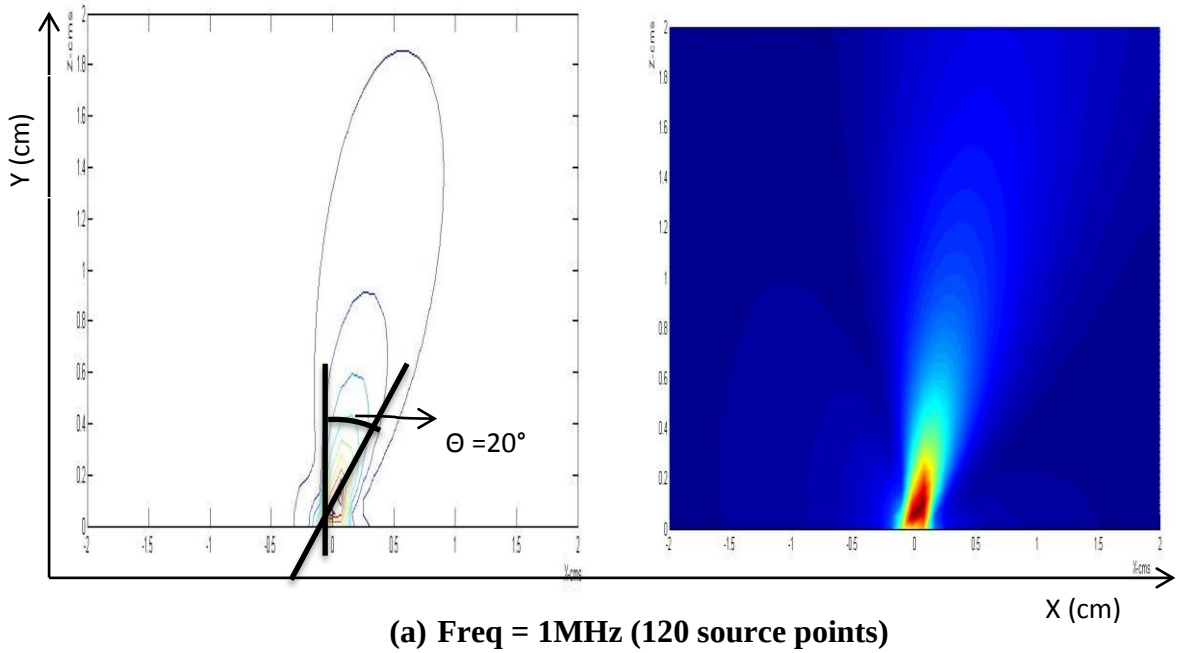

(a) Freq = 1MHz (120 source points)

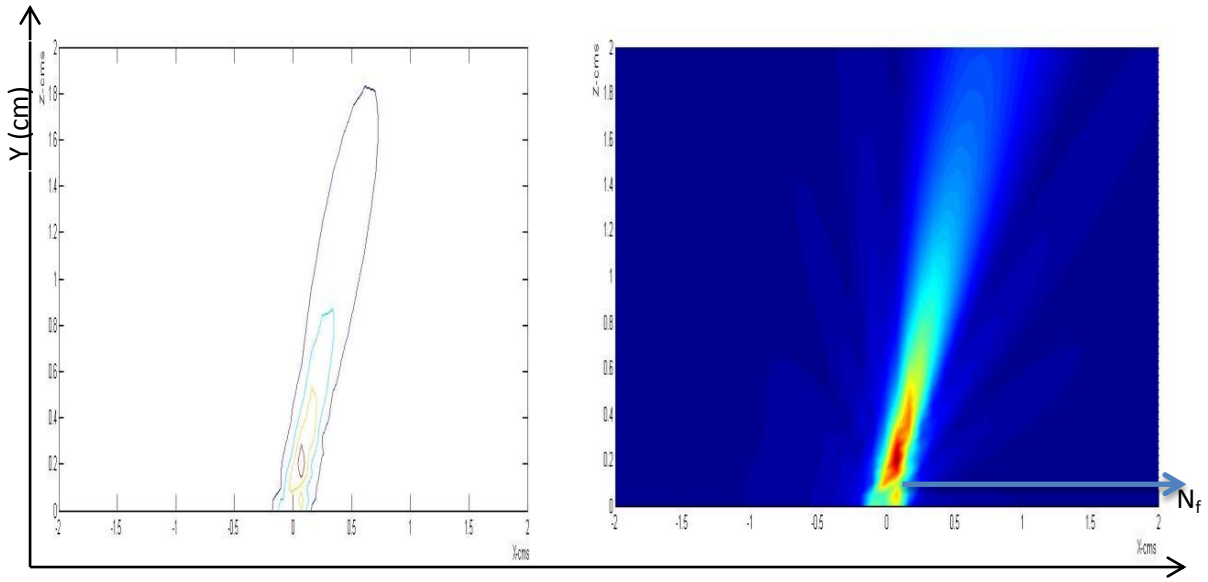

(b) Freq = 2.25MHz (286 Source points)

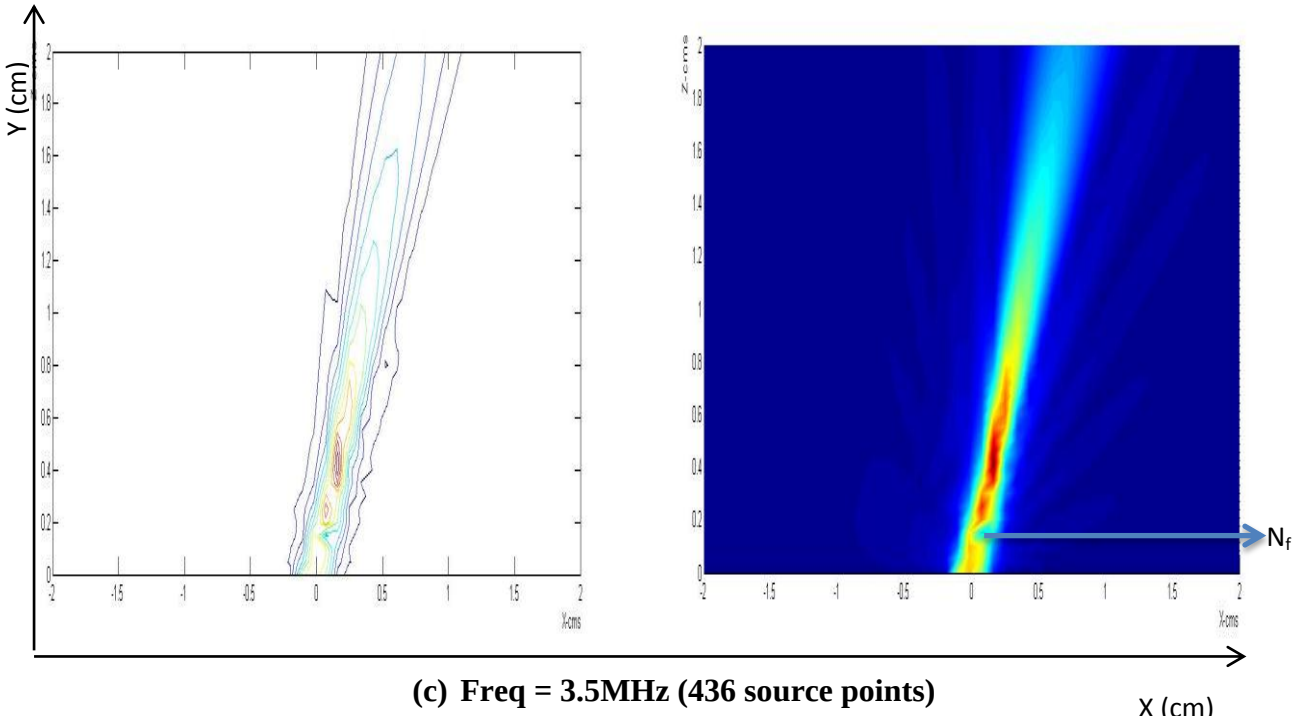

(c) Freq = 3.5MHz (436 source points)

Figure 5.19: Pressure Plots of Homogeneous Fluid at 20 Degree

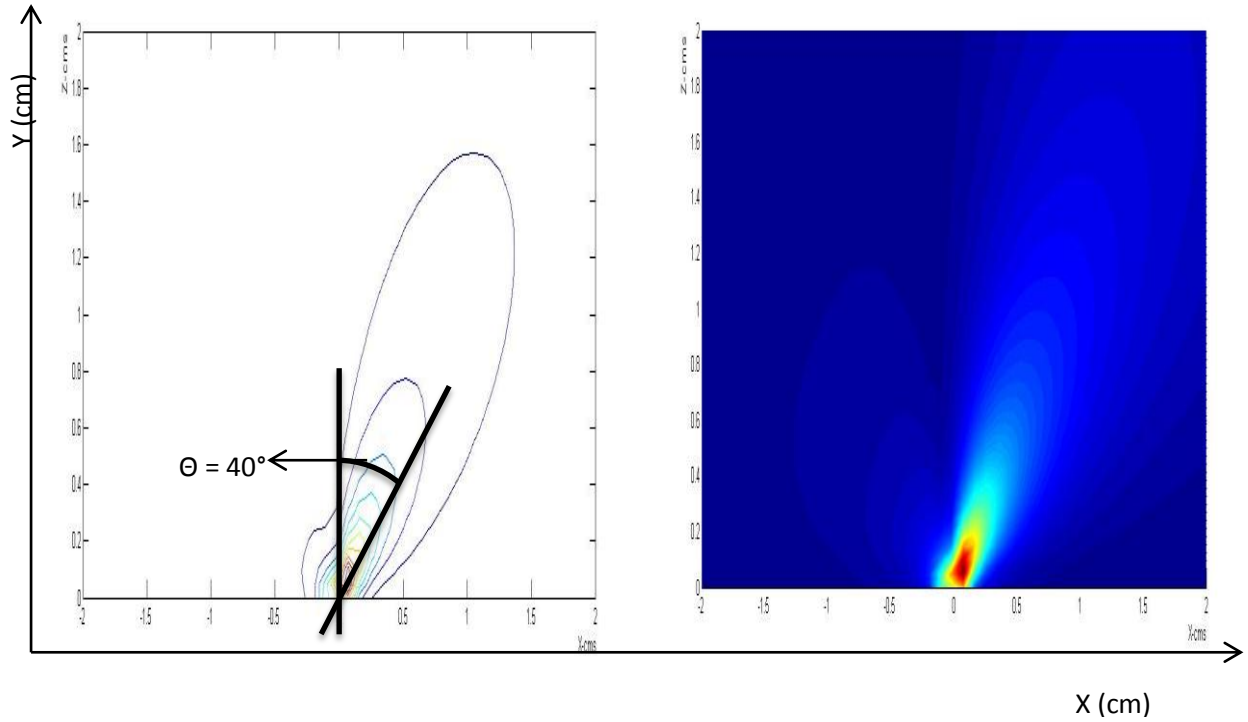

(a) Freq = 1MHz (120 Source points)

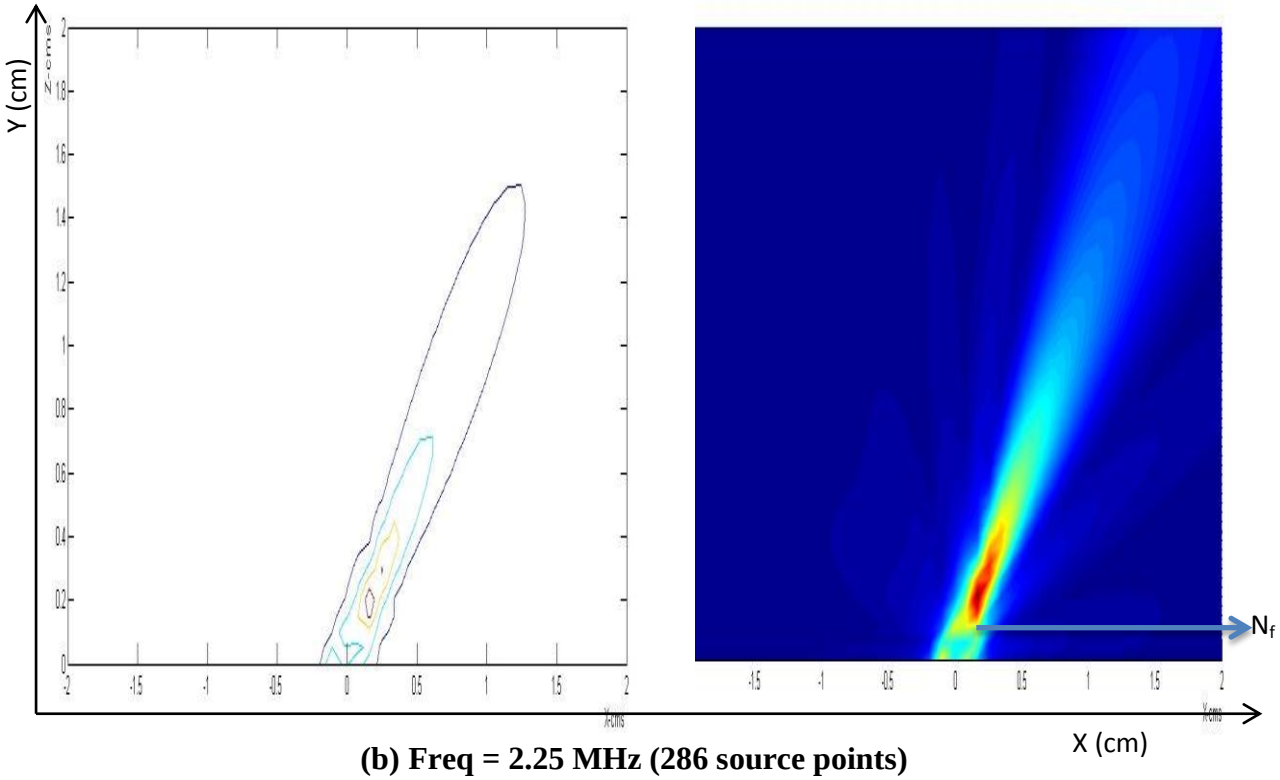

(b) Freq = 2.25 MHz (286 source points)

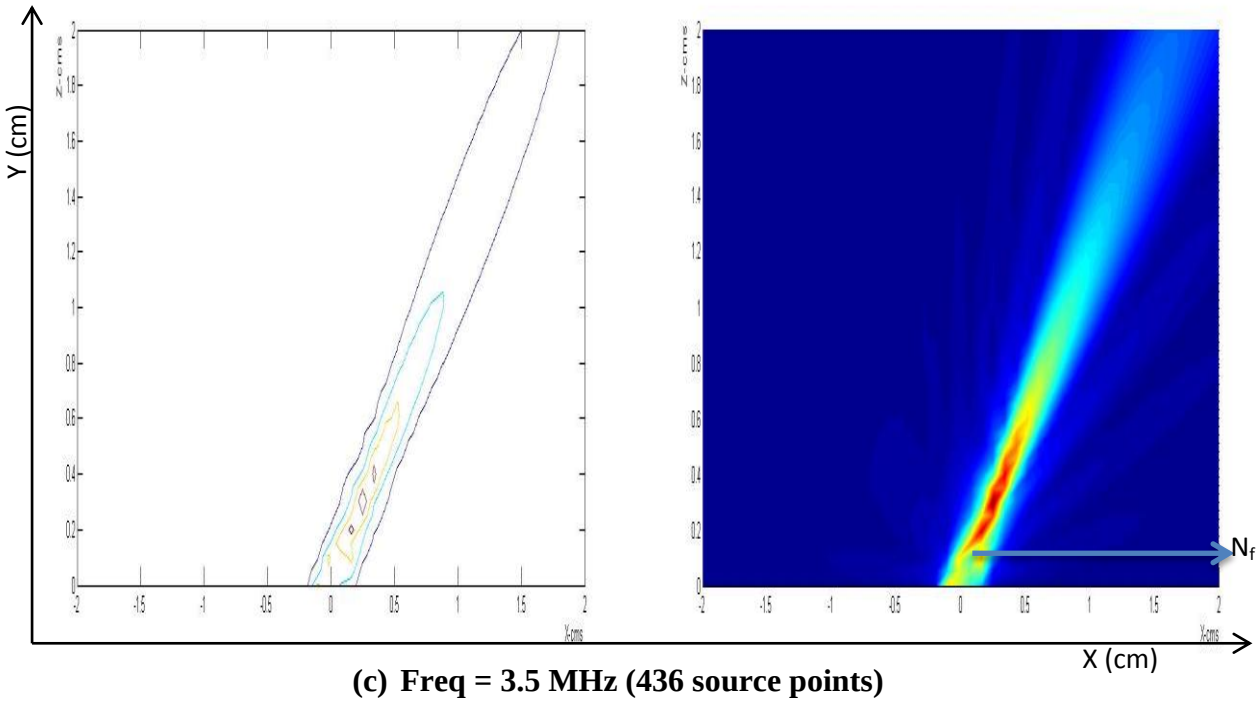

(c) Freq = 3.5 MHz (436 source points)

Figure 5.20: Pressure Plots of Homogeneous Fluid at 40 Degree

From the above shown **Figure 5.19** & **Figure 5.20** the ultasonic field were found on two different angles as given 20° & 40°, and it was concluded that transducer was placed at non-normal incidence the effect of divergance & Near Field was found & the same as was concluded in the case of transducer at normal incidence.

5.3.2 Transient Wave Propagation in Homogenous Fluid

Same steady state model was used to predict transient wave propagation in homogeneous fluid. Fast Fourier transform (FFT) was used to convert time domain impulse into frequency domain pulse. Then for each frequency, DPSM method was applied and obtained response was again transformed to time domain using inverse Fourier transforms (IFFT). Frequencies up to Nyquist frequencies were used for analysis and effect of remaining frequencies were taken care by superimposing antisymmetric behaviour of imaginary part about Nyquist frequency. **Figure 5.4** shows the flowchart for reconstruction of transient wave program in homogenous fluid using DPSM techniques.

For Water Fluid:

Figure 5.21((a), (b), (c), (d)) shows the acoustic pressure at four different target points lying along Z-axis of transducer face. Transducer is immersed in homogeneous fluid (water) having density (ρ) =1 gm/cc and wave speed is (C_f) = 1.49 km/sec.

- For point close to transducer face (Z= 0) acoustic wave pressure peak lies around 95 μ-sec as shown in **Figure 5.21**(a) with markers.
- Acoustic pressure pulse response at target point 2 at a distance of 2.5 cm from Transducer face shows that a peak arrives at 111 μ-sec as shown in the **Figure 5.21**(b) (having time lag 16 μ-sec).
- For third point at a distance 3.7 cm from transducer face, pressure peak reaches at time 119 μ-sec as shown in the **Figure 5.21**(c) (having time lag 24 μ-sec).
- For fourth point at a distance 4.9 cm from transducer face, pressure peak reaches at time 127 μ-sec as shown in the **Figure 5.21**(d) (having time lag 32 μ-sec).

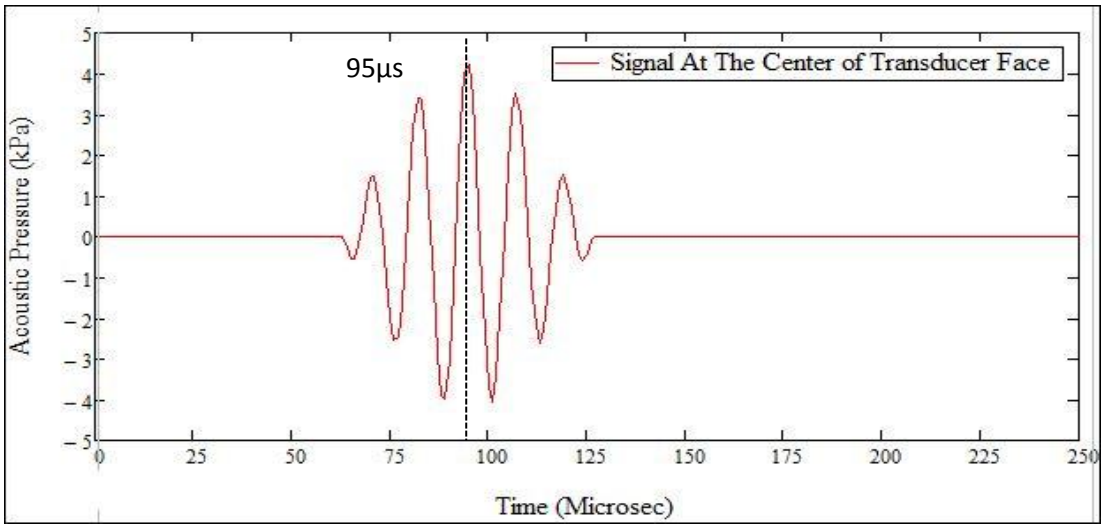

(a) Acoustic Pressure at the Transducer Face

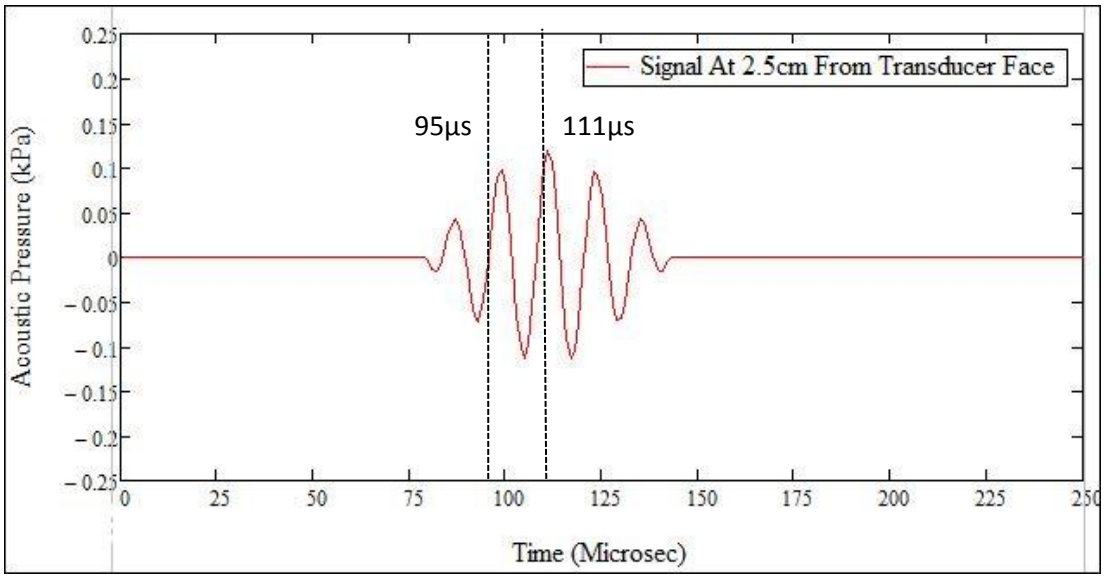

(b) Acoustic Pressure at T2

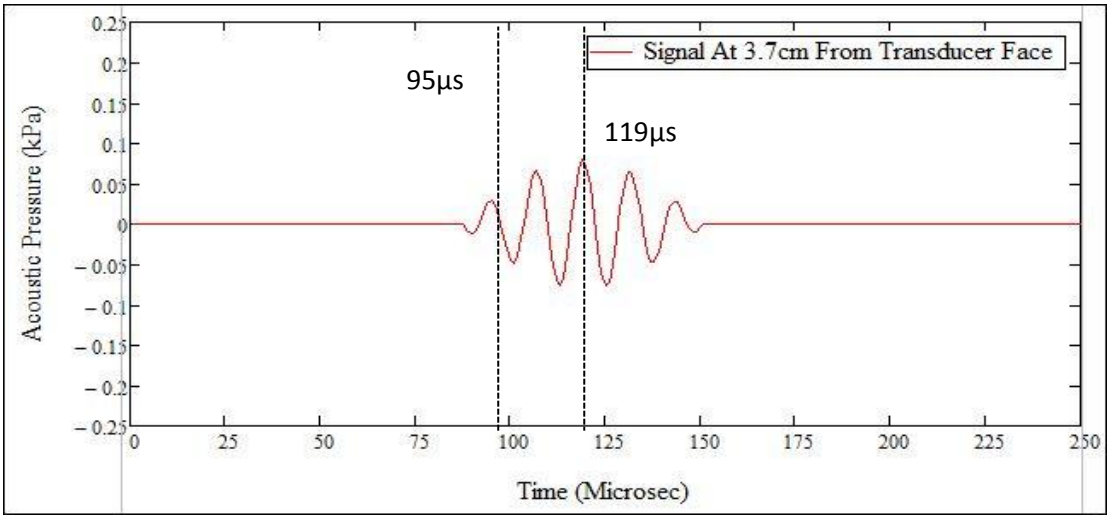

(c) Acoustic Pressure at T3

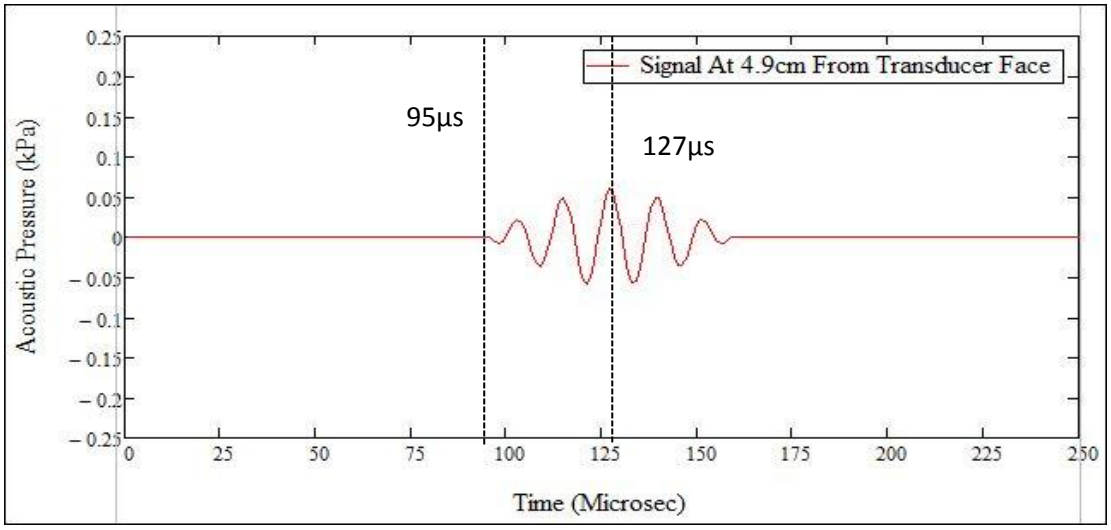

Figure 5.21: Acoustic Pressure Response at Various points along Transducer axis (Z-direction)

From the above signals, it can be seen that as the distance between the transducer surface and the target point is increasing the time lag between the signals can be seen. These uneven distances are used , as these same distances have been used for the practical implementation for the medium water. This whole process have been resused for another homogeneous fluid having different properties than water.

For Glycerine Fluid:

Figure 5.22((a), (b), (c), (d)) shows the acoustic pressure at four different target points lying along Z-axis of transducer face. Transducer is immersed in homogeneous fluid (glycerine) having density (ρ) =1.26 gm/cc and wave speed is (C_f) = 1.92 km/sec.

- For point close to transducer face (Z= 0) acoustic wave pressure peak lies around 95 μ-sec as shown in **Figure 5.22**(a) with markers.
- Acoustic pressure pulse response at target point 2 at a distance of 2.5 cm from Transducer face shows that a peak arrives at 107 μ-sec as shown in the **Figure 5.22**(b) (having time lag 12 μ-sec).
- For third point at a distance 3.7 cm from transducer face, pressure peak reaches at time 114 μ-sec as shown in the **Figure 5.22**(c) (having time lag 19 μ-sec).
- For fourth point at a distance 4.9 cm from transducer face, pressure peak reaches at time 120 μ-sec as shown in the **Figure 5.22**(d) (having time lag 25 μ-sec).

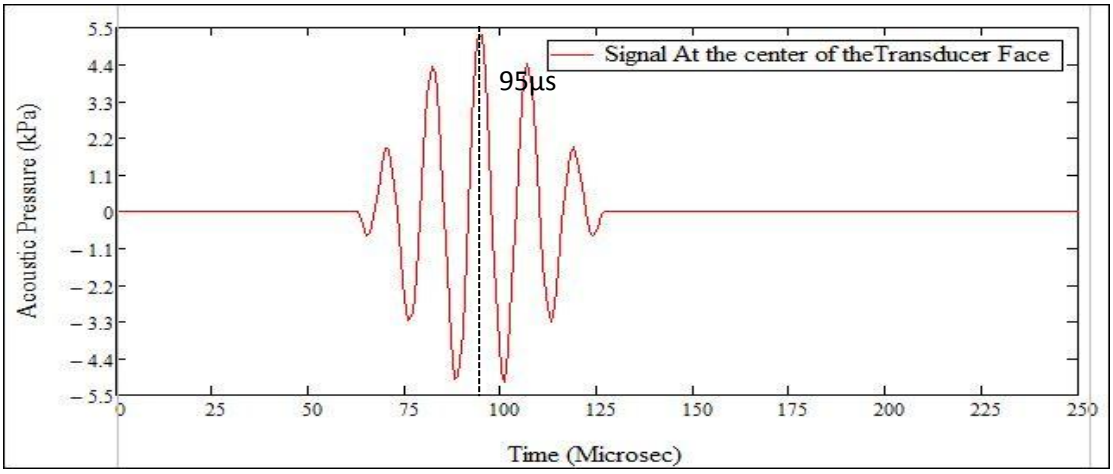

(a) Acoustic Pressure at the Transducer Face

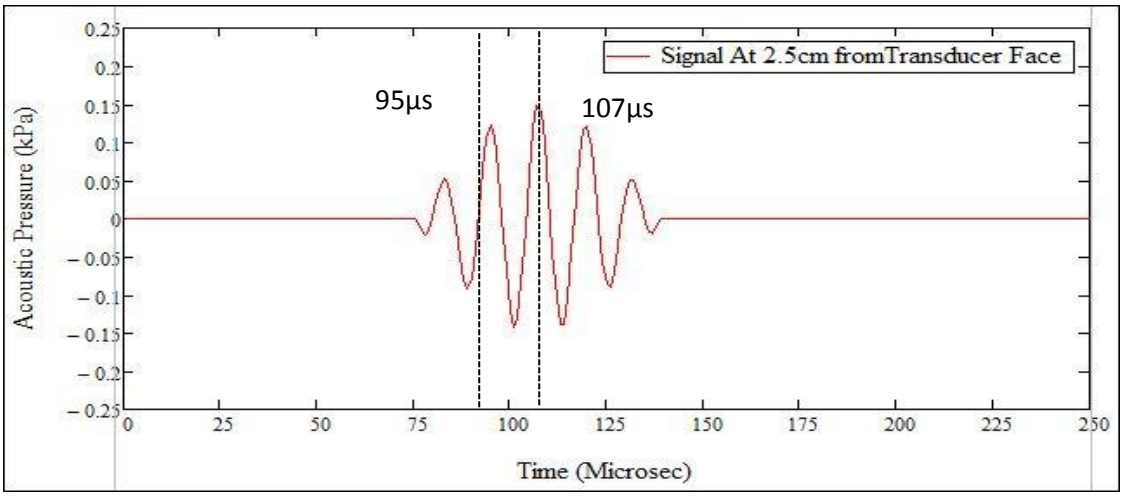

(b) Acoustic Pressure at T2

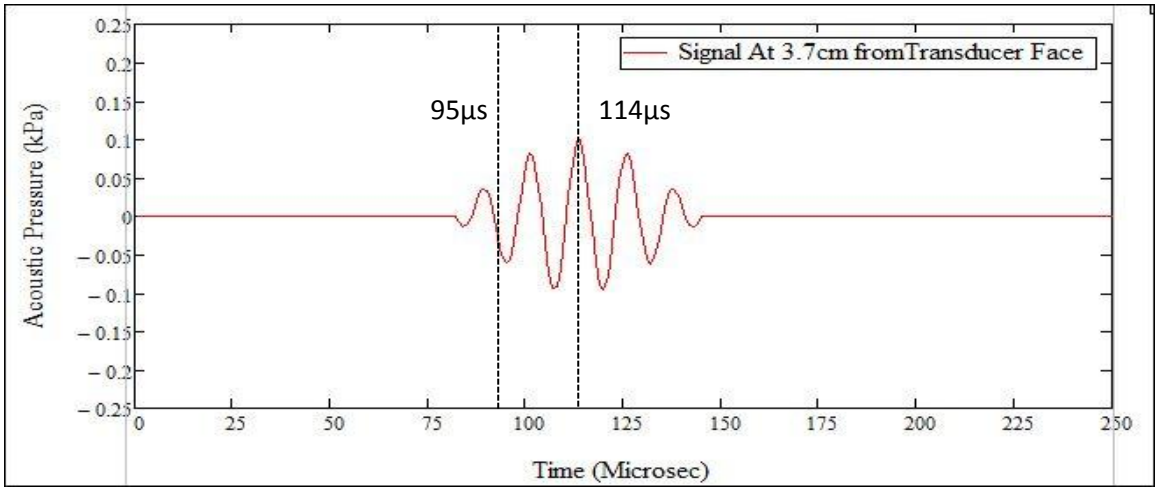

(c) Acoustic Pressure at T3

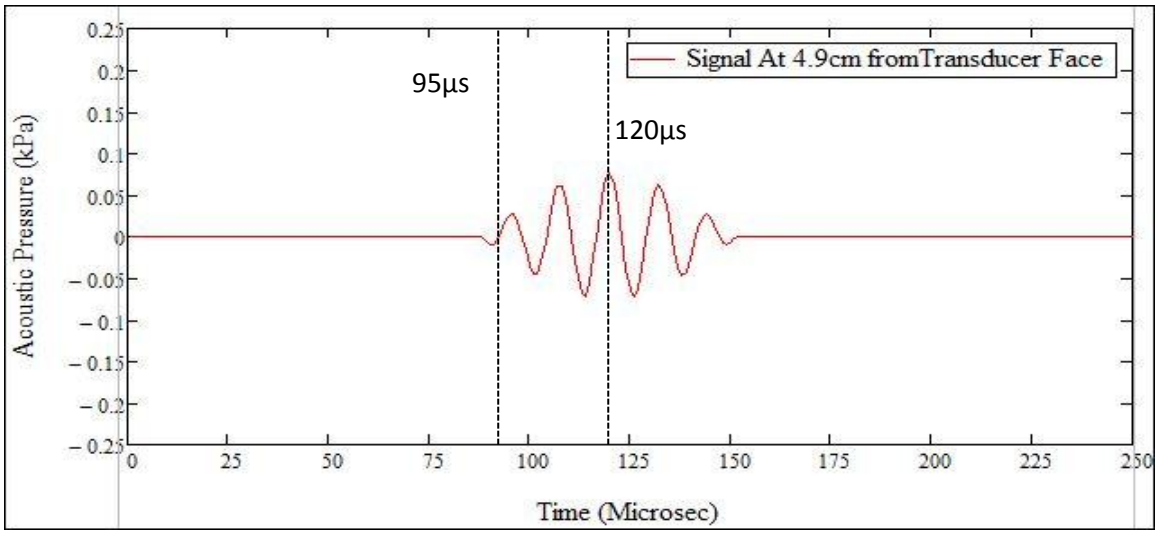

(d) Acoustic Pressure at T4

Figure 5.22: Acoustic Pressure Response at Various points along Transducer axis (Z-direction)

From the above signals, it has been observed that as the distance between the transducer surface and the target point is increasing the time lag between the signals can be seen. These time lags are different from water because of the difference in properties of both water and glycerine. The signal has been approaching the target in advance as compared to the water as the wave speed in glycerine is much more that water's. The same process has been done for Mobil Oil disscussed in next segment.

For Mobil Oil Fluid:

Figure 5.23((a), (b), (c), (d)) shows the acoustic pressure at four different target points lying along Z-axis of transducer face. Transducer is immersed in homogeneous fluid (mobil oil) having density (ρ) =0.87 gm/cc and wave speed is (C_f) = 1.72 km/sec.

- For point close to transducer face (Z= 0) acoustic wave pressure peak lies around 95 μ-sec as shown in **Figure 5.23**(a) with markers.
- Acoustic pressure pulse response at target point 2 at a distance of 2.5 cm from Transducer face shows that a peak arrives at 109 μ-sec as shown in the **Figure 5.23**(b) (having time lag 14 μ-sec).
- For third point at a distance 3.7 cm from transducer face, pressure peak reaches at time 116 μ-sec as shown in the **Figure 5.23**(c) (having time lag 21 μ-sec).
- For fourth point at a distance 4.9 cm from transducer face, pressure peak reaches at time 123 μ-sec as shown in the **Figure 5.23**(d) (having time lag 28 μ-sec).

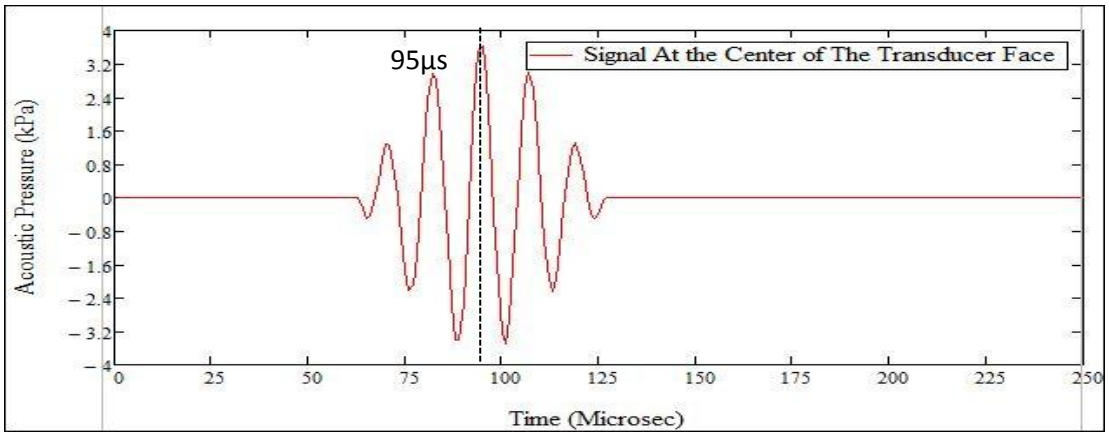

(a) Acoustic Pressure at the Transducer Face

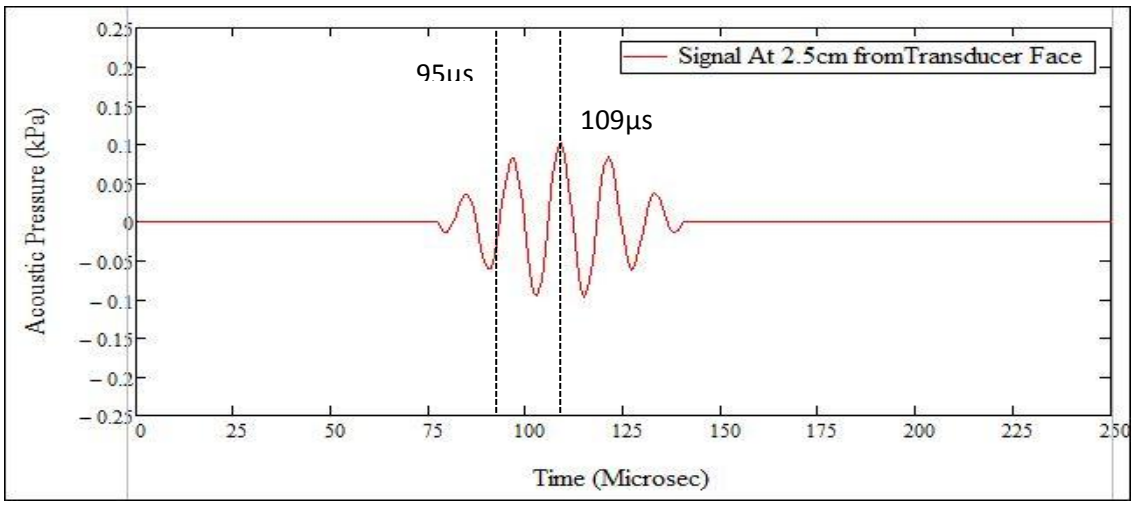

(b) Acoustic Pressure at T2

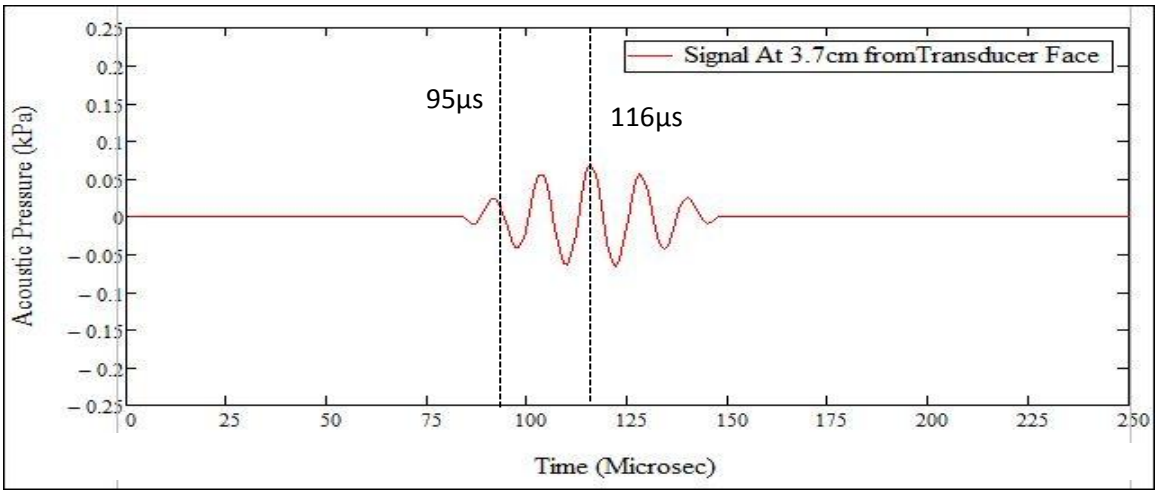

(c) Acoustic Pressure at T3

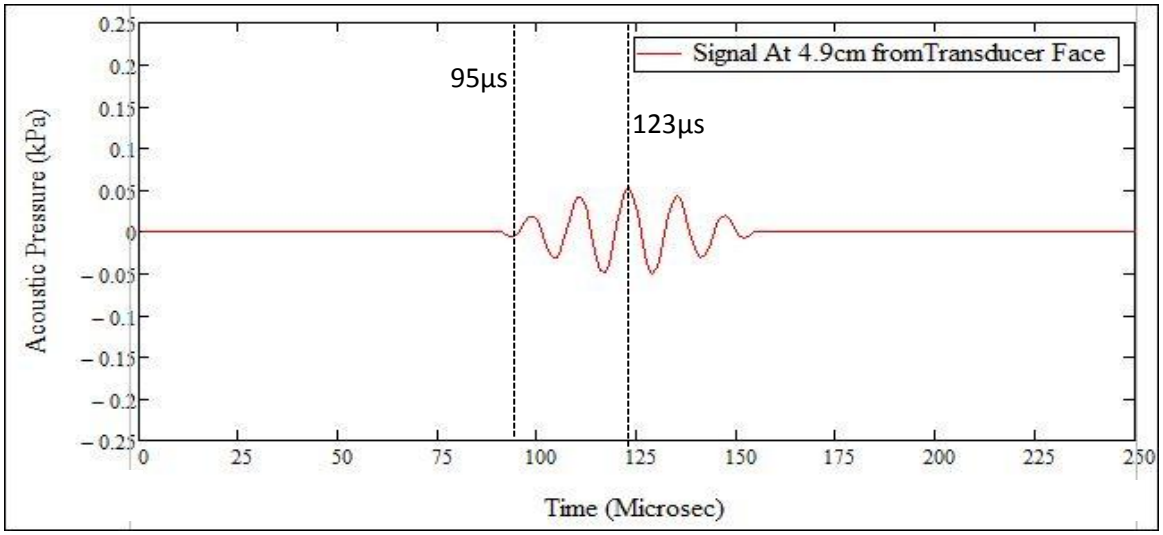

(d) Acoustic Pressure at T4

Figure 5.23: Acoustic Pressure Response at Various points along Transducer axis (Z-direction)

From the above signals, it has been observed that as the distance between the transducer surface and the target point is increasing the time lag between the signals can be seen. These time lags are different from both glycerine and water because of the difference in properties of both water and glycerine. The signal has been approaching the target in between the time of both water and glycerine because of its wave speed, which lies in between them.

5.4 Wave Propagation in a Non-Homogeneous Fluid

In this case three layers of fluids were arranged such that their monotonically increases from bottom layer to top layer and both steady wave and transient wave has been studied in this.

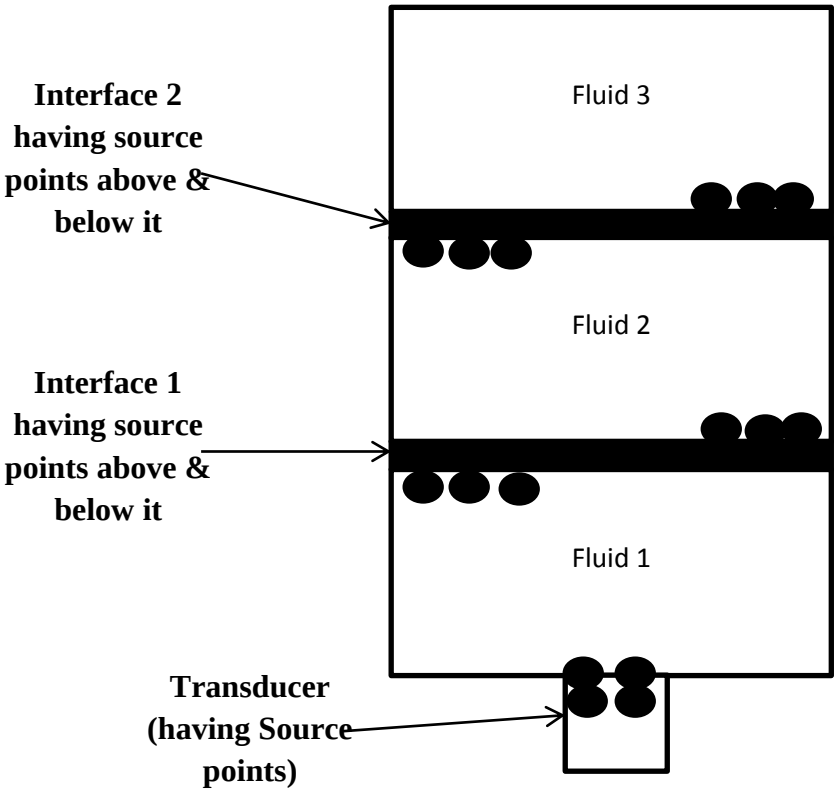

Figure 5.24: Schematic of the Triple Layered Non-Homogeneous Fluid

In the **Figure 5.24,** Schematic showing the arrangement of the triple layered Non-Homogeneous Fluid. Transducer has been showing the source points on its surface, and then these source points are shifted back at $-r_s$ distance from the surface so as to avoid singularity problem. **Figure 5.25,** showing the actual arrangement followed in the modeling software. The source points could be seen having two layers of it on every surface, like on the first interface, at a distance of 1cm from the transducer surface, two sets of source points could be observed in green colour. And on second interface the two set of source points could be seen in red colour at a distance of 2cm from transducer surface.

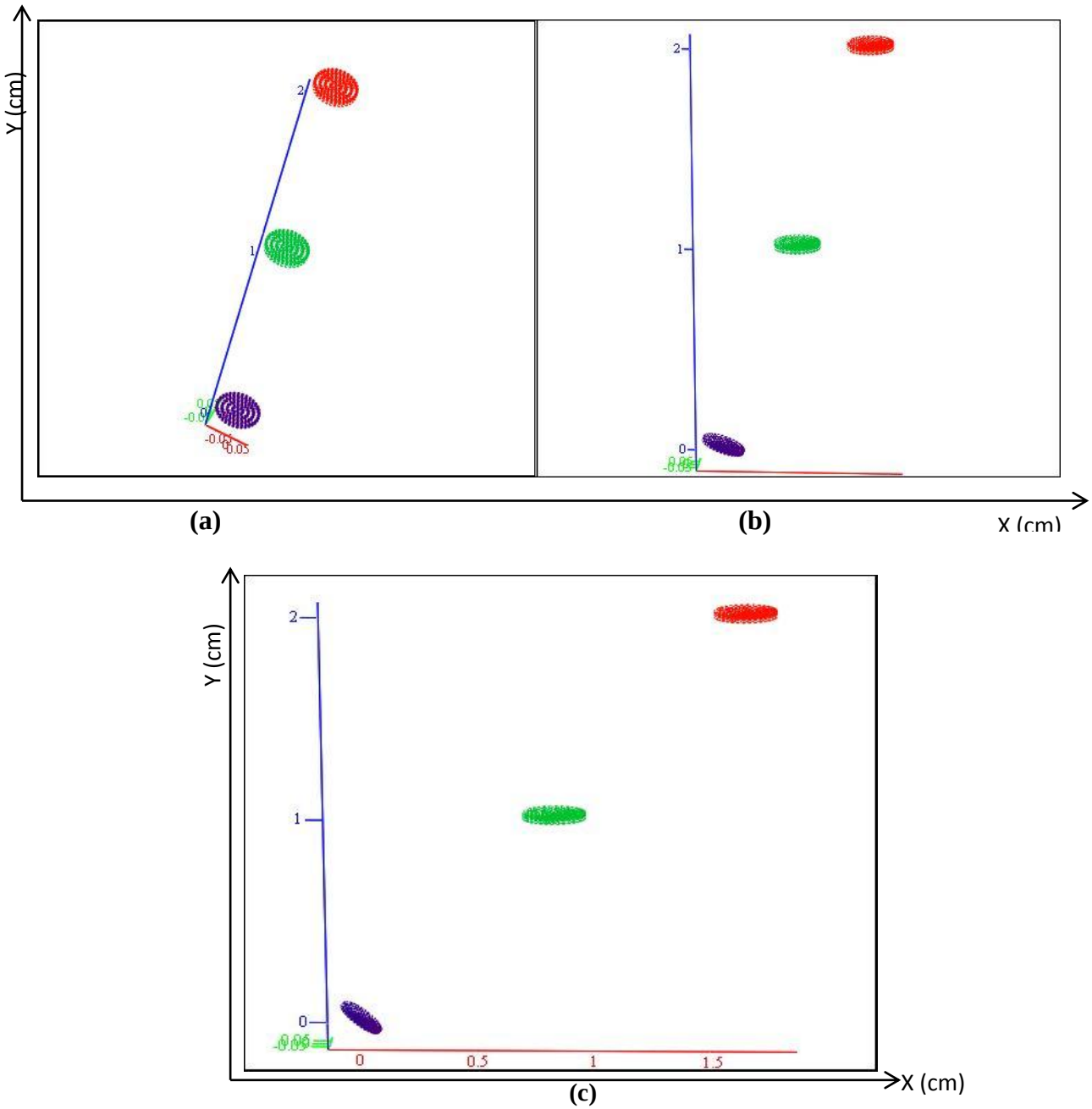

Figure 5.25: Non Homogeneous Fluid at (a) Normal Incidence (b) Non-Normal Incidence 20° (c) Non-Normal Incidence 40°

Name of Fluid	Density (gm/cc)	P-Wave Speed (C_P) (Km/sec)
Fluid 1 (Glycerine)	1.26	1.92
Fluid 2 (Water)	1	1.49
Fluid 3 (Mobil Oil)	0.87	1.72

Table 5.1: Fluid Properties for Fluid 1, Fluid 2 & Fluid 3 Interface

The main emphasis has been to compute the ultrasonic field in multilayered fluid systems. In the multilayered problem geometry several interfaces may be present. The fluids with different densities and acoustic properties form a multilayered system, the fluid density should be monotonically vary from top to bottom. For a system with *n* number of fluids there will be (*n-1)* number of interfaces. The source points are also divided into two types (a) active source points (b) passive source points. The active source points are mainly taken on the transducer surface. On the interface those are passive point source. Depending upon the source points, which are sending energy and which are not would be labeled as active and passive point source. The source points on each interface act as a transmitter as well as a reflector of elastic wave energy generated by the ultrasonic transducers.

5.4.1 Results for Steady State in Triple Layered Non-Homogeneous Fluid:

Routine was developed for modeling ultrasonic field when emiting energy at normal angle or other then normal angle. The fluids are placed according to the density. At the bottom glycerine has been placed, then water has been placed above it & after that mobil oil has been placed. The mentioned approach, was used to find the source strength for a given velocity at any point within three fluids, can be calculated using Eq-4.36 and Eq-4.37 of Chapter Four. To generate the ultrasonic field in three fluids a rectangular grid were created for the target points.

For 1MHz Frequency:

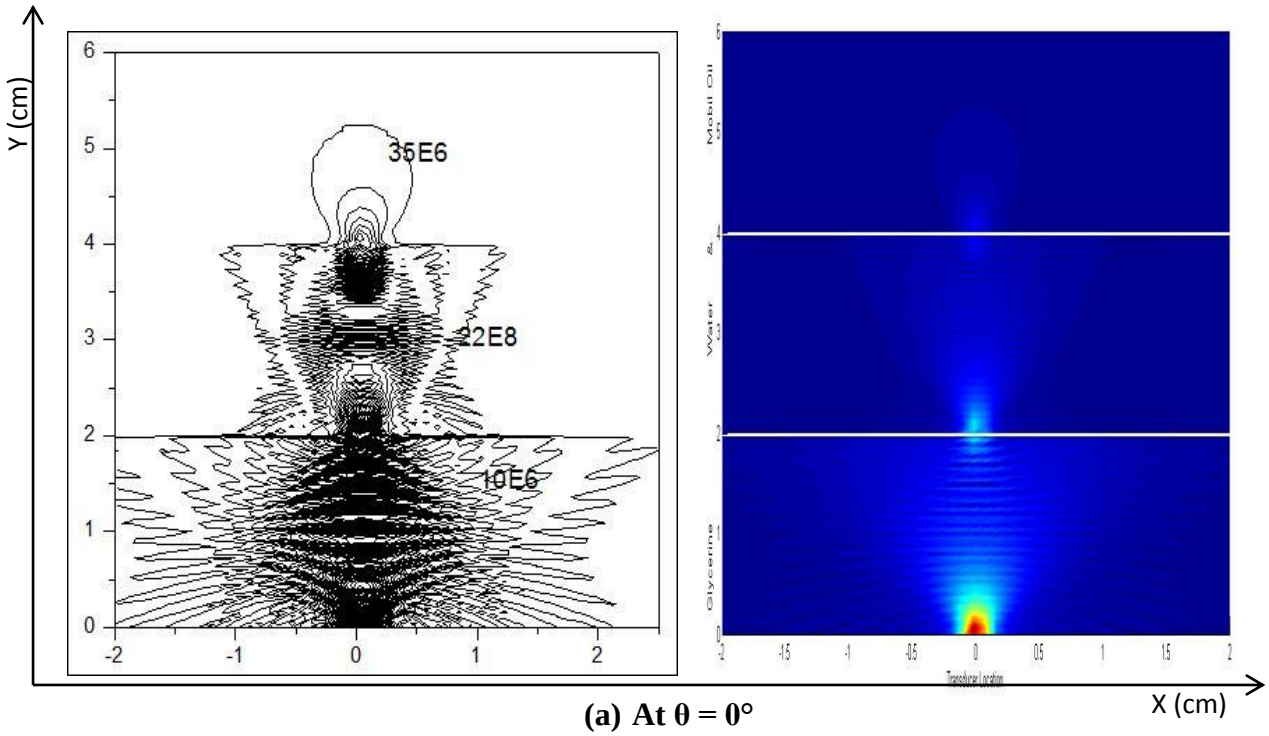

(a) At θ = 0°

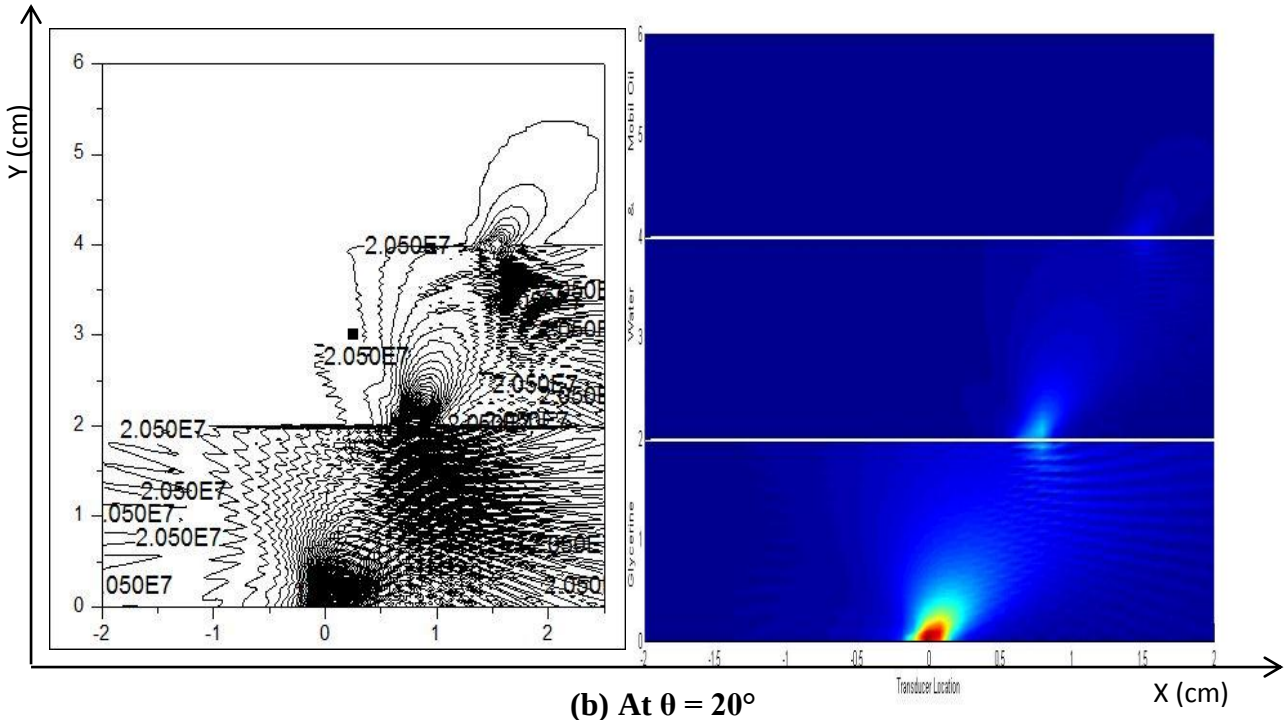

(b) At θ = 20°

Figure 5.26: Pressure Plot at Different Angles in Non-Homogeneous (Freq-1MHz) (a) & (b)

The **Figure 5.26,** shows the triple layered non-homogeneous fluid having glycerine at the bottom , water in the middle and mobil oil at the top. The wave has been developed at angle Zero degree and 20 degree for 1MHz frequency of transducer. In this case the 1MHz wave has been going through first two fluids easily but has diminished in the third fluid because some part of the energy has been reflected back from the interfaces. The various labels of the pressure has been marked on the contour plots as shown.

For 2.25 MHz Frequency:

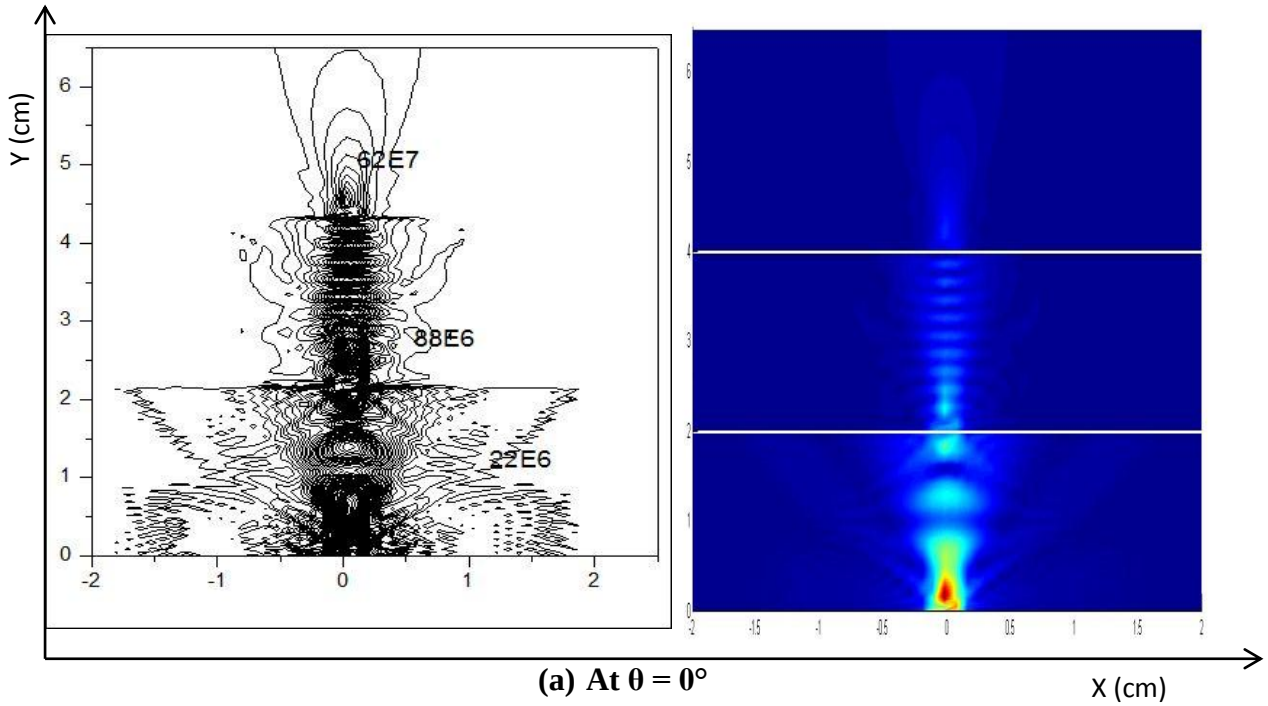

(a) At θ = 0°

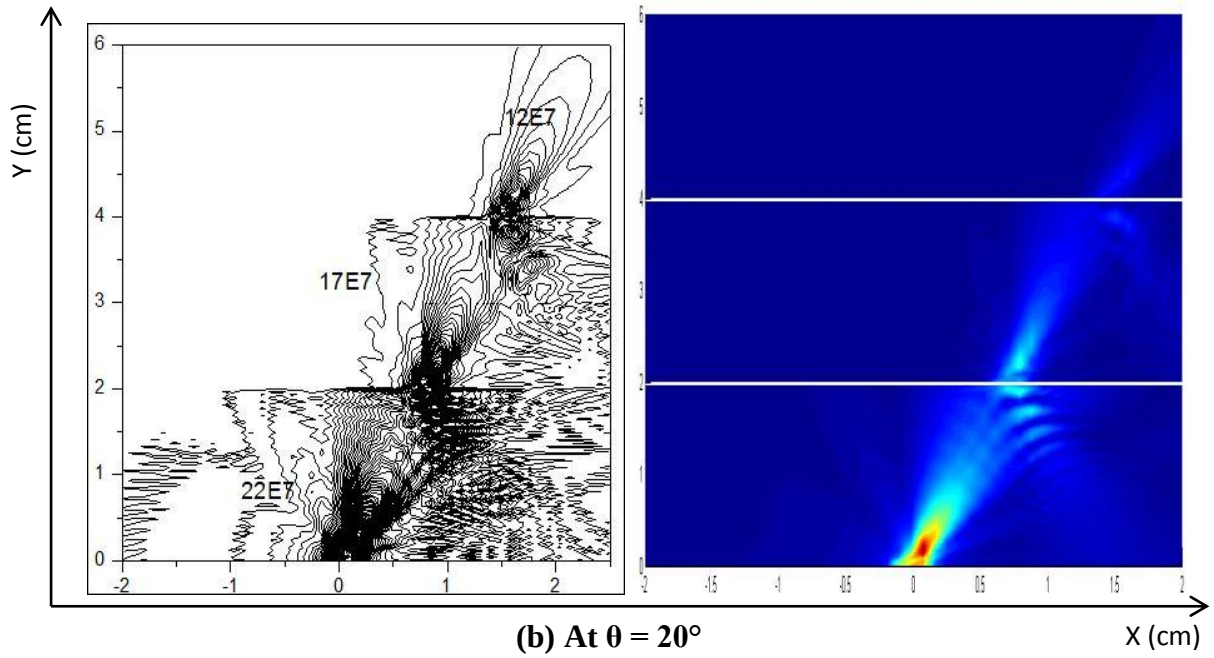

Figure 5.27: Pressure Plot at Different Angles in Non-Homogeneous Fluid (Freq-2.25MHz) (a) & (b)

The **Figure 5.27, t**he wave has been developed at angle Zero degree and 20 degree for 2.25MHz frequency of transducer. In this case the 2.25MHz wave has been going through first two fluids easily but has diminished in the third fluid because of the same reason some energy has been reflected back and some transmitted through the interfaces. It has been observed as the frequency has become 2.25MHz the pressure energy has been in the collimated position. The various labels of the pressure has been marked on the contour plots as shown.

For 3.5 MHz Frequency: The plots for 3.5MHz frequency has been developed and are shown in **Figure 5.28,** in this case the pressure energy has been collimated because of the increase in the frequency of the transducer.

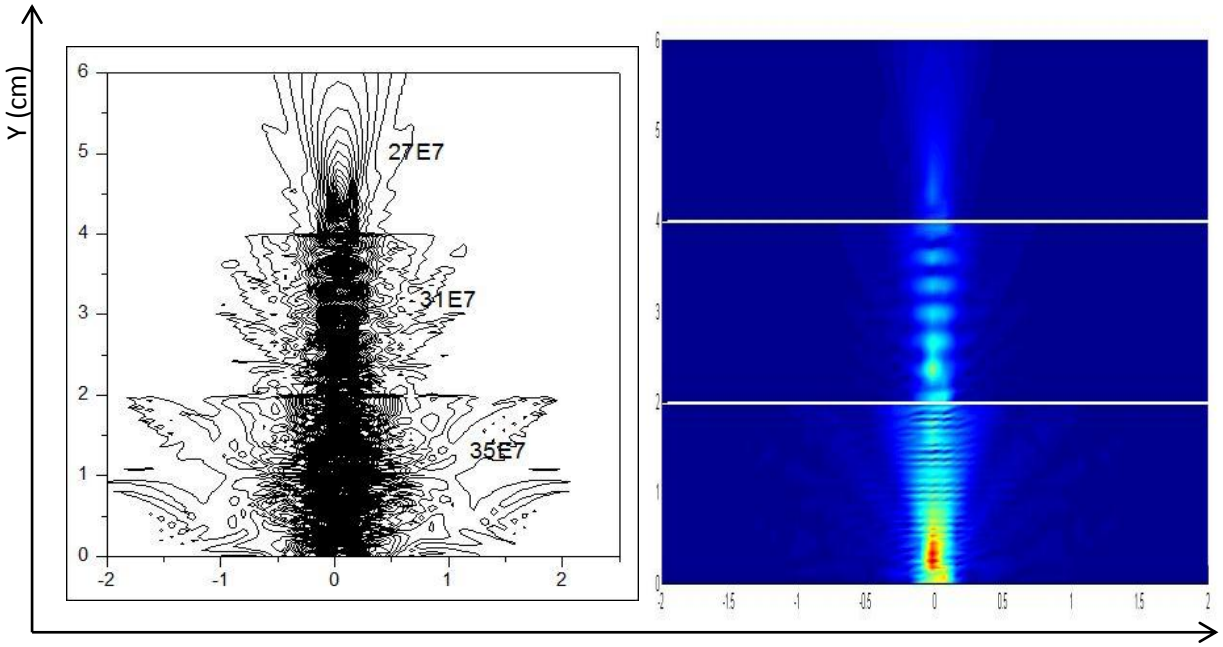

(a) At θ = 0°

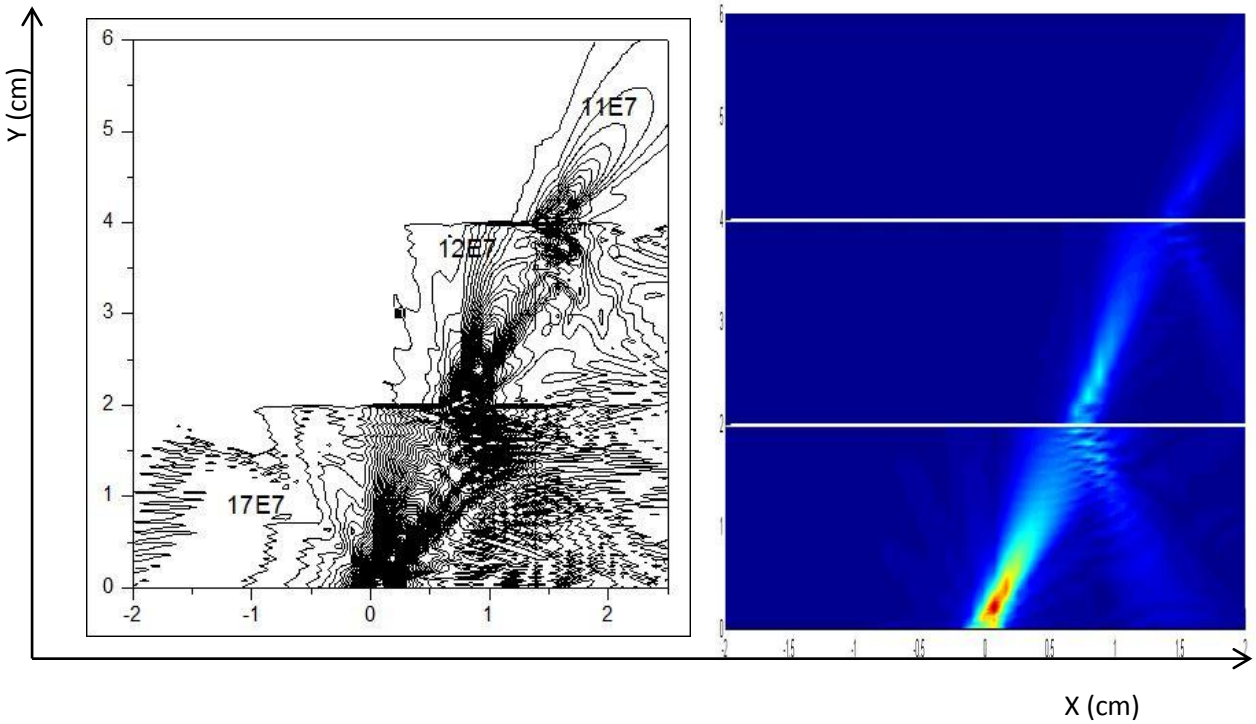

(a) At θ = 20°

Figure 5.28: Pressure Plot at Different Angles for Non-Homogeneous Fluid (Freq-3.5 MHz) (a) & (b)

The **Figure 5.28, t**he wave has been developed at angle Zero degree and 20 degree for 3.5MHz frequency of transducer. In this case the 3.5MHz wave has been going through all the three fluids but some part of the wave energy has been lost because some energy has been

reflected back and some transmitted through the interfaces. It has been observed as the frequency has become 3.5MHz the pressure energy has been in the collimated position. The various labels of the pressure has been marked on the contour plots as shown.

It has been observed that the pressure energy is being reflected back and some part goes through. It has been happening because of Snell's Law the pressure energy is following Snell's Law. The next section will discuss the Snell's Law.

5.4.2 Snell's Law of Refraction & Reflection:

As discussed earlier in Chapter One, Snell's Law describes the relationship between the angles and the velocities of the waves. Snell's law equates the ratio of material velocities V_1 and V_2 to the ratio of the sine's of incident (Q_1) and refracted (Q_2) angles, as equation is

$$\frac{Sin\ \theta_1}{V_{L_1}} = \frac{Sin\ \theta_2}{V_{L_2}} \qquad \text{from Eq-1.1}$$

where, V_{L_1} & V_{L_2} are the longitudinal wave velocities in material 1 and material 2 respectively.

From previous section the case for 2.25MHz frequency has been taken with transducer placed at angle of 20° for the Snell's Law

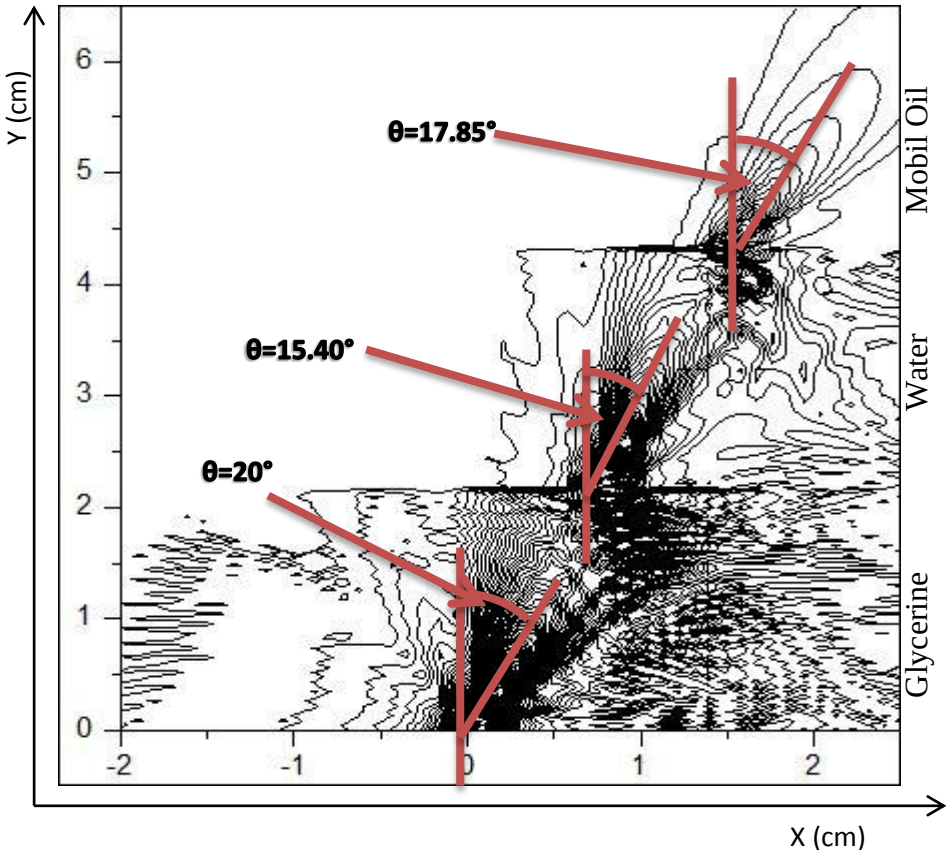

Figure 5.29: Transmitted Angles from the Interfaces

Figure 5.29, showing angles transmitted from the interface. At the first instance the transducer is placed at an angle of 20°. The angle at the first interface is calculated by Snell's Law (as shown in **Figure 5.29**) is 15.40°, this is less than the measured angle, which is coming out to be 17° approximately. This difference in angles is coming due to difference in wave speed of the fluids. In the next interface the transmitted angle becomes greater than the previous interface angle as calculated by Snell's Law is 17.85°, and measured angle is 19°.

In another case, the fluid2 and fluid3 has been interchanged to observe the variations in transmitted angles at the interfaces. This is in programming because in practical it is not possible to alter the fluid with different densities.

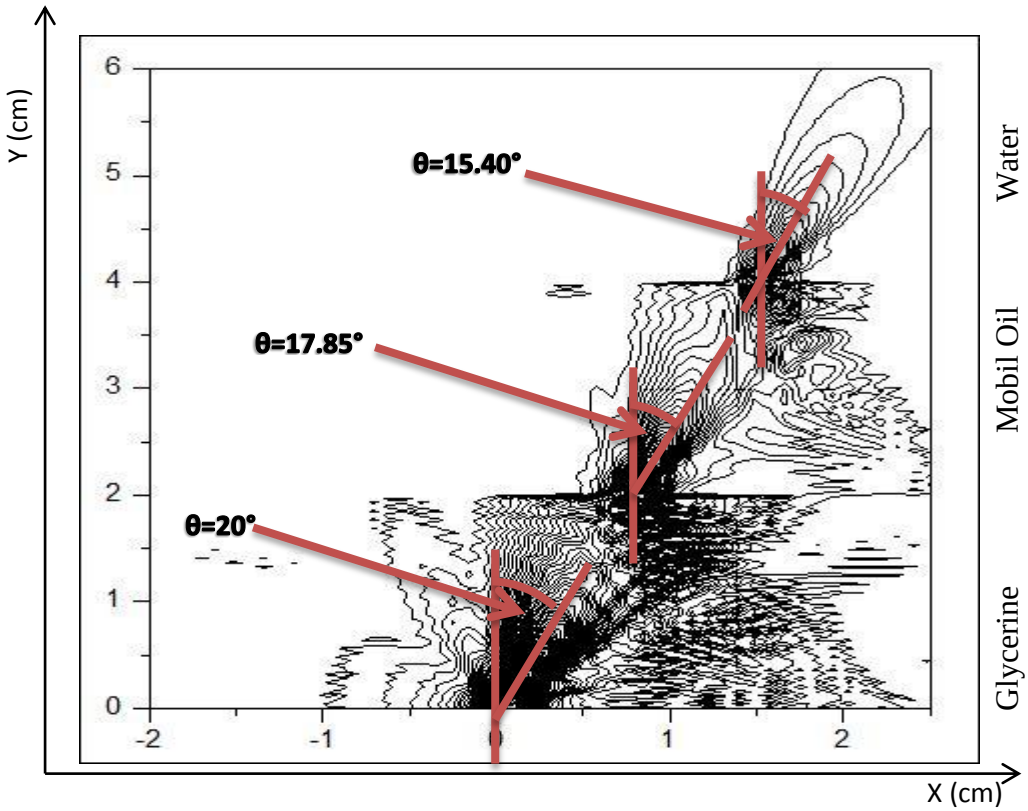

Figure 5.30: Transmitted Angles from the Interfaces with change in fluid densities

Figure 5.30, showing angles transmitted from the interface. In this case fluid 2 and fluid 3 have been interchanged, to see the outcome of Snell's Law. At the first instance the transducer is placed at an angle of 20°. The angle at the first interface is calculated by Snell's Law (as shown in **Figure 5.30**) is 17.85°, this is less than the measured angle, which is coming out to be 19° approximately. This difference in angles is coming due to difference in wave speed of the fluids. In the next interface the transmitted angle becomes less than the previous interface angle as calculated by Snell's Law is 15.40°, and measured angle is 17°. As

it can be observed that the value of the transmitted angles from the interface have also been interchanged as the fluids were interchanged, so by this observation, it can be said that Snell's Law holds good for Non-Homogeneous Fluid with triple layered. When the steady state has been observed, the transient state in triple layered non-homogeneous has been discussed in next section.

5.4.3 Results for Transient State in Triple Layered Non-Homogeneous Fluid:

Same steady state model was used to study the transient wave using FFT engine. 5 cycles Tone burst signal was used as input signal and the acoustic pressure was recorded at five points lying along transducer axis at Z=0 as shown in **Figure 5.31** as target points. To get clear distinct pulse peak, first interface was kept at 20 cm from the transducer face and second interface was kept at 40 cm from the transducer face and also the FFT sampling points were taken as 512.

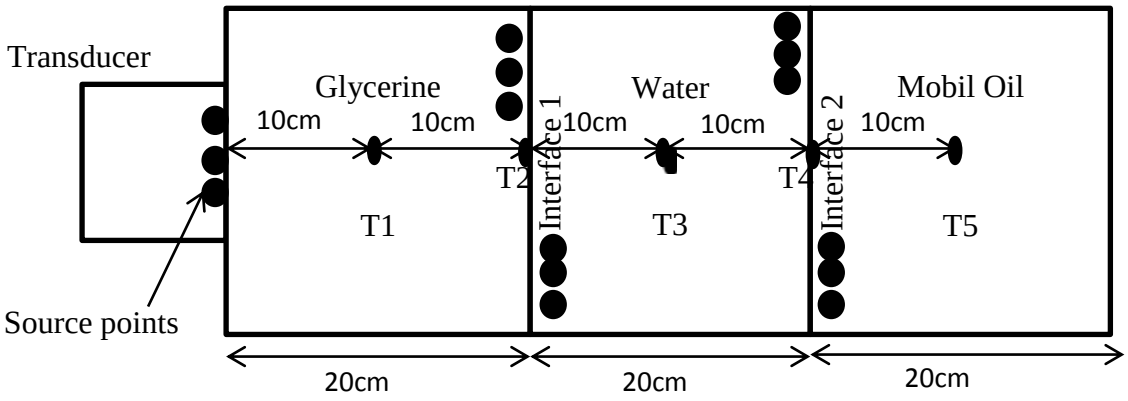

Figure 5.31: Schematic Location of Target points (T1 to T5) where the response of ultrasonic field was observed

In **Figure 5.31,** the order of the triple layered non-homogeneous fluid has been shown. First fluid has been placed near the transducer face and second and third fluids have been placed at a distance of 20cm from the transducer face. The black dots shown, they represent source points on transducer surface and on the two interfaces as well. And the symbols from T1 to T5 are the target points placed at a distance of 10 cm from each other. Now by using the programming code the various input signal, reflected signal and transmitted signals have been generated and discussed.

Input Pulse from the Transducer Face:

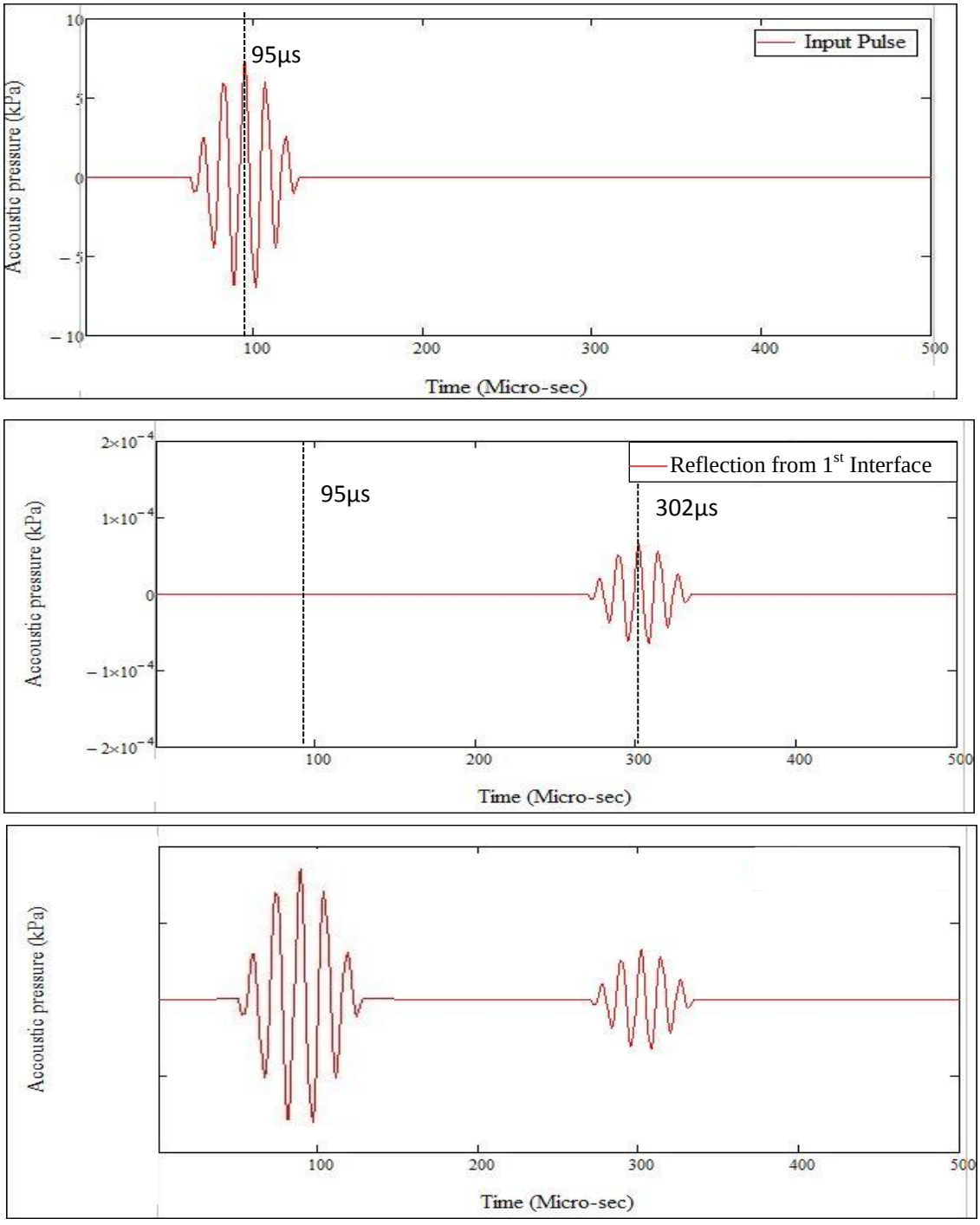

Figure 5.32: Tone Burst Signal -Pressure response at Transducer Face

At the transducer face the input signal had the highest peak at 95µs and when it reflected back from the first interface, which was located at T2 = 20cm from the transducer face, then its reflected signal had the highest peak at 302µs. This gave the time lag between these two peaks as 207µs. This was the matching with the theoretical time that the wave should take to reach interface and rebound back to transducer face. To calculate the time, the equation of pulse echo has been used and given by,

$$T = \frac{D}{S} \qquad \text{Eq-5.4}$$

where, T is the time taken, D is the distance travelled, S is the wave speed of the material. So by using this Eq-5.4 the time lag has been calculated for all the cases.

Input Pulse at Target Point T1:

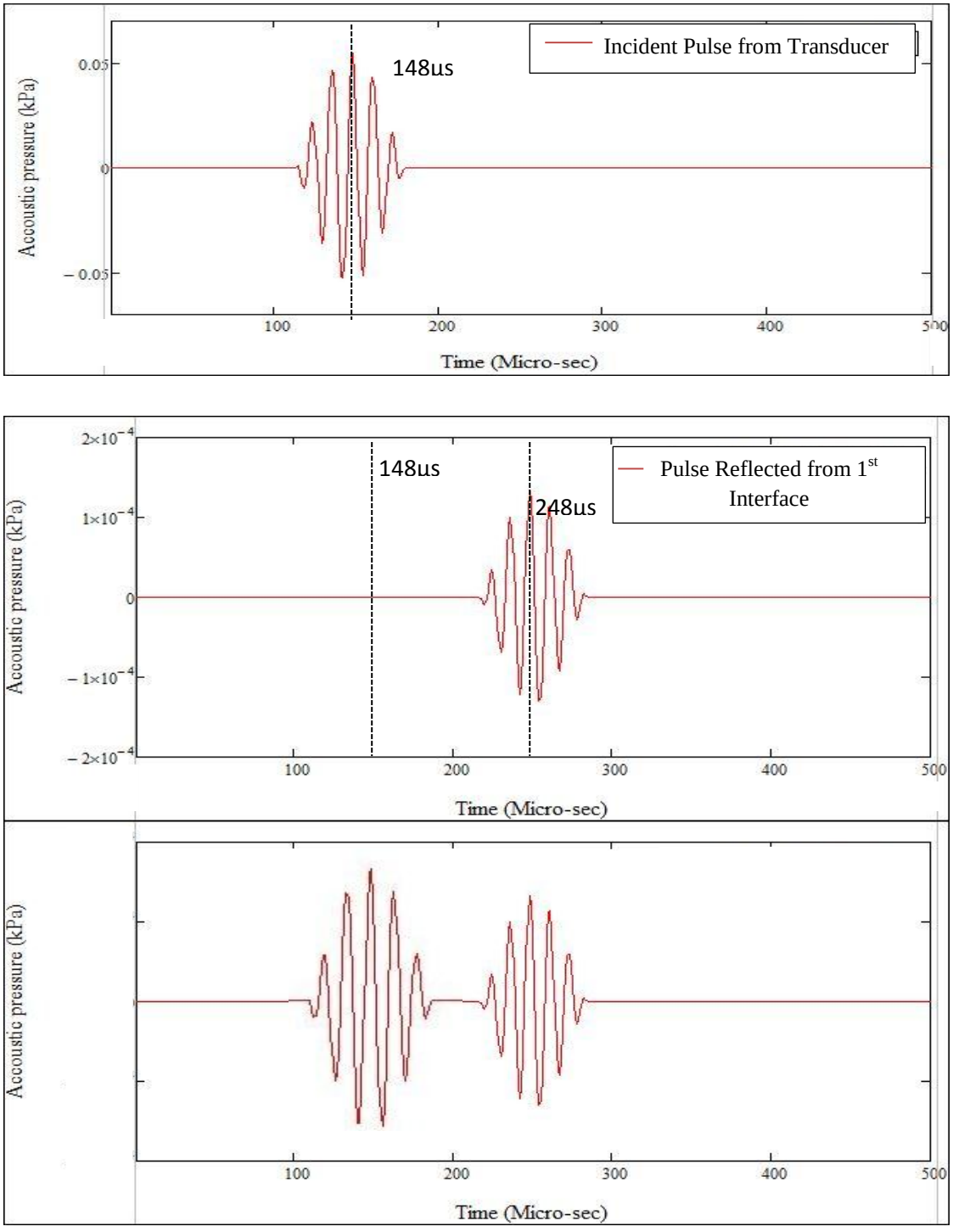

Figure 5.33: Tone Burst Signal -Pressure response at T1

At the target point T1 from the transducer face the input signal had the highest peak at 148μs and when it reflected back from the first interface, which was located at T2 = 20cm from the transducer face, then its reflected signal had the highest peak at 248μs. This gave the time lag between these two peaks as 153μs. This was the matching with the theoretical time calculated using Eq-5.4 that the wave should take to reach interface and rebound back to transducer face.

Input Pulse at Target Point T2 (on the first interface):

On the first interface the input signal will have very low amplitude value because the distance from the transducer face has been increasing. The signals are as shown.

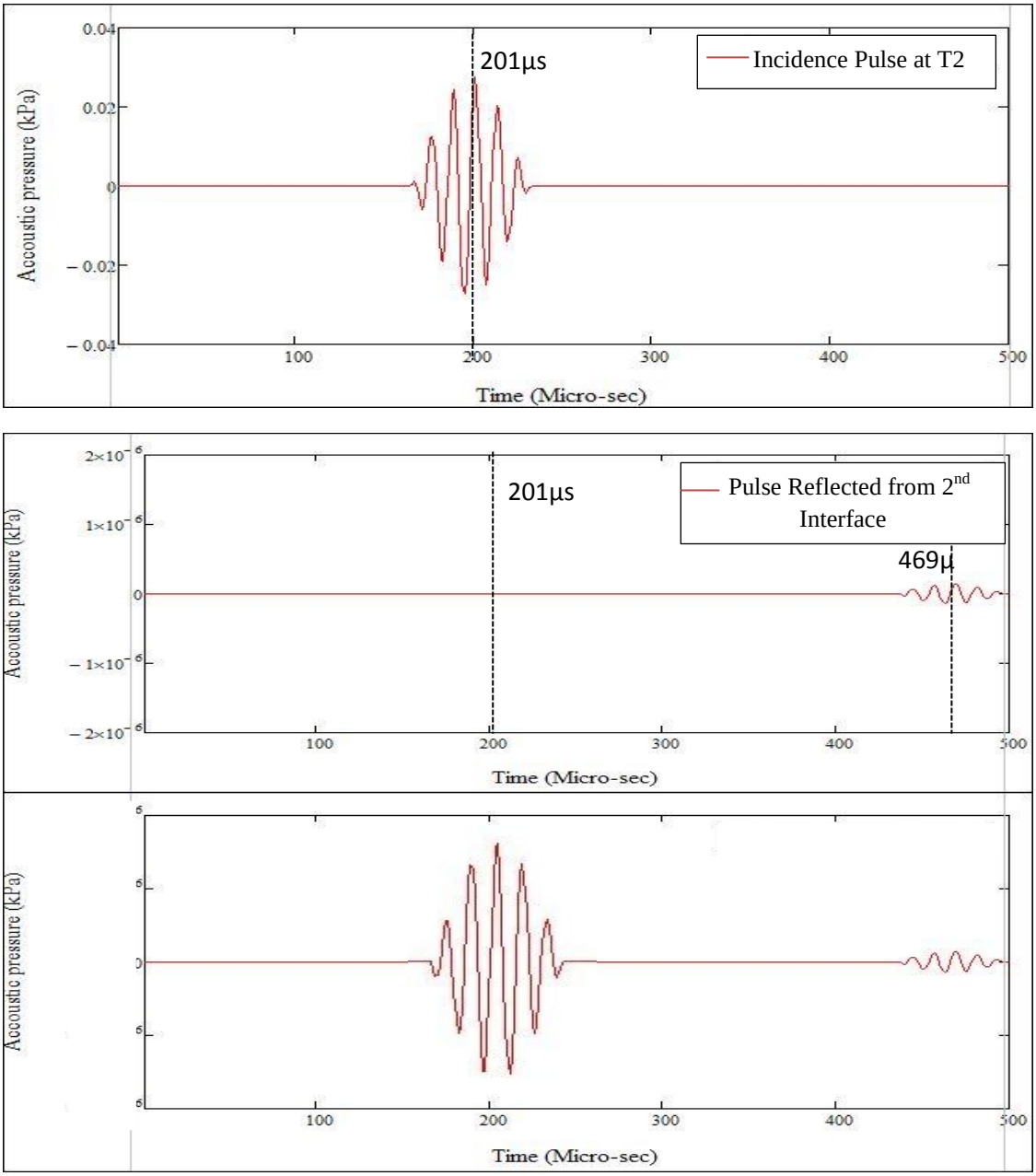

Figure 5.34: Tone Burst Signal -Pressure response at T2

At the target point T2 (on the first interface) from the transducer face the input signal had the highest peak at 201µs in the second fluid and when it reflected back from the second interface, then its reflected signal had the highest peak at 469µs. This gave the time lag between these two peaks as 372µs. This was the matching with the theoretical time that the wave should take to reach interface and rebound back to transducer face.

Transmitted Pulse at T3:

Now the signal, that has been generated, has been a transmitted signal as it will be coming through the first interface and going towards the target point T3, located in the second fluid. The signals are as shown.

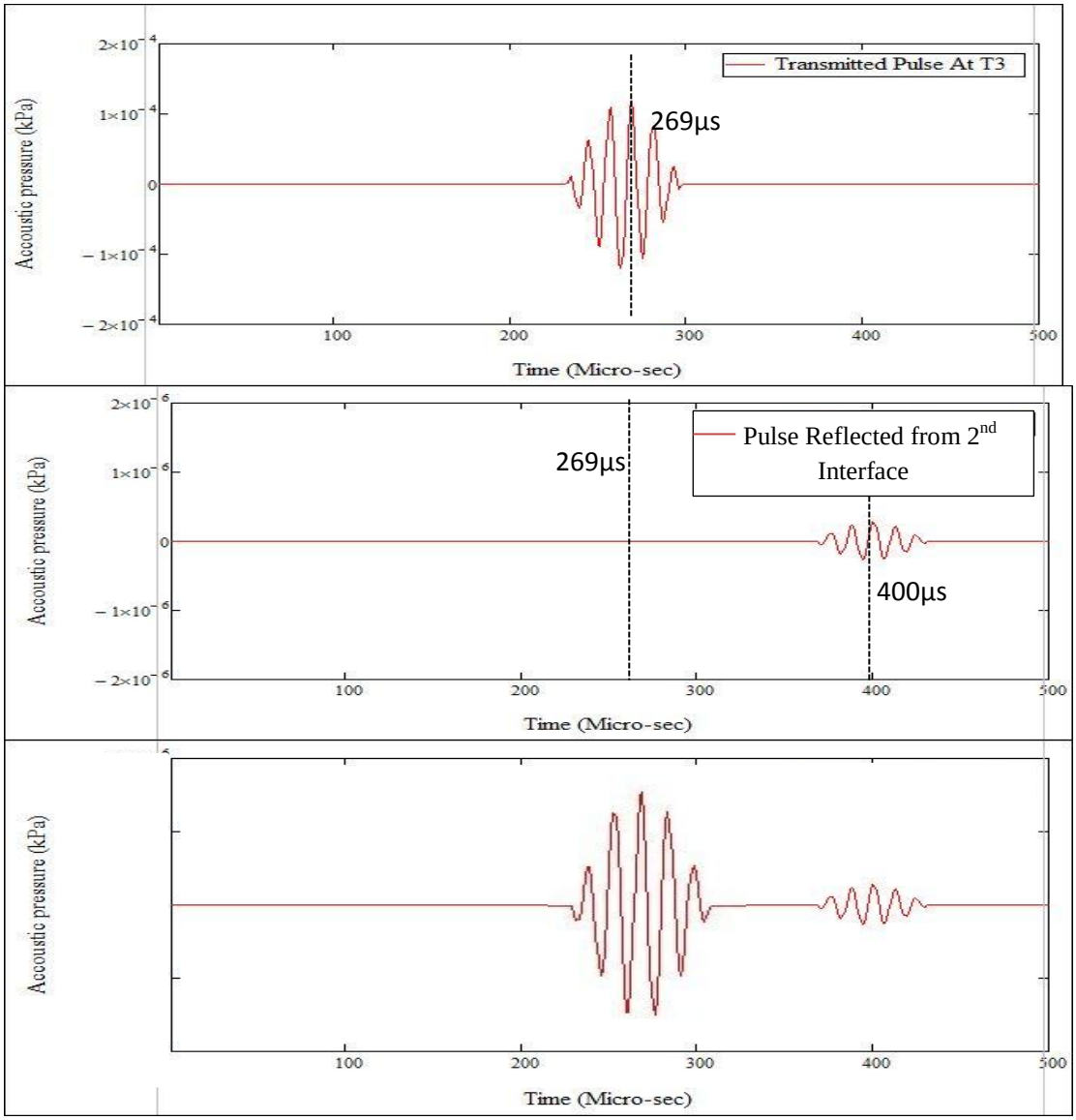

Figure 5.35: Tone Burst Signal -Pressure response at T3

At the target point T3 (after the first interface) from the transducer face the transmitted signal had the highest peak at 269μs in the second fluid and when it reflected back from the second interface, which was located at T4 = 40cm from the transducer face, then its reflected signal had the highest peak at 400μs. This gave the time lag between these two peaks as 131μs. This was the matching with the theoretical time that the wave should take to second interface and rebound back to target point T3. This also showed that as the distance increased the time increased to reach the target point T3. And also this took less time to come back from the second interface compared to the time taken by the signal to reach the target point T3 after reflection at Z= 30 cm.

Transmitted Pulse at T4 (on the second interface) & at T5:

Now the wave has reached the second interface and it has been decaying with respect to the increasing distance and fluid change. The signals are as shown.

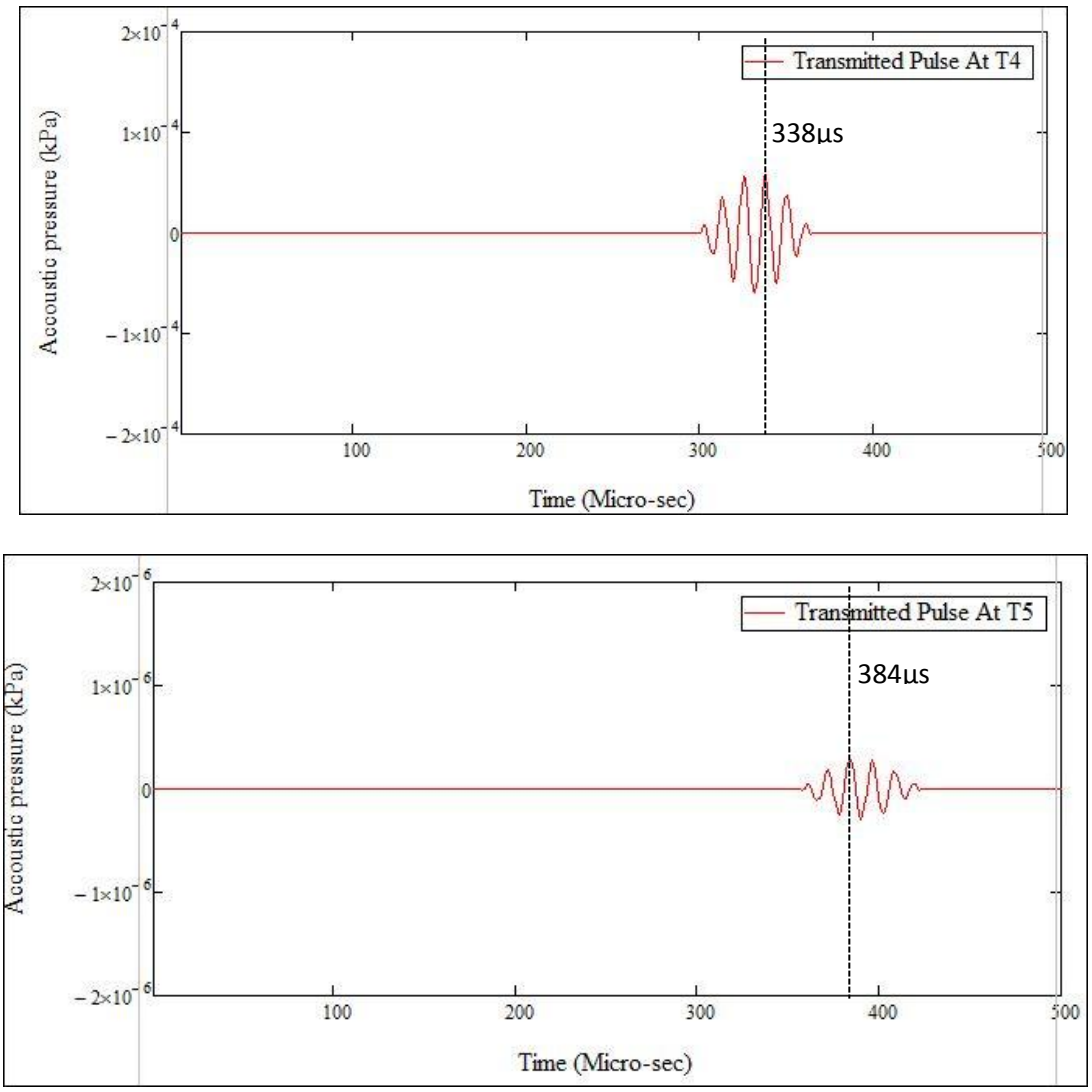

Figure 5.36: Tone Burst Signal -Pressure response at T4 & T5

At the target point T4 (on the second interface) from the transducer face the transmitted signal had the highest peak at 338μs in the second fluid and when it was further transmitted to target point T5 then it had the highest peak at 384μs in the third fluid.

In the end it can be concluded that as the distance has been increasing so did the wave decaying. Also the time taken to reach various target points was different.

5.4.3 Acoustic Pressure Distribution with respect to Time

Acoustic pressure contours (tomograms) were plotted at various times interval on X-Z plane as shown in the **Figure 5.29**. Input velocity pulse at transducer face was given tone burst pulse as per **Figure. 5.5**. Transducer having diameter 0.254 cm was immersed in water and in the water target point grid has been generated. In the following figures different colours showed intensity of pressure.

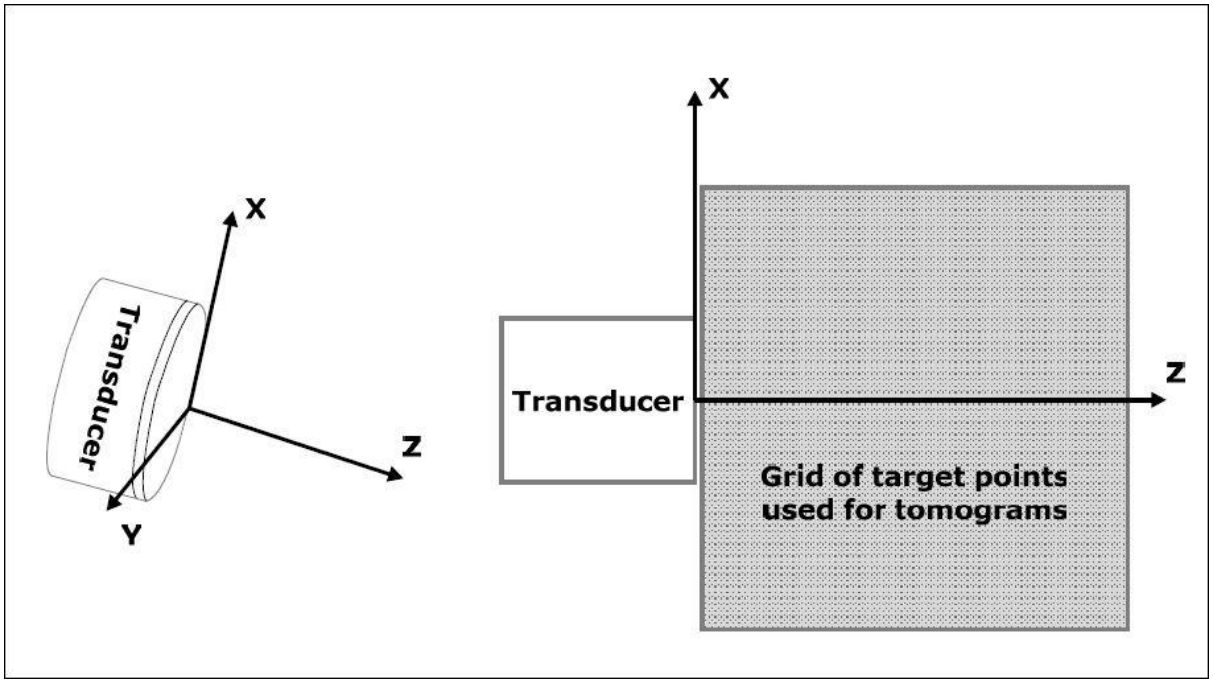

Figure 5.37: Location of X-Z plane and the target point grid used to generate tomo-grams

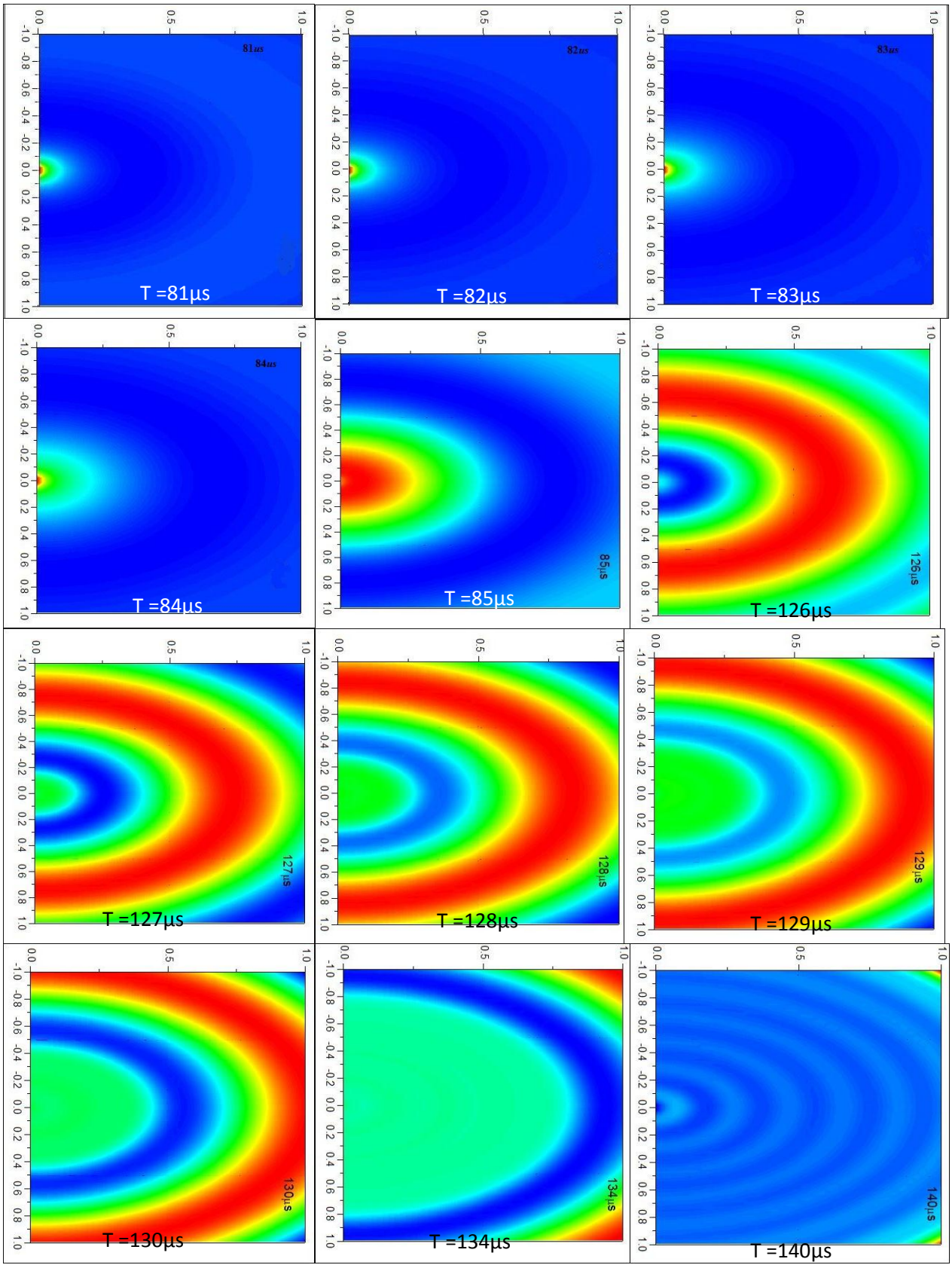

Figure 5.38: The acoustics pressure snap shots of homogenous fluid at different time instances

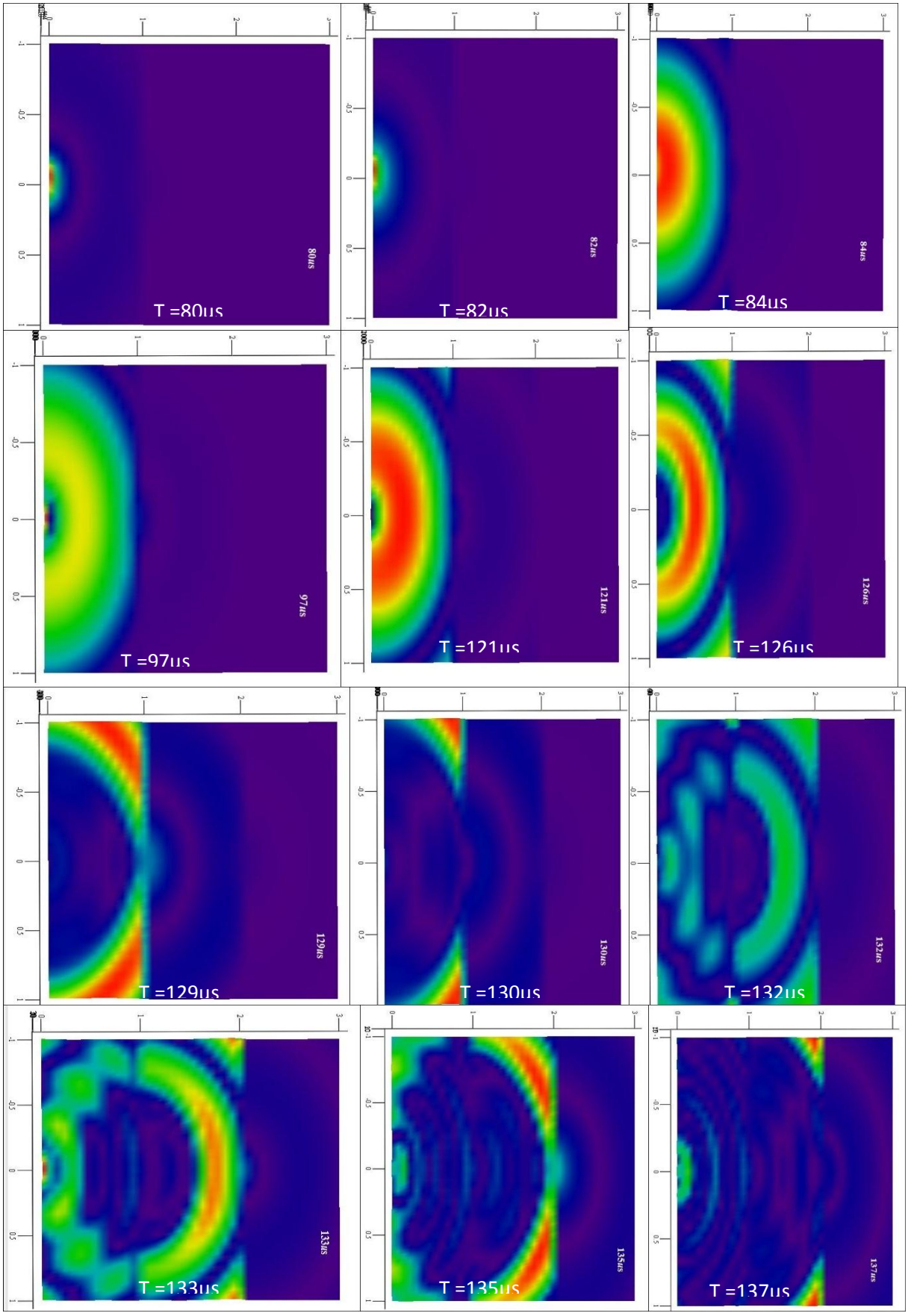

Figure 5.39: The acoustics pressure snap shots of Triple Layered Non Homogenous fluid at different time instances

.

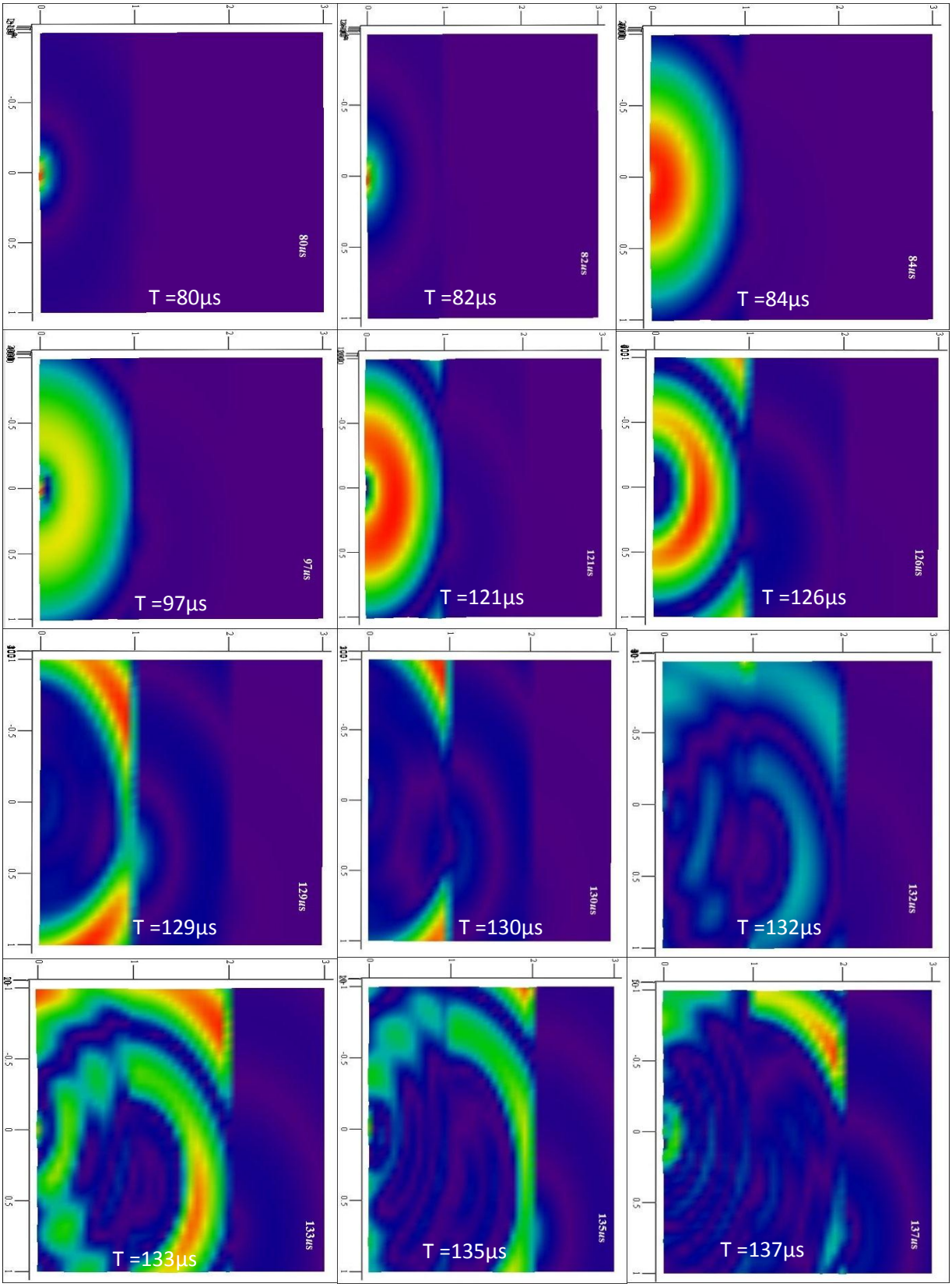

Figure 5.40: The acoustics pressure snap shots of Triple Layered Non Homogenous fluid at different time instances at an angle of 20°.

5.5 Concluding Remarks

In this chapter key characteristic of ultrasonic wave propagation like Near field Zone & Divergence Angle have been found exactly as calculated using DPSM technique in homogeneous fluids i.e. water, mobil oil & glycerine and triple layered non-homogeneous fluid (combination of all three fluids).

Transient state analysis have been done in homogeneous fluids and in triple layered non-homogeneous fluid. Analysis has been done indiviually on all the three homogeneous fluids. And these analysis have been compared with the practical work. The next chapter will explain this.

CHAPTER SIX

EXPERIMENTAL VALIDATION

6.1 Experimental Setup:

In the previous chapter the numerical results for pressure fields generated in both homogeneous and triple layered non-homogeneous fluid and their snap shots have been presented. This chapter deals to validate the numerical results with the experimental results the following setup have been used.

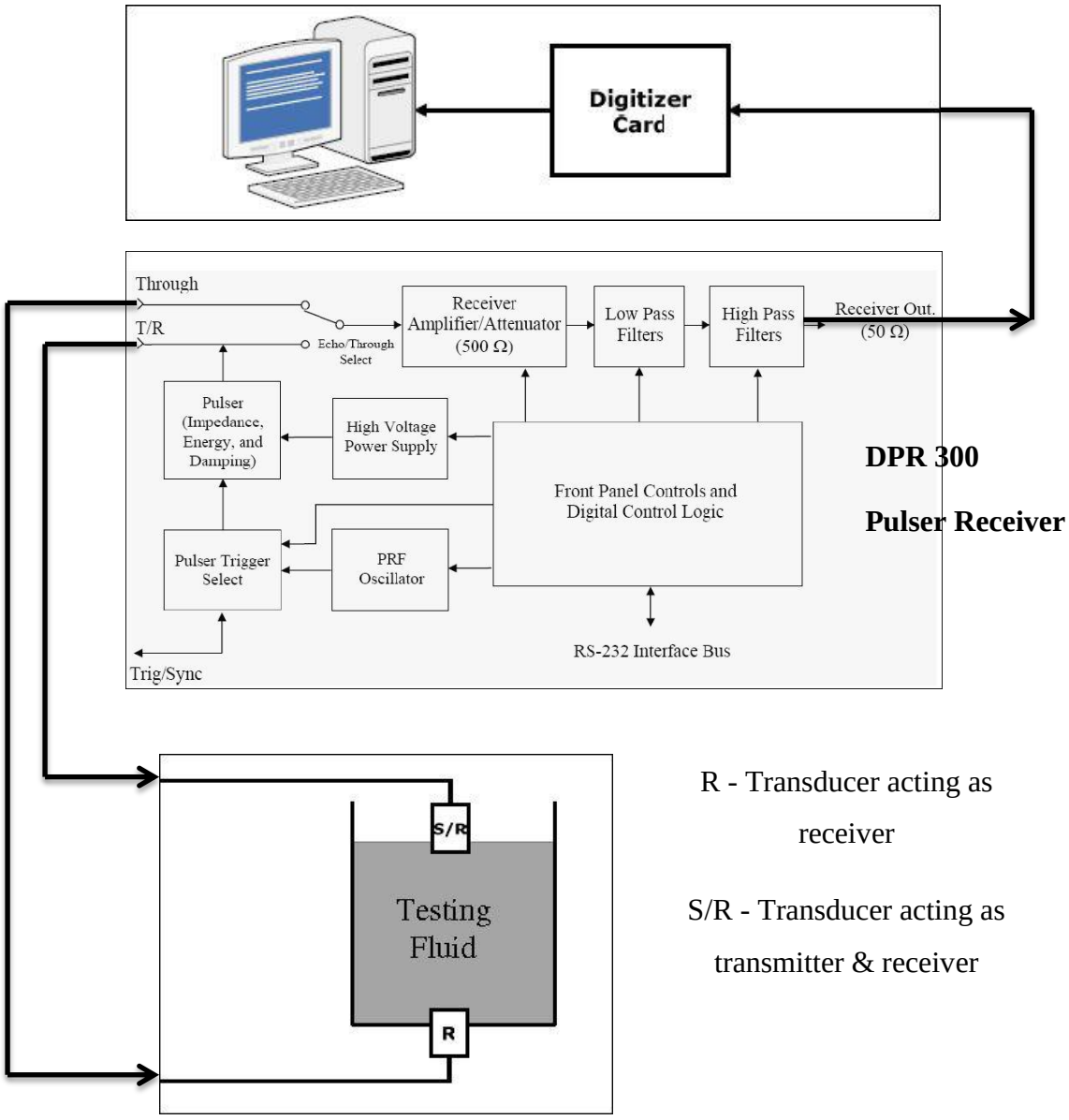

Figure 6.1: Experimental Setup

Following are the salient features of the Pulser/ receiver system used:

PRF Oscillator & Pulser Trigger control: The internal PRF oscillator generates repetitive trigger pulses for the pulser subsystem under the control of the PRF control. Pulser Trigger control selects between the internal PRF oscillator and an external source applied to the Trig/Sync connector as trigger sources for the DPR 300 Pulser.

Pulser (Impedance/Energy/Damping): The pulser generates an excitation pulse upon receiving a trigger event from a selected source. There are four energy values and two impedance values, and the single Energy and impedance control adjusts the pulse energy and the pulser impedance.

Receiver amplifier: It controls the amplification or attenuation of signals processed by the DPR300 receiver. The receiver gain can be varied from -13dB to 66 dB.

Low Pass and High Pass filters: Low filters are available for reducing the bandwidth of the DPR300 receiver. High Pass filters are available for eliminating undesirable low frequency energy from the DPR300 receiver signal. High pass filtering can be used as a means of providing faster receiver recovery from strong signals such as the excitation pulse or strong interface echoes.

Digitizer Card: It converts the analog signal which is coming from DPR 300 in to Digital signal and fed to computer.

7.2 Experimental Procedure:

Pulser/receiver system sends a negative spike signal (100 V to 475 V) to the transducer as an input pulse. Depending upon the method (pulse echo or through) the output pulse will be sensed by the respective transducer. The received output pulses are then amplified and filtered by DPR 300 and sends to digitizer card where it converts analog signal to digital form and on computer screen the waveform can be seen with the help of software (Acquiris) and also graphical data can be captured. Thus different waveforms for different types of fluids and interfaces are obtained from experimental setup.

7.2.1 Experimental Results for homogeneous fluids

The experiments have been performed on homogeneous fluids i.e. water, glycerine & mobil oil one by one by varying the level of the fluid in the small tank (**Figure 6.2)** manufactured for this purpose only. The set up details and results of these fluids has been described as

7.2.1.1 Results for Mobil Oil:

The setup has been prepared for the testing of the signal in mobil oil at different levels. The transducers have been adjusted on the tank. Then mobil oil was filled in this tank.

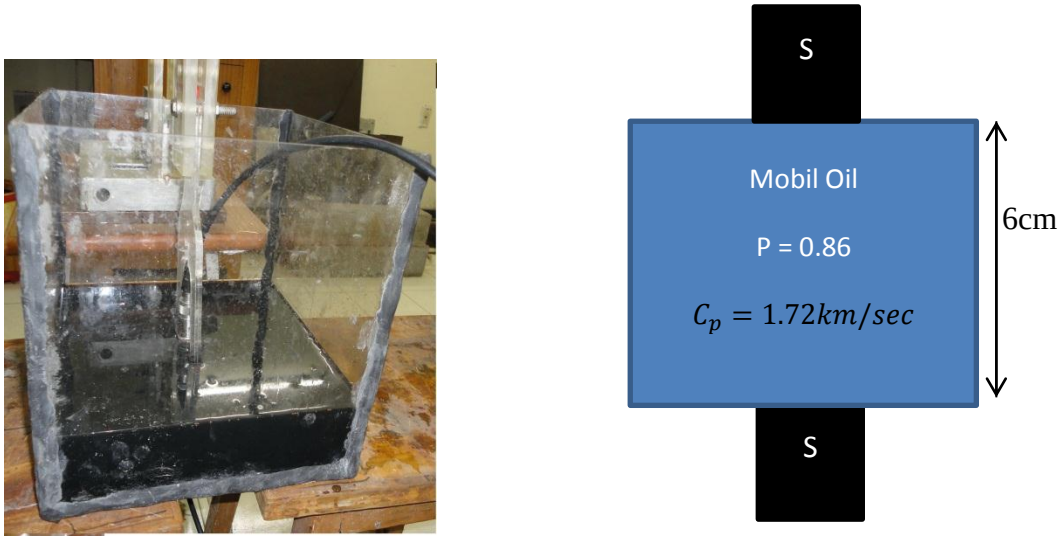

Figure 6.2: Setup for Mobil Oil

As shown in **Figure 6.2,** the actual photograph of the tank with transducer inside the mobil oil. And the schematic is also drawn. Same target points have been used in this case. The results are as follows

Mobil oil Level kept at 2.5cm from Transducer:

The tank was filled with mobil oil up to 2.5cm from the transducer in the pulse through mode with 2.25MHz frequency the result has been shown as

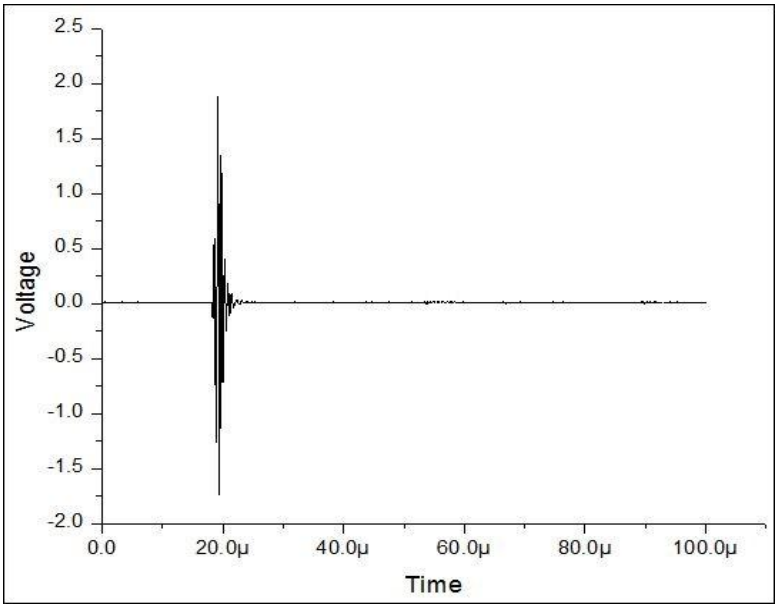

Figure 6.3: Mobil Oil Level kept at 2.5cm from Transducer Surface

Mobil oil Level kept at 3.7cm from Transducer:

The tank was filled with mobil oil up to 3.7cm from the transducer in the pulse through mode with 2.25MHz frequency the result has been shown as

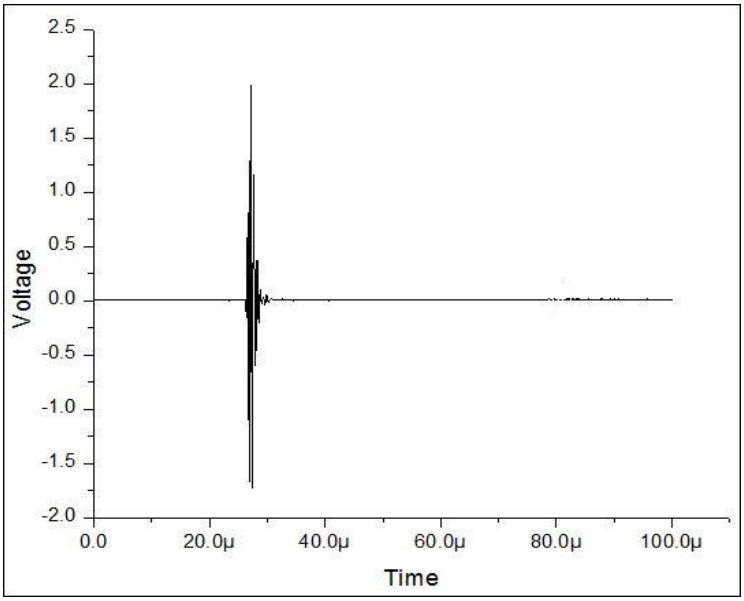

Figure 6.4: Mobil Oil Level kept at 3.7cm from Transducer Surface

It can be seen from the **Figure 6.4,** as the level of the mobil oil has been increased the pulse is taking more time to reach there.

Mobil oil Level kept at 4.9cm from Transducer:

The tank was filled with mobil oil up to 4.9cm from the transducer in the pulse echo mode with 2.25MHz frequency the result has been shown as

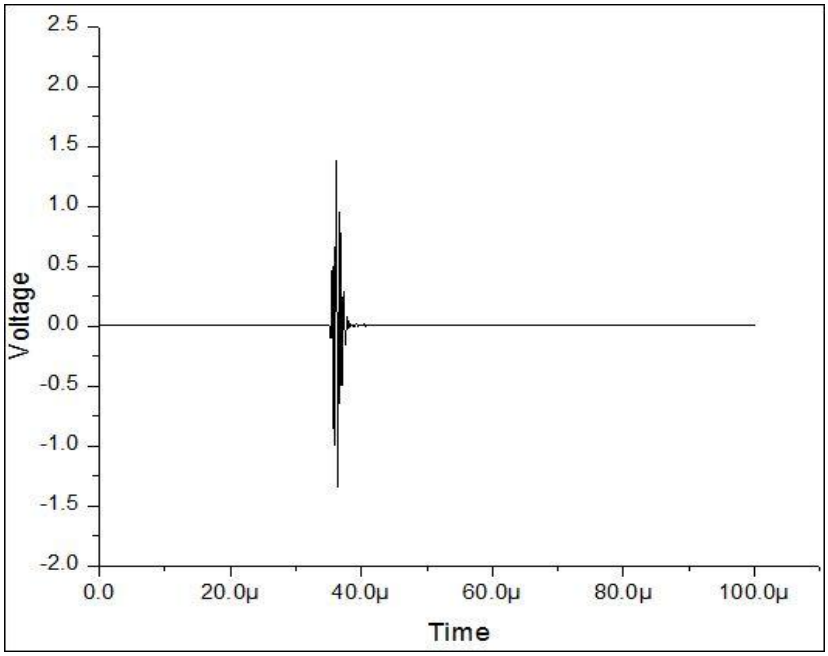

Figure 6.5: Mobil Oil Level kept at 4.9cm from Transducer Surface

It can be seen from the **Figure 6.5,** as the level of the mobil oil has been increased the pulse is taking more time to reach there.

Combining the results from DPSM programing & experimental readings of mobil oil are as shown.

Table 6.1: Comparison of DPSM & Experimental results for Mobil Oil

Location	Time of Arrival (in μs)			
	Experimental		DPSM	
	Actual	Incremental	Actual	Incremental
T1	0	0	95	0
T2	19	19	109	14
T3	28	9	116	7
T4	35	8	123	7

It has been observed that in both the methods, the wave signal has been taking time to reach its target points located at three different positions. It has been concluded that the DPSM has been taking the same incremental time to reach different targets as in the experimental work

7.2.1.2 Results for Glycerine:

The setup has been prepared for the testing of the signal in glycerine at different levels. The transducers have been adjusted on the tank. Then glycerine was filled in this tank. Set up Photograph has been shown on next page.

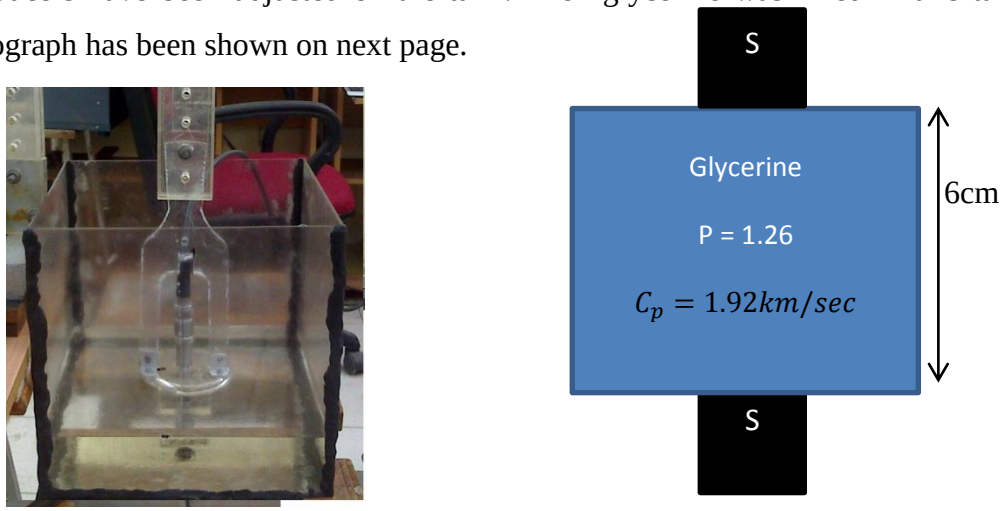

Figure 6.6: Set up for Glycerine

As shown in **Figure 6.6,** the actual photograph of the tank with transducer inside the glycerine. And the schematic is also drawn. Same target points have been used in this case. The results are as follows

Glycerine Level kept at 2.5cm from Transducer:

The tank was filled with glycerine up to 2.5cm from the transducer in the pulse through mode with 2.25MHz frequency the result has been shown as

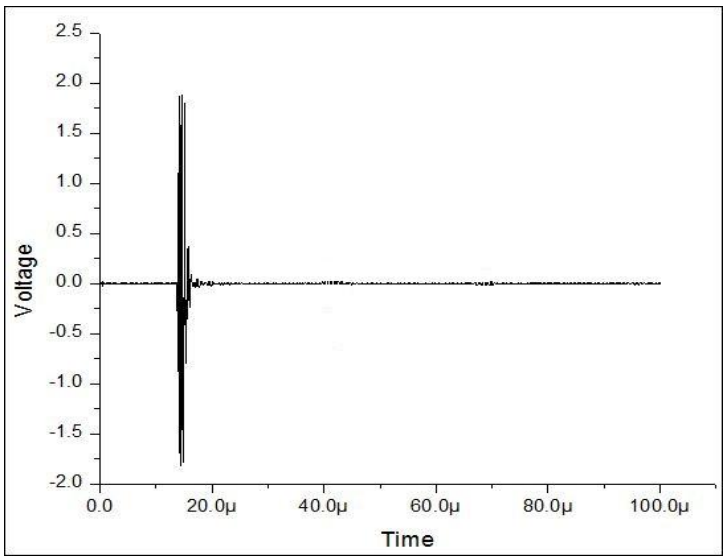

Figure 6.7: Glycerine Level kept at 2.5cm from Transducer Surface

Glycerine Level kept at 3.7cm from Transducer:

The tank was filled with glycerine up to 3.7cm from the transducer in the pulse through mode with 2.25MHz frequency the result has been shown

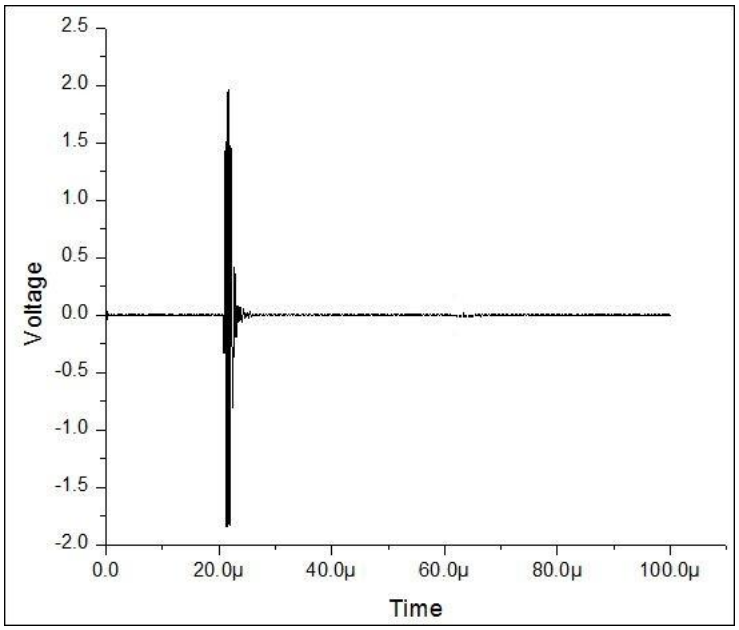

Figure 6.8: Glycerine Level kept at 3.7cm from Transducer Surface

It can be seen from the **Figure 6.8,** as the level of the glycerine has been increased the pulse is taking more time to reach there.

Glycerine Level kept at 4.9cm from Transducer:

The tank was filled with mobil oil up to 4.9cm from the transducer in the pulse through mode with 2.25MHz frequency the result has been shown as

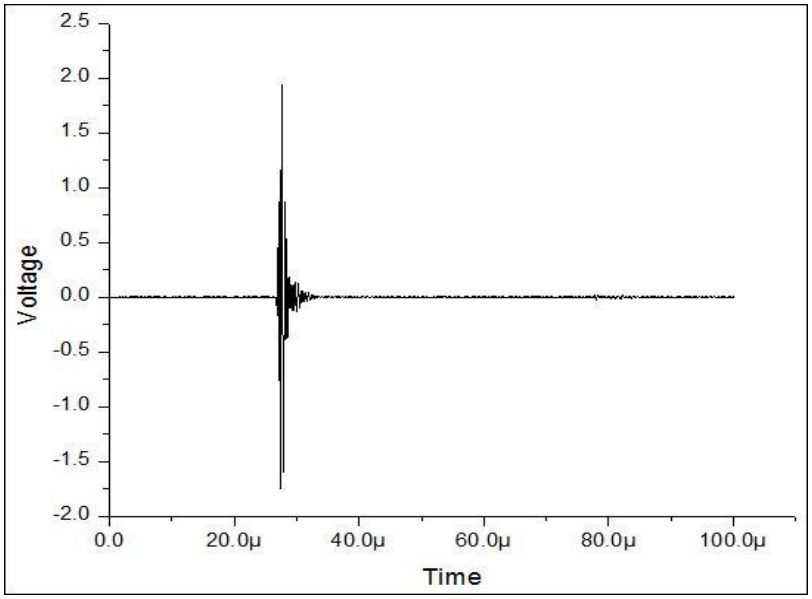

Figure 6.9: Glycerine Level kept at 4.9cm from Transducer Surface

It can be seen from the **Figure 6.9,** as the level of the glycerine has been increased the pulse is taking more time to reach there.

Combining the results from DPSM programing & experimental readings of glycerine are as shown.

Table 6.2: Comparison of DPSM & Experimental results for Glycerine

Location	Time of Arrival (in μs)			
	Experimental		DPSM	
	Actual	Incremental	Actual	Incremental
T1	0	0	95	0
T2	17	17	107	12
T3	22	5	114	7
T4	28	6	120	6

It has been observed that in both the methods, the wave signal has been taking time to reach its target points located at three different positions. It has been concluded that the DPSM has been taking the same incremental time to reach different targets as in the experimental work.

7.2.1.3 Results for Water:

The setup has been prepared for the testing of the signal in water at different levels. The transducers have been adjusted on the tank. Then water was filled in this tank.

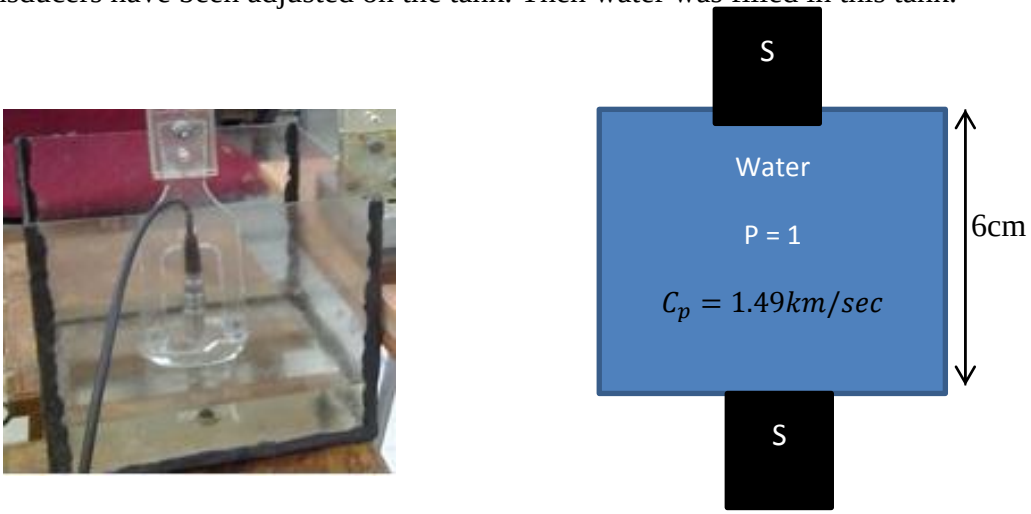

Figure 6.10: Setup for water

As shown in **Figure 6.10,** the actual photograph of the tank with transducer inside the water. And the schematic is also drawn. The water level was kept maximum at 6cm in the tank and the readings have been noted at different target points, which were perpendicular to the transducer surface. The frequency of the transducer has been selected as 2.25MHz in the pulse through mode.

Water Level kept at 1.2cm from Transducer:

The water level was kept at 1.2cm from transducer surface in the pulse through mode with frequency of 2.25MHz.

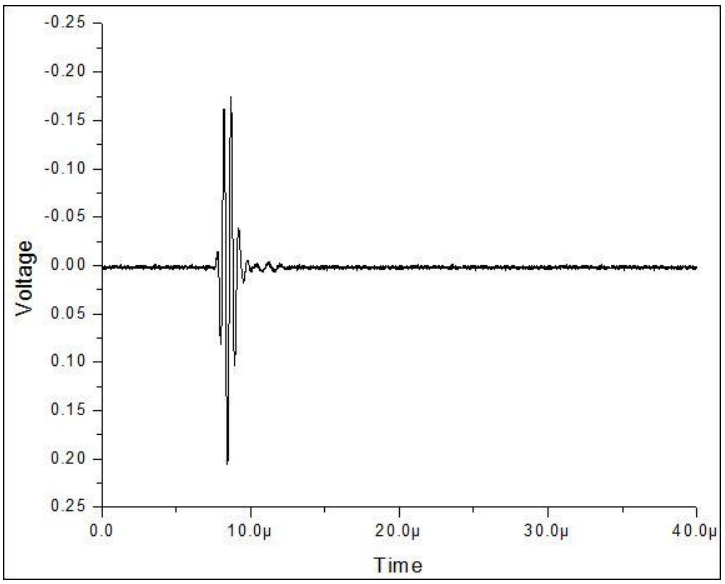

Figure 6.11: Water level kept at 1.2cm from Transducer Surface

Water Level kept at 2.5cm from Transducer:

The water level was kept at 2.5cm from transducer surface in the pulse through mode with frequency of 2.25MHz.

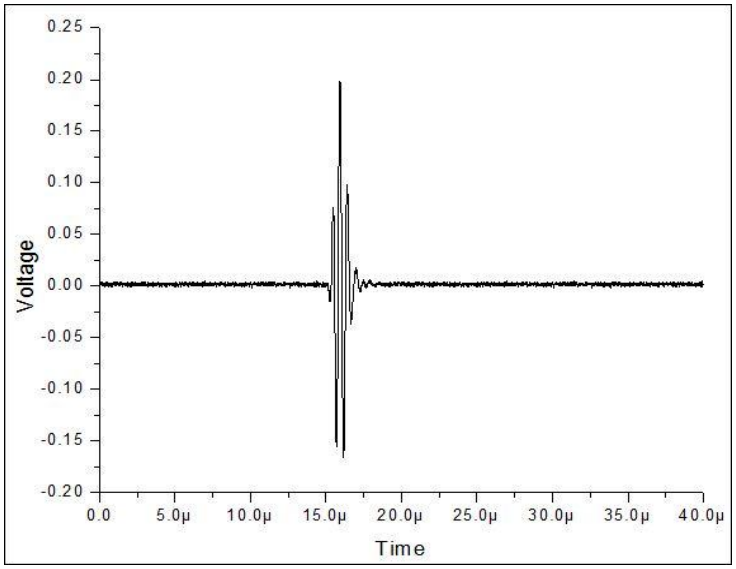

Figure 6.12: Water level kept at 2.5cm from Transducer Surface

It can be seen from the **Figure 6.12,** as the level of the water has been increased the pulse is taking more time to reach there & also the voltage has been observed decreasing.

Water Level kept at 3.7cm from Transducer:

The water level was kept at 3.7cm from transducer surface in the pulse through mode with frequency of 2.25MHz.

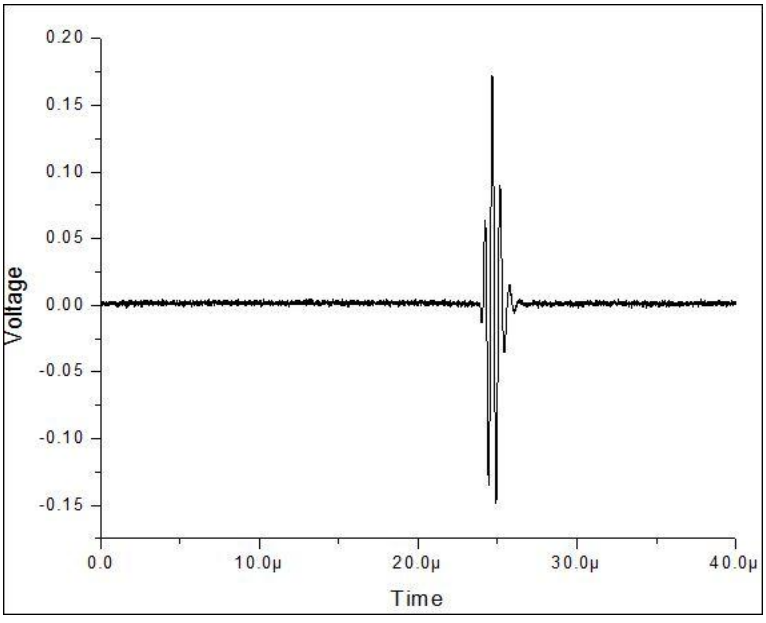

Figure 6.13: Water Level kept at 3.7cm from Transducer Surface

It can be seen from the **Figure 6.13,** as the level of the water has been increased the pulse is taking more time to reach & as well as the voltage has been decreasing.

Water Level kept at 4.9cm from Transducer:

The water level was kept at 4.9cm from transducer surface in the pulse through mode with frequency of 2.25MHz.

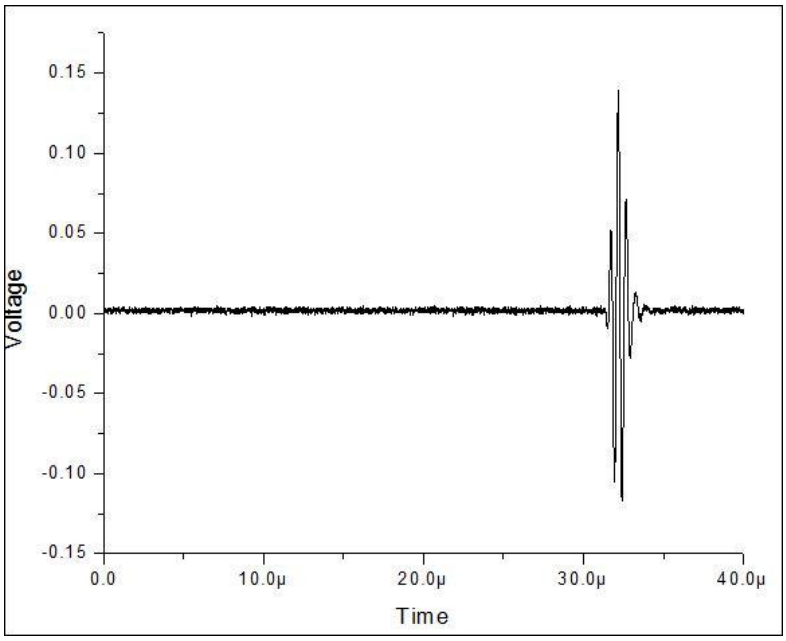

Figure 6.14: Water Level kept at 4.9cm from Transducer Surface

It can be seen from the **Figure 6.14,** as the level of the water has been increased the pulse is taking more time to reach & as well as the voltage has been decreasing.

After results of water has been observed, it has been concluded that the arrival time of the pulse at different target points has been increasing as the distance of the target points increased. And the voltage drop has been observed too as the distance between the transducer and target points increased. This can be explained by the **Figure 6.15.**

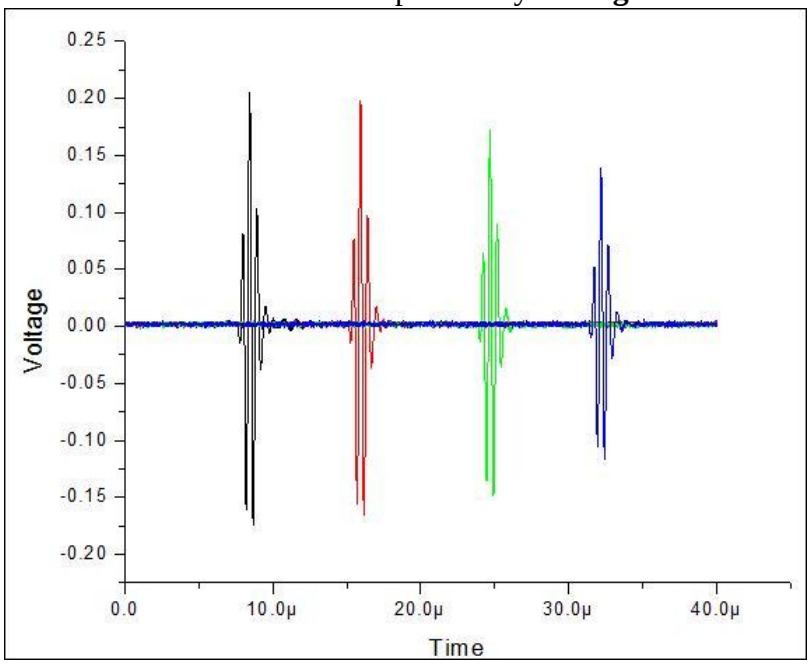

Figure 6.15: Water Signatures at Different Target Points

As shown, the water signatures at different target points, the voltage of the wave pulse has been decreasing as the distance was increasing from the transducer face. The arrival time of each signal has been found different for different locations. So, it has been concluded that voltage and arrival time varies as the distance varies.

Combining the results from DPSM programing & experimental readings of water are as shown.

Table 6.3: Comparison of DPSM & Experimental results for Water

Location	Time of Arrival (in μs)			
	Experimental		DPSM	
	Actual	Incremental	Actual	Incremental
T1	0	0	95	0
T2	8	8	102	7
T3	16	8	111	8
T4	25	9	119	8
T5	33	8	127	8

It has been observed that in both the methods, the wave signal has been taking time to reach its target points located at three different positions. It has been concluded that the DPSM has been taking the same incremental time to reach different targets as in the experimental work. The results for this comparison have been plotted on a graph as shown in **Figure 6.16.**

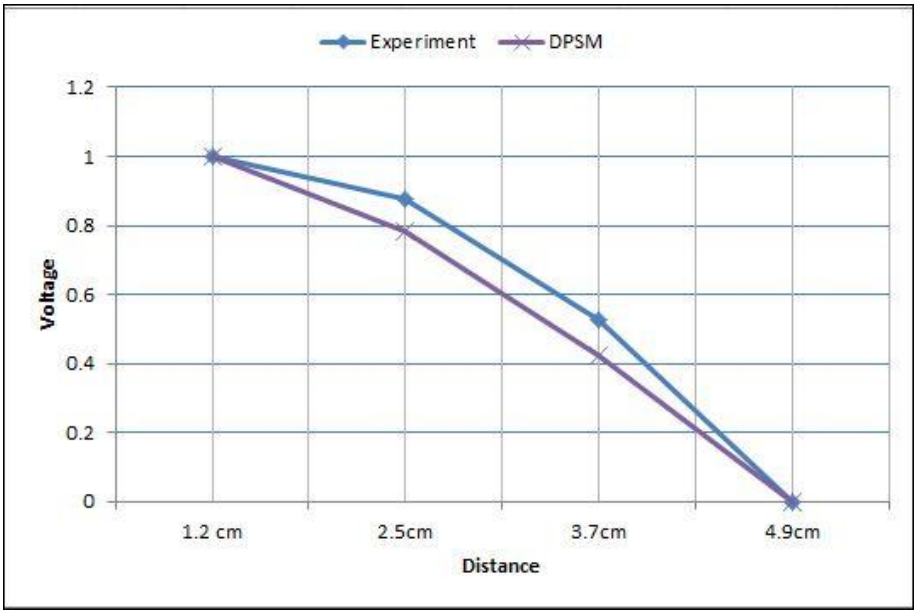

Figure 6.16: Comparison between DPSM & Experimental Results

Before plotting this comparison, the voltage variation has been normalized into the limit from 0 to 1 voltage. After normalization the plot was generated between DPSM & Experimental results, it has been concluded that the DPSM has been following the same trend as the experimental results. With the increase in distance, the drop in the voltage has been observed.

There is not exact time matching between the two methods but it is the incremental time matching between the DPSM & Experimental Work, because in theoretical programming we assumed the signal to be the tone burst signal but in actual it is pulse signal. And also in practical the wave speed of these three fluids can vary but in programming it has been assumed.

Now, it has been seen that the DPSM is following the trend by decreasing the signal as the distance from the transducer surface is increasing in all three homogeneous fluids. After doing the experiment in homogeneous fluid the triple layered non-homogeneous fluid has been done as discussed in next section

7.2.2 Experimental Results for triple layered non-homogeneous fluid

The experiment has been performed in triple layered non-homogeneous fluid. The fluids have been placed according to their densities i.e. glycerine, having high density, placed at the bottom of the tank, then water and at the top mobil oil has been placed as shown in **Figure 6.17**

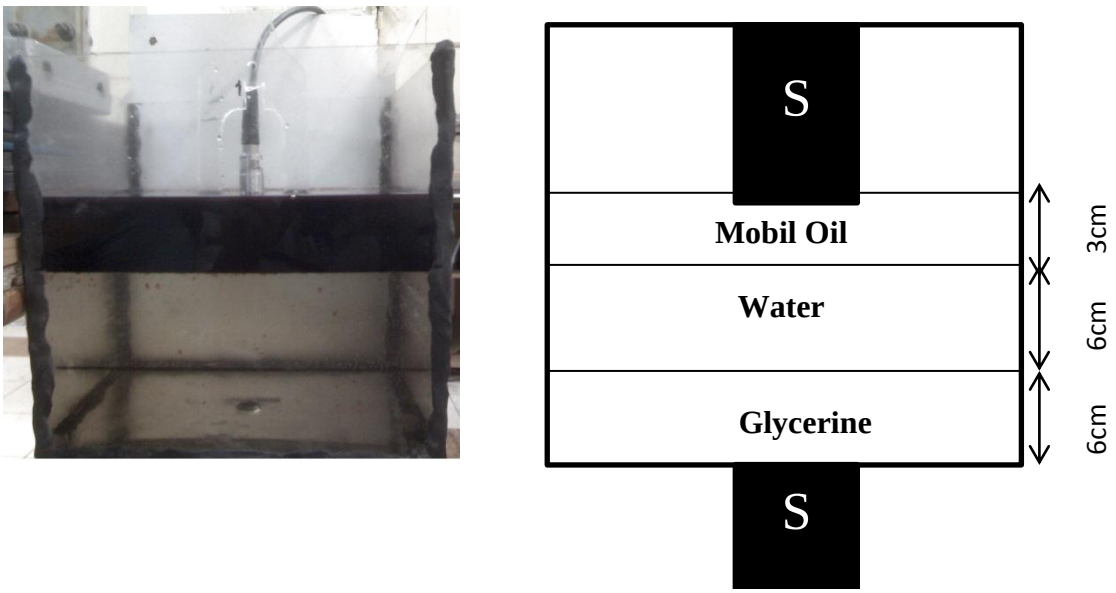

Figure 6.17: Set up for Triple Layered Non-Homogeneous Fluid

The triple layered set up and its schematic has been shown in **Figure 6.17** and the level of each fluid has also been shown.

In this case five set of readings have been complied at different target points along the transducer surface in Z-axis.

- The first reading has been taken in the glycerine at a distance of 3.5cm, with the frequency of 2.25MHz in pulse through mode.
- The second reading has been taken at the first interface of glycerine & water the voltage drop has been observed here, it is because of change in the wave speed of both the fluids.
- The third reading has been taken in the water at a distance of 9cm from the transducer surface. The voltage drop has also been observed here because of the interface in the path of the input signal.
- The fourth reading has been observed at the second interface of water and mobil oil. The voltage drop here is even more than the previous reading. It is because of the interface and then different fluid's properties.
- The final reading was observed in the mobil oil, here the voltage drop has been maximum because of the two interfaces in the path of input signal.

The graph has been made between the voltage and distance of both DPSM results & Experimental results in triple layered non-homogeneous fluid.

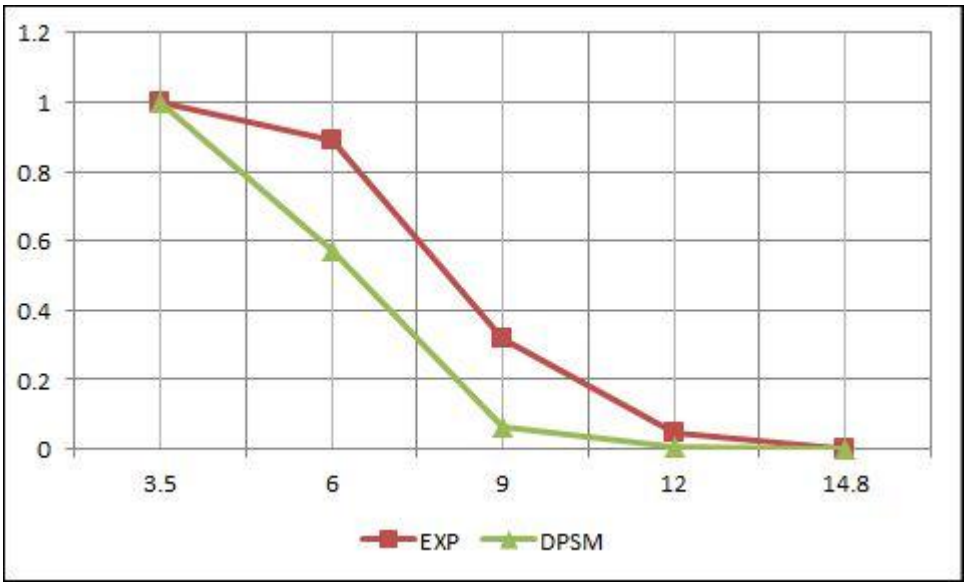

Figure 6.18: Comparison of the Voltage & Distance between DPSM & Experimental results

In the **Figure 6.18,** the voltage variation has been normalized between 1 to 0. And it has been observed that the voltage has been decreasing as the distance between the target point and transducer surface increases. It can be concluded that DPSM results are following the same trend as the experimental result.

7.3 Concluding Remarks

In this chapter, the results have been discussed, which have been done experientially and analytically. And the results have been compared between DPSM & Experimental work. It has been observed that the DPSM is following the same trend as the practical work. As the distance increases the signal decreases in all the homogeneous & non-homogeneous fluid.

CONCLUSIONS

- The DPSM technique has been used to model the ultrasonic fields generated by both steady state and transient state wave propagation in Homogeneous & Triple layered Non-Homogeneous fluid having two interfaces.
- In the DPSM modeling, it has been observed that as the number of point sources increases the accuracy increases i.e. Near Field has been compared both by calculating & by measuring. The DPSM followed the Exact solution as the number of point sources increased.
- It has been observed that to reduce the divergence angle in the field modeling one can increase the size of the diameter of the transducer or by increasing the frequency of the transducer.
- It follows Snell's Law accurately it has been shown by changing the order of the fluid 2 and fluid 3.
- The snap shots presented in the previous chapter, the transmission, reflection in both homogeneous and triple layered non-homogeneous fluid can be observed at different time instances.
- The DPSM results are following the same trend (peak arrival time delay as the distance increases) as in the experimental work.

Scope for Future Work

- In DPSM modeling of transducer surface, it was assumed that the velocity is constant at the transducer surface. It can be extended to model the piezoelectric behaviour of the transducer in that way transducer will not rely on constant velocity to give output. Then instead of constant velocity one can give voltage as one of the input parameter.
- This developed model can be extended to triple layered non-homogeneous solid fluid interaction problem.
- This model can be extended to four layered three interface non-homogeneous fluid but with high frequency transducer modeling.
- The developed model can be extended to model the bubble interface also

REFERENCES

1. Rose, J.L., (2004) “Ultrasonic Guided Waves in Structural Health Monitoring” , Key Engineering Materials Vols. 270-273, pp.14-21
2. http://www.ndt-ed.org dated 04-02-2012 4:05pm
3. http://edinformatics.com dated 20-11-2011 6:15pm
4. http://www.allshookup.org dated 20/11/2011 6:15pm
5. http://www.earthquake.usgs.gov dated 20/11/2011 6:15pm
6. http://www.ndt-specialist.com dated 04/02/2012 4:01pm
7. Ginzel E., (2006) “NDT Modelling overview”, Materials Research Institute, Waterloo, Ontario, Canada
8. http://www.ndt.net dated 12/05/2012 8:01pm
9. Barauskas R., Daniulaitis V., (2000) “Simulation of the ultrasonic wave propagation in solids” ISSN 1392-2114 ULTRAGARSAS, Nr.4 (37), 2000, Kaunas University of Technology, Mickeviciaus, Kaunas
10. Tirukkavalluri R.R., (2008) “Ultrasonic field modelling of transient wave propagation in homogenous and non-homogenous fluid media using Distributed Point Source Method (DPSM)”, M.E. Thesis, Department of Mechanical Engineering, Thapar University, Patiala
11. Gomez Y.U., Espinosa F.M. de, (2006) “Selective Excitation of Lamb Wave modes in thin aluminium plates using bonded piezoceramics: FEM modelling and measurements”, ECNDT 2006 - Poster 205**,** Instituto de Acustica, Madrid, Spain
12. Han S., (2007) ”Finite Element analysis of Lamb Waves acting within a thin aluminium plate”, M.S. Thesis, Department of The Air Force Air University, Air Force Institute of Technology, Wright-Patterson Air Force Base, Ohio
13. Vermani G., (2008) ”Damage detection in reinforcing steel bars using ultrasonic wave propagation”, M.E. Thesis Department of Civil Engineering, Thapar University, Patiala
14. Ahmad, R., Kundu, T., Placko, D (2003) "Modeling of the Ultrasonic Field of Two Transducers Immersed in a Homogeneous Fluid Using Distributed Point Source Method". I2M (Instrumentation, Measurement and Metrology) Journal; Vol.3, pp.87-116

15. Kundu T., (2004) “Ultrasonic non-destructive evaluation: Engineering and Biological material characterization”, International Standard Book Number 0-8493-1462-3, CRC Press, Boca Raton London
16. Placko D., Kundu T., (2007) “ DPSM Modeling Engineering Problems”, Wiley
17. Bartoli I., Marzani A., Matt H., Scalea F.L. di, Viola E., (2006) ”Modelling guided wave propagation for structural health monitoring application”, Department of Structural Engineering, University of California, San Diego, USA
18. Raisutis R., Zukauskas E., Mazeika L., (2011) “Application of analytical and semi-analytic modelling methods for investigation of ultrasonic guided wave propagation in composites”, ISSN 1392-2114 ULTRAGARSAS (ULTRASOUN D), Vol. 66, No. 3, 2011, Ultrasound Institute, Kaunas University of Technology, Kaunas
19. Kessler S.S., (2002) “Piezoelectric based In-Situ damage detection of composite materials for structural health monitoring systems”, PhD Thesis, Department of Aeronautics and Astronautics, Massachusetts Institute of Technology
20. Daniulaitis V., Barauskas R., (1998) “Modelling techniques of ultrasonic wave propagation in solids”, ISSN 1392-2114 ULTRAGARSAS, Nr.1 (29), 1998, Kaunas University of Technology, Department of Engineering Mechanics, Mickeviciaus, Kaunas
21. Kundu T., Banerjee S., (2007) “Ultrasonic Field Modeling in Plates Immersed in Fluid”, International Journal of Solids & Structures 44 (2007) 6013-6029, Department of Civil Engg. & Engg. Mechanics, University of Arizona, Tucson, AZ85721, USA
22. Banerjee S., Kundu T., Alnuaimi Nasser A., (2007) “DPSM Technique for Ultrasonic Field Modeling near Fluid Solid Interface”, Ultrasonic 46 (2007) 235 250, Department of Civil Engg. & Engg. Mechanics, University of Arizona, Tucson, AZ 85721, USA
23. Banerjee S., Kundu T., (2007) “Semi-analytical Modeling of Ultrasonic Fields in Solids with Internal Anomalies Immersed in a Fluid”, Wave Motion 45 (2008) 581 595, Department of Civil Engg. & Engg. Mechanics, University of Arizona, Tucson, AZ 85721, USA
24. Das S., Banerjee S., Kundu T., (2008) “Elastic wave scattering in a solid half-space with a circular cylindrical hole using the Distributed Point Source Method”, International Journal of Solids and Structures 45 (2008) 4498-4508, Department of Civil Engg. & Engg. Mechanics, University of Arizona, Tucson, AZ 85721, USA

25. Sharma S., (2009) “Ultrasonic field modeling using Distributed Point Source Method (DPSM)”, M.E. Thesis, Department of Mechanical Engineering, Thapar University, Patiala
26. Dao M. C., Das S., Banerjee S., Kundu T., (2009) “Wave propagation in a fluid wedge over a solid half-space-Mesh-free analysis with experimental verification”, International Journal of Solids and Structures 46 (2009) 2486-2492, Department of Civil Engg. & Engg. Mechanics, University of Arizona, Tucson, AZ 85721, USA
27. Banerjee S., Das S., Kundu T., Placko D., (2009) “Controlled Space Radiation concept for mesh-free semi-analytical technique to model wave fields in complex geometries”, Ultrasonics 49 (2009) 615-622, Department of Civil Engg. & Engg. Mechanics, University of Arizona, Tucson, AZ 85721, USA, Ecole Normale Superieve, SATIE, 62, av. Du President Wilson, F-94235 Cachan Cedex, France
28. Fan Z., (2010) “Application of Guided Wave Propagation on waveguides with irregular cross-section”, PhD Thesis, Department of Mechanical Engg., Imperial College London, London SW7 2AZ
29. Placko D., Yanagita T., Rahani E. K., Kundu T., (2010) “Mesh-Free Modeling of the Interaction between a Point-Focused Acoustic Lens and a cavity”, IEEE Transactions on Ultrasonics, Ferroelectrics & Frequency Control, Vol. 57 No. 6, June 2010, Department of Civil Engg. & Engg. Mechanics, University of Arizona, Tucson, AZ 85721, USA, Ecole Normale Superieve, SATIE, 62, av. Du President Wilson, F-94235 Cachan Cedex, France
30. Placko D., Yanagita T., Rahani E. K., Kundu T., Dao C. M., (2010) “Ultrasonic Field Modeling: A comparison of Analytical, Semi-Analytical, and Numerical Techniques”, IEEE Transactions on Ultrasonics, Ferroelectrics & Frequency Control, Vol. 57 No. 12, December 2010, Department of Civil Engg. & Engg. Mechanics, University of Arizona, Tucson, AZ 85721, USA, Ecole Normale Superieve, SATIE, 62, av. Du President Wilson, F-94235 Cachan Cedex, France
31. Rahani E. K., Kundu T., (2011) “Modeling of Transient Wave Propagation Using the Distributed Point Source Method”, IEEE Transactions on Ultrasonics, Ferroelectrics & Frequency Control, Vol. 58 No. 10, October 2011, Department of Civil Engg. & Engg. Mechanics, University of Arizona, Tucson, AZ 85721, USA